MSc in Sustainable Energy

Design and economic analysis of a Solar Thermal Pre-cooling System for Agro-Produce Cold Chain in Lesotho

Dissertation

***Student**: Mpho Lucas Yengane*

201200737

Signature:

Date: September 2023

***Main Supervisor**: Prof. Mpholo/Mr. Mokeke*

Signature: _____

Date: _____

Abstract

The agricultural sector in Lesotho faces considerable challenges related to post-harvest losses. When fresh vegetables are exposed to field temperatures of up to 35°C, even for a short period, it can lead to compromised cold storage quality, shortening their shelf-life by 20 hours. These post-harvest losses amount to an estimated 30-40% of the harvest, exacerbating poor economic performance and poverty. Solar thermal cooling, leveraging Lesotho's abundant solar energy resources (4.5-6.5 kWh/m^2/day), holds great potential for solar-powered refrigeration. This research aims to design a solar thermal cooling system tailored to the specific needs of preserving fresh agricultural produce. Also, a comprehensive economic analysis, encompassing TRNSYS and MATLAB evaluations, is conducted to assess the system's financial viability.

The TRNSYS simulation determines optimal values for the coefficient of performance, solar fraction, collector efficiency, exergy efficiency, and primary energy savings, while the MATLAB economic analysis scrutinizes various key economic metrics, including levelized cost of energy, net present value, savings to investment ratio, and discounted pay-back period, to thoroughly evaluate the system's performance and economic feasibility. The outcomes reveal that even at the lowest considered coefficient of performance value (0.5), the solar thermal absorption cooling system demonstrates a more cost-effective levelized cost of energy when compared to the average electricity cost for refrigeration in Lesotho.

The proposed solar thermal cooling system incorporates evacuated tube collectors and an auxiliary boiler to effectively manage a cooling load of 7.318 kW, ensuring the preservation of fresh vegetables at a temperature of 6.1°C. The optimized system design entails the selection of a chiller with a coefficient of performance value of 0.8, a collector area of 12 m^2, and a hot storage volume of 0.2 m^3. This configuration maximizes solar energy utilization, resulting in higher solar fraction values and improved energy efficiency. Remarkably, this optimized configuration yields the best values for levelized cost of energy ($0.085/kWh), net present value ($9,200), discounted pay-back period (12 years), and savings to investment ratio (achieving 1 in year 13). These findings unequivocally highlight the financial feasibility and profitability of the solar thermal cooling system, positioning it as a highly promising investment option for addressing refrigeration needs in Lesotho.

Acknowledgments

I would like to extend my sincere gratitude to those who have supported and guided me throughout the completion of this master's thesis.

First and foremost, I express my heartfelt appreciation to my thesis supervisors, Professor M. Mpholo and Mr. S. Mokeke, for their invaluable guidance, expertise, and unwavering support. Their insights and feedback have been instrumental in shaping this work.

I would like to acknowledge the faculty and staff of The National University of Lesotho for creating a conducive academic environment and providing resources that facilitated my research. I am indebted to my family and friends for their constant encouragement and support throughout this journey. Their belief in my abilities has been a source of motivation and strength.

1 Table of Contents

List of Figures

List of tables

1. Introduction

1.1. Background

Since the 18th century, it has been acknowledged that food preservation is essential [1]. In the past, reducing the moisture content of fresh vegetables was a common way to extend their shelf life. However, in the 21st century, consumers demand high-quality food, rendering this older practice limited [2, 3]. Although food can still be preserved through methods such as drying, curing, salting, fermenting, smoking, or oxygen removal, refrigeration is currently the most popular method. Proper refrigeration at the appropriate temperature and humidity enables food to maintain its moisture content and weight, thereby staying fresh for a longer time. The need for fresh produce has driven early innovations in food storage technology, such as Smock and Neubert's research on controlled atmosphere storage of apples in 1950, which paved the way for groundbreaking advances in fresh food preservation and refrigeration [1].

Preserving food at high-quality levels requires a multi-dimensional chain system in which food is kept at low temperatures to slow down metabolic processes that lead to spoilage [4]. Since its inception, the refrigeration of fresh produce has continued to improve. In the early 2000s, this was accelerated by the increasing demand for premium quality fruits and vegetables, where global production witnessed significant growth, increasing by 30% from 1980 to 1990 and further by 56% from 1990 to 2003 [5, 6]. However, many refrigeration technologies rely heavily on the electricity generated from burning fossil fuels, thus presenting an environmental challenge of climate change. This has led researchers worldwide to develop new technologies for more environmentally friendly refrigeration, such as solar thermal cooling.

Due to its wide-ranging agriculture and food security applications, solar radiant energy can be utilized for solar thermal cooling [7]. Solar thermal cooling systems use solar energy to heat a secondary fluid, which flows through collectors to gain thermal energy and transfer it to the generator chamber of the chiller for the necessary condensation and evaporation processes that create the cooling effect. Solar thermal cooling systems have an advantage over solar photovoltaic (PV) systems in that they can harvest up to 98% of incident radiation and provide efficiencies of 60-70%, compared to solar PV panels that can only harvest up to 46% of visible light and offer a maximum efficiency of 30% [24–26]. However, the major obstacle to the growth of solar thermal cooling technology is its high initial cost and low overall system

efficiency, making it difficult to compete commercially with conventional cooling technologies [11].

The surge in research on solar thermal cooling technology for air conditioning and refrigeration can be attributed to the energy crises of the 1970s; it also gained even more popularity in the early 90s as a solution to low electrification and off-grid cooling [12]. Two decades ago, a review by Best and Ortega on solar refrigeration and cooling found that the global system efficiencies achieved using evacuated tube collectors in conjunction with ammonia/water absorption systems were only 7-20%, depending on solar irradiation [13]. These efficiencies have since improved to 48% [14]. They also discovered that concentrating collectors are necessary for achieving lower temperatures ranging from 4 to 10°C. Furthermore, Brosnan suggests that swiftly pre-cooling agricultural produce to temperatures between 0 and 5°C before transportation using solar thermal cooling can help prolong its shelf life by halting metabolic processes for 8 hours or more [15].

Reducing reliance on fossil fuel energy sources, which contribute to climate change, has been a significant driver in the development of solar thermal cooling technologies in the past two decades [16]. Absorption, adsorption, and desiccant cooling are the three most researched technologies in this niche market. Still, they have not been able to provide consistent optimal cold storage temperatures and humidity levels of 0-12°C and 80-95%, respectively, without an auxiliary heat supply [16, 17]. This is a major challenge in food refrigeration since maintaining steady temperatures and humidity is essential for optimal food quality.

Despite progress being slow, there has been a significant advancement in solar thermal cooling technologies in recent years. With the continued effort in research and development, solar thermal cooling systems can potentially provide a more sustainable solution for air conditioning and refrigeration, reducing reliance on fossil fuel energy sources and contributing to the ongoing fight against climate change.

1.2. Problem Statement

Agriculture contributes 17% to Lesotho's gross domestic product (GDP), and more than 70% of Basotho depend on agriculture for food and income [17–19]. It is crucial for ensuring food security, economic growth, and development [22]. Despite the importance of agriculture, farmers in the country face a significant challenge in the form of post-harvest losses due to the

absence of cold storage facilities for perishable agricultural produce such as fruits and vegetables. This is primarily due to the metabolic processes that cause fresh produce to deteriorate and lose value. Fruits and vegetables can lose up to 20 hours of their shelf life due to field heat exposure [18–20]. In addition, perishable commodities are known to experience a faster deterioration rate as the temperature increases and the deterioration can increase two to three times with every 10°C rise in temperature [26]. To ensure the quality and safety of perishable fruits and vegetables, storing them at their lowest safe temperature is recommended.

Sub-Saharan Africa (SSA) has estimated 30-40% post-harvest food losses, which amounts to more than a third of all harvest [4–6]. These losses not only lead to financial difficulties for farmers but also discourage large-scale farming of perishable agricultural products, impeding the growth of the agriculture sector and exacerbating poverty and poor economic performance. This, in turn, leads to more deaths among children each year than the combined toll of AIDS, malaria, and tuberculosis [29].

Implementing post-harvest management systems such as cold room storage is crucial in reducing losses and shifting Lesotho from a food-deficient country dependent on South Africa to a more food-secure nation [22, 30]. Cold rooms provide a solution to the post-harvest loss challenge by preserving produce for extended periods before distribution to consumers. However, traditional cold rooms can be costly to purchase and maintain, which can increase storage expenses and decrease profit margins, particularly for small-scale farmers [2, 5]. Furthermore, these conventional cold rooms may not be easily accessible for off-grid usage near farming lands for pre-cooling purposes. Pre-cooling is vital not only for extending the shelf life of produce by eliminating field heat, but also for reducing temperature variations in cold storage facilities which can impact the quality of other products in storage [8, 9]. Additionally, the operation of cold rooms can lead to exorbitant electricity or fuel costs over time, even with low agricultural yield [17]. Nevertheless, the adoption of solar thermal cooling technologies remains limited in Lesotho due to a lack of awareness regarding their benefits, insufficient research, and limited financial resources.

1.3. Research Questions and Objectives

The following research questions frame the conducting of this research:

a. What is the potential of solar thermal energy for refrigeration in Lesotho?

b. What are the design considerations for solar thermal refrigeration in Lesotho, including sizing, efficiency, and cost-effectiveness?
c. How can solar thermal refrigeration systems be integrated into the existing infrastructure in Lesotho?
d. What are the environmental and socio-economic benefits of solar thermal refrigeration in Lesotho?

This research aims to design a solar thermal cooling system to address the challenge of spoilage of fresh agricultural produce and to perform an economic analysis of the model.

The following objectives are targeted in the system design:

a. To assess the current state of refrigeration in Lesotho, including the demand for refrigeration, the types of refrigeration systems used, and the challenges faced.
b. To evaluate the potential of solar thermal energy for refrigeration in Lesotho, including the availability of solar resources, the suitability of solar thermal technology, and the potential for integration with the existing infrastructure.
c. To design a solar thermal refrigeration system for Lesotho that is efficient, costeffective, and appropriate for the local context.
d. To evaluate the economic benefits of solar thermal refrigeration in Lesotho.

The objectives are further defined within the following specific constraints.

i. Achieving pre-cooling temperatures of 0-12°C for the following products:
    - cabbage
    - tomato
    - green pepper
    - green beans ii. Designing the system for:
    - high collector efficiency
    - high coefficient of performance (COP)
    - high solar fraction
    - high exergy efficiency
    - high primary energy savings

iii. Perform an economic analysis to determine if the system can reach parity or, better yet, be cheaper than the available conventional cooling systems considering the following economic metrics:
    - Levelized cost of energy (LCOE)

- Net present value (NPV)
- Savings to investment ratio (SIR)
- Discount pay-back period (DPP)

1.4. Justification

Without considering the cold rooms used for agricultural produce, it is worth noting that cooling loads currently account for 30-40% of global power consumption [33]. It is therefore crucial to develop cleaner and more sustainable energy sources for large-scale cooling systems to reduce post-harvest losses for agricultural produce while minimizing the environmental impact. Designing and performing an economic analysis of a solar thermal cooling system in Lesotho has several justifications including the following:

1. Abundant solar energy: Lesotho is just 30,355 km^2 in size and solar irradiation is generally evenly distributed across the country with solar insolation levels at 5.57kWh/m^2, meaning that the country receives a significant amount of sunlight throughout the year as shown in Figure 1 [34], [35]. This makes it an ideal location for installing solar thermal absorption cooling systems, which rely on solar energy to power the cooling process. In addition, solar radiation is most intense during the hours of peak cooling loads, which coincide with the hottest hours of the day. Therefore, less cooling is required after sunset or during cloudy weather.

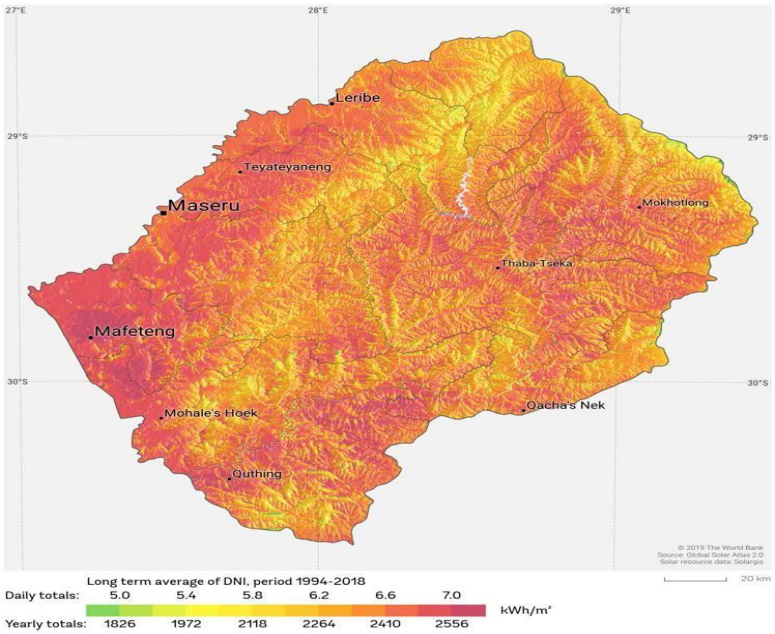

Figure 1. Direct normal radiation patterns for Lesotho [35].

2. Reducing electricity demand: Lesotho currently relies heavily on electricity imports to meet its energy needs. The installation of solar thermal absorption cooling systems can help reduce the country's electricity demand, freeing up more electricity for other uses and reducing the country's dependence on foreign energy sources. In 2010, Wang [36] discovered that using solar-assisted cooling systems in Southern, European, and Mediterranean regions could result in energy savings of up to 40-50%. This is particularly relevant to Lesotho, where there is already a capacity shortage, with a national peak load of 180.57 MW and a domestic generation capacity of only 74.7 MW as of 2022 [37].
3. Cost savings: Solar thermal absorption cooling systems can provide cost savings over traditional cooling systems in the long run. While the initial investment may be higher, the lower operating costs of solar thermal absorption cooling systems can result in significant savings over time. Furthermore, by 2030, the total cost of solar thermal cooling systems is projected to drop significantly by 35-45%, according to the International Energy Agency (IEA) [38]. This highlights the need for increased investment and research into solar thermal cooling.
4. Environmental benefits: Solar thermal absorption cooling systems are a clean and renewable technology, producing no greenhouse gas emissions or other pollutants. By using this technology, Lesotho can reduce its carbon footprint and contribute to global efforts to mitigate climate change.
5. Economic development: Installing and maintaining solar thermal cooling systems can create local jobs and support economic development in Lesotho. Additionally, by reducing energy costs and increasing energy independence, this technology can help stimulate economic growth and improve the overall standard of living.
6. Lesotho's low electrification: Solar thermal cooling technologies have the potential to address the challenge of low electrification in Sub-Saharan African countries such as Lesotho. Despite an increase in electrification since the 2000s, less than half of the country's population has access to electricity as indicated in Figure 2 [39]. Solar thermal cooling systems can operate in the rural areas which are not covered by the national grid.

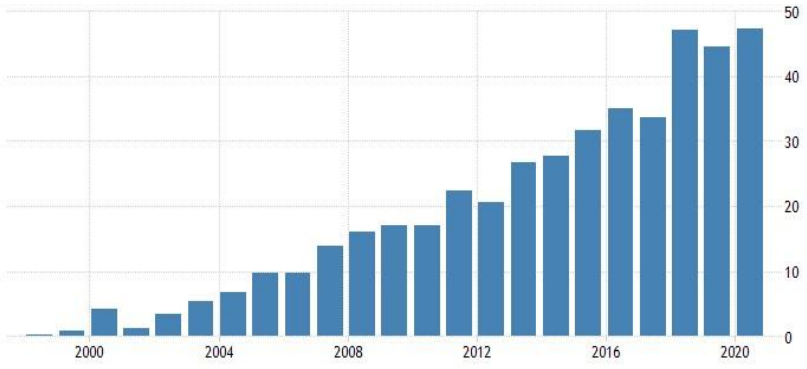

Figure 2. Access to electricity in Lesotho (% of the population) over 24 years [39].

1.5. Report Structure

This report is organized and coordinated into five major chapters. The first chapter is the introduction which lays down the background, problem statement, research questions, and justification for conducting this research. The second chapter is the literature review which encompasses theoretical and mathematical definitions of the technologies (absorption, desiccant, and adsorption) that the research focuses on as well as the design and economic parameters. Moreover, the literature review gives a critical overview of the relevant work that relates to the study and technologies used in the research. The third chapter is the methodology. In this chapter, the precise system of methods used as well as simulation technologies are described. The fourth chapter is the results and discussion, where the simulation results are tabulated, analyzed, discussed, and criticized in reference to the literature. The fifth and final chapter is the conclusion. This is where the main findings are summarized, conclusions are drawn, and recommendations are presented for future research.

2. Literature Review

The following literature review corroborate and justify the objectives of this research, which are to design and simulate a solar thermal cooling system using mathematical modeling and TRNSYS software modeling, with emphasis on both the technical and economic performance of the system.

A solar thermal refrigeration system is a type of refrigeration system that uses solar energy to power the refrigeration cycle, in lieu of electricity. This type of system utilizes the principle of thermodynamic refrigeration, where a working fluid is compressed, condensed, and expanded to produce cooling. The common thermal refrigeration methods are absorption, adsorption, and desiccant cooling [7, 40–42].

The basic components of a solar thermal refrigeration system include a solar collector, a thermal storage unit, a refrigeration cycle, and a cooling load. The solar collector is responsible for capturing the solar energy and transferring it to the thermal storage unit, which stores the thermal energy until it is needed for the refrigeration cycle. The refrigeration cycle generally includes a compressor, a condenser, an expansion valve, and an evaporator, which work together to produce cooling. Additionally, there is also an adsorber bed and desiccant wheel depending on the refrigeration method used [14, 43].

The process starts with the solar collector absorbing solar radiation and converting it to thermal energy. This thermal energy is transferred to the thermal storage unit which can be a tank or a bed of rocks. When cooling is needed, the thermal energy is released from the storage unit and used to power the refrigeration cycle [14]. In an event where solar radiation is in short supply, an auxiliary heater is used to provide the necessary thermal energy.

The refrigeration cycle starts with the compressor which compresses the working fluid, usually a refrigerant such as ammonia or water, to high pressure and temperature [44]. The compressed gas is then sent to the condenser, releasing heat to the surroundings and condensing into a liquid. The liquid then flows through the expansion valve, where it is expanded to low pressure and temperature. This causes the liquid to evaporate and absorb heat from the surroundings, which provides a cooling effect. The evaporated gas is then sent back to the compressor to restart the cycle. The cooling effect produced by the system can be used for various applications such as air conditioning, food preservation, and medical storage.

The advantages of a solar thermal refrigeration system include low operating costs, no greenhouse gas emissions, and the ability to operate in remote areas without access to electricity [42, 43]. However, the system requires a significant upfront investment and may have limited cooling capacity compared to the traditional electrically powered refrigeration systems.

2.1. Cooling Technologies

Absorption cooling, adsorption cooling, and desiccant cooling are all types of thermally-driven cooling technologies that use the principles of heat transfer and thermodynamics to produce cooling effects. However, they differ in their working principles, performance characteristics, and applications. The choice of cooling technology depends on the specific application requirements and the availability of heat sources. These technologies are part of a cooling method referred to as sorption cooling [43–45].

Sorption cooling uses sorbent materials to absorb and release a refrigerant, allowing for the transfer of heat and the production of cooling. The process works by exposing the sorbent material to a source of heat, causing it to release the refrigerant that it has previously absorbed. This process of absorption generates cooling which can then be used to cool a space or object.

Sorption cooling has several advantages over traditional vapor compression cooling systems, including lower energy consumption, reduced noise levels, and the ability to operate using waste heat or other low-grade heat sources [48–51]. However, sorption cooling systems can be more complex and expensive to build and maintain than traditional cooling systems.

2.1.1. Adsorption Cooling

Adsorption cooling is a type of refrigeration cycle that uses the adsorption process to produce cooling. The basic principle of adsorption cooling is that a working pair of materials, typically a solid adsorbent and a refrigerant, are used to produce cooling through an adsorptiondesorption process.

2.1.1.1. Theoretical Background

During the adsorption process, the refrigerant is adsorbed onto the surface of the solid adsorbent, which leads to a decrease in the partial pressure of the refrigerant in the surrounding

environment [52]. The vapor then flows to the condensing chamber. Heat is rejected in the condenser where the refrigerant vapor is cooled down and turned to liquid. This decrease in pressure results in a lowering of the temperature of the adsorbent and the surrounding environment, which can be used to produce cooling.

Adsorption chillers are equipped with an adsorbent bed to adsorb and desorb the refrigerant, a condenser, an expansion valve, and an evaporator, as shown in Figure 3 [53]. The adsorbent temperature and the refrigerant vapor pressure govern the operation of the adsorption chiller by allowing reversible adsorption between the adsorbent and refrigerant. The adsorbent bed has two different sections; the first adsorber is heated to perform desorption, while the second adsorber is cooled to perform adsorption. Further cooling is achieved by passing the refrigerant through an expansion valve to lower pressure, hence lowering the temperature more. In the evaporation chamber, heat is absorbed, the refrigerant liquid is evaporated, and the vapor returns to the solid adsorbent bed. Here, it is adsorbed, and the cycle is repeated. When the desired cooling temperatures are reached, the heating and cooling are reversed on the adsorbent bed.

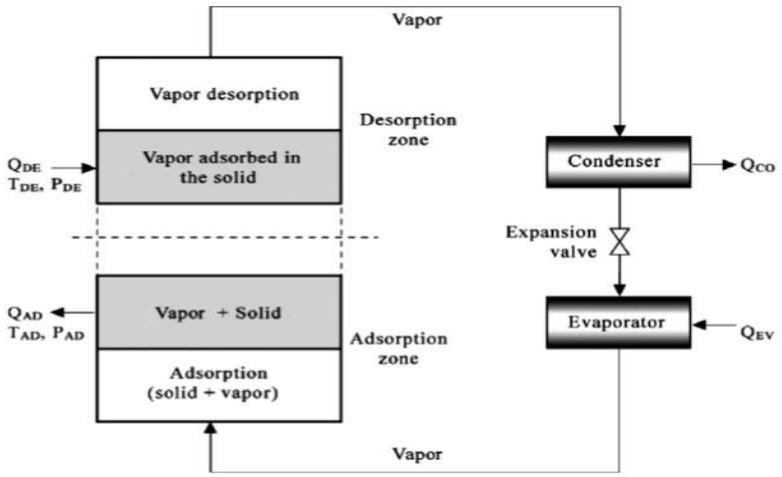

Figure 3. Adsorption cooling cycle [53].

Once the adsorbent is saturated with refrigerant, the desorption process is initiated by heating the adsorbent. This causes the refrigerant to be released from the adsorbent, which can be condensed to liquid form, thereby producing cooling.

The performance of an adsorption cooling system is determined by several factors, including the selection of the adsorbent and refrigerant pair, the operating conditions, and the design of

the system [54]. One of the main advantages of adsorption cooling is that it can operate using low-grade heat sources such as waste heat from industrial processes or solar energy, making it a potentially attractive option for sustainable cooling applications.

2.1.1.2. Mathematical Representation

The adsorption cooling process can be represented mathematically using the following equations that can be used to model and optimize the performance of the system:

The mass balance equation:

$$m_1 Cp_1 + Q = m_2 Cp_2 \quad (1)$$

Where m_1 and m_2 are the masses of the adsorbent material in the adsorber and desorber, respectively; Cp_1 and Cp_2 are the specific heat capacities of the adsorbent in the adsorber and desorber, respectively; Q is the amount of heat added to the system.

The heat balance equation:

$$Q = m_1 H_s - m_2 H_s \quad (2)$$

Where H_s is the enthalpy of adsorption of the adsorbent material.

The equation of state:

$$PV = mRT \quad (3)$$

Where P is the pressure, V is the volume, m is the mass, R is the gas constant, and T is the temperature.

The Langmuir adsorption isotherm equation:

$$\frac{P}{P_s} = \frac{a_x}{1+aX} \quad (4)$$

Where P is the pressure, P_s is the saturation pressure, a is the Langmuir constant, and X is the fraction of the adsorption sites occupied by the adsorbate. Langmuir isotherm originates from an assumption that adsorption on an adsorbent surface occurs on an energetically uniform surface without any adsorbent molecules interaction [55].

2.1.1.3. Relevant Literature

Although adsorption cooling systems use green and renewable technologies, their major drawback is the low COP and low specific cooling power, together with a complex system design [48]. Wang conducted the research on adsorption cooling technology and found that low-temperature coolers driven by solar thermal heat sources using activated carbon-methanol can yield COP of 0.5 [56]. While not high, the COP value was an improvement from previous research. Moreover, Wang et al. designed a modified adsorption cooling system consisting of an adsorption bed, condenser, insulated receiver, and evaporator [28, 29]. The system resulted in a COP of 0.487 which is relatively low but still an improvement from previous lower COP values.

The adsorption cooling system driven by compound parabolic collectors (CPC) was simulated in Tokyo (Japan) with the following design parameters: 2.81×10^6 J/kg adsorption heat, 963.89 W/m^2 solar radiation, maximum and minimum temperatures of 24.2 and 30.8 °C respectively, and 18 collectors of 2.415 m^2 [52]. These resulted in chilled water temperatures ranging from 9.8 to 12°C, and a cooling capacity of 10 kW. The resulting solar COP was 0.3 which was much lower in comparison to other systems.

Teng et al. have found that primary energy savings and COP in an adsorption cooling system can be improved through the use of heat recovery strategies [55]. This is achieved by reusing energy wasted during adsorption as sensible heat and heat of adsorption. This reduces the energy required for the desorption phase and improves COP by 34.4%.

2.1.2. Desiccant Cooling

2.1.2.1. Theoretical Background

Desiccant cooling systems, just like adsorption cooling, use evaporation to create the chilling effect. However, this potential of evaporation in desiccant cooling is increased due to the dehumidification of air by the desiccant material, which removes moisture from the air, resulting in cooling [59]. The basic principle behind desiccant cooling is the ability of certain materials, known as desiccants, to absorb moisture from the air. This process is known as adsorption, which occurs when water molecules bond with the surface of the desiccant material.

Desiccant cooling systems typically consist of two main components: the desiccant wheel and the evaporative cooling system. The desiccant wheel, shown in Figure 4, is a rotating wheel that is coated with a desiccant material [60]. The wheel rotates slowly between the dry air stream and the heated air stream. This effectively splits the wheel into adsorption and desorption sections. Air is passed through the wheel, and the desiccant material absorbs moisture from the air. This results in air dehumidification, which is affected by operating conditions such as regeneration temperature and wheel rotation speed. The now dry air is then passed through an evaporative cooling system, which uses the evaporation of water to cool the air further. There are two types of desiccant cooling systems: solid desiccant systems and liquid desiccant systems. Solid desiccant systems use a solid desiccant material such as silica gel or activated alumina, while liquid desiccant systems use a liquid desiccant such as lithium bromide or calcium chloride.

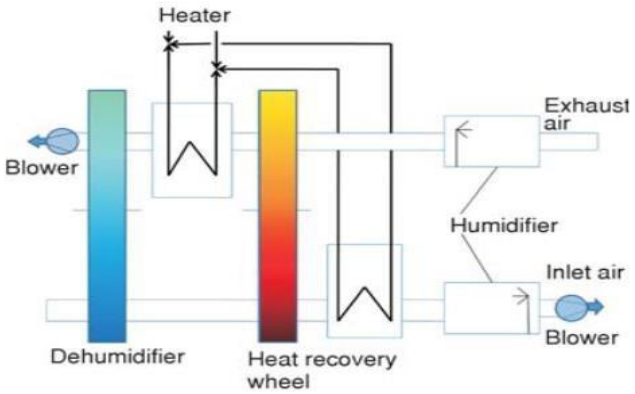

Figure 4. Desiccant cooling system schematic [60].

The theoretical background of desiccant cooling is based on the principles of thermodynamics and psychrometrics [61]. The thermodynamic principle at work is the fact that when a material

absorbs moisture, it releases heat. This is known as the heat of adsorption, and it is the basis for the cooling effect of desiccant cooling systems.

In the context of desiccant cooling, psychrometrics is used to determine the optimal conditions for the desiccant wheel and evaporative cooling system. This involves calculating the dew point temperature, which is the temperature at which water vapor in the air begins to condense. The air can be dehumidified and cooled simultaneously by maintaining the air below the dew point temperature.

2.1.2.2. Mathematical Representation

Mathematical representation of desiccant cooling involves a combination of the following thermodynamic, psychrometric, and heat and mass transfer equations, as well as the use of graphical representations such as the psychrometric chart:

Humidity ratio (W): This is the amount of water vapor in the air per unit of dry air.

$$W = 0.622 \frac{P^v}{P - P_v} \quad (5)$$

Where P_v is the partial pressure of water vapor, P is the atmospheric pressure, and 0.622 is a constant.

Dew point temperature (T_d): This is the temperature at which the air becomes saturated with water vapor and condensation occurs.

$$T_d = \frac{237.7 ln(\frac{P^v}{6.112})}{17.27 - ln(\frac{6.112 P_v}{6.112})} \quad (6)$$

The basic energy and mass balance equations for a desiccant cooling system are used to design and optimize desiccant cooling systems by balancing the energy and mass flows within the system described as follows:

$$Q_1+Q_2+Q_3+Q_4 = WQ_c \quad (7)$$

Where Q_1 is the energy required to regenerate the desiccant, Q_2 is the sensible heat added to the process air during the regeneration process, Q_3 is the latent heat added to the process air during the regeneration process, Q_4 is the sensible heat added to the desiccant during the regeneration process, W is the energy required to run the air handling unit (AHU), and Q_c is the cooling capacity of the system

Mass balance equation:

$$ma_1 + ma_2 = ma_3 + ma_4 \quad (8)$$

Where ma_1 is the mass flow rate of the incoming air, ma_2 is the mass flow rate of regeneration air, ma_3 is the mass flow rate of conditioned air, and ma_4 is the mass flow rate of exhaust air.

Psychrometric chart: This is a graphical representation of the thermodynamic properties of air, including dry-bulb temperature, humidity ratio, and dew point temperature shown in Figure 5. It can be used to determine the state of the air and the cooling potential of a desiccant system.

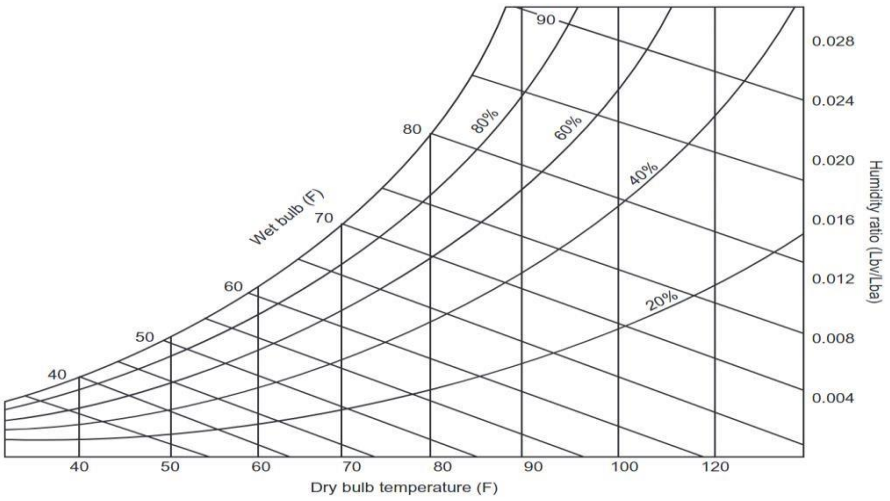

Figure 5. Psychrometric chart [62].

2.1.2.3. Relevant Literature

Enteria et al. designed a solar thermal desiccant cooling system with an incorporated hot water system at Tohoku University in Japan [63]. The system performance showed a decrease in COP from 0.44 to 0.35 as the temperature increased from 60 °C to 75 °C. This shows the complexity of attempting to improve the COP of a desiccant cooling system. Unlike other cooling technologies that respond positively to the increase in temperature, desiccant cooling shows a negative effect. Therefore, a more complex system design would be required to improve performance.

In addition, Mansuriya et al. also simulated a desiccant cooling system using a weak calcium chloride solution to dehumidify the air, which is then blown into the evaporator and cooled down [64]. This study showed that for the same inlet temperature and air velocity, the COP increases with increased desiccant concentration. Moreover, Cui found that the refrigeration capacity of desiccants generally increases slightly with decreasing air humidity [50]. In opposition, Gagliano et al. suggest that desiccant cooling is likely to be more efficient in hot and humid regions since it shows high performance in dealing with latent loads rather than sensible loads [60]. This makes it less favorable for temperate climate regions such as Lesotho. Furthermore, desiccant cooling can reasonably be used for flexible applications with higher cooling temperatures, such as air conditioning rather than food refrigeration, which requires lower temperatures [65].

2.1.3. Absorption Cooling

Absorption cooling technology is attractive as it uses natural refrigerants such as water, ammonia, and methanol while being driven by solar radiation or free waste heat [66]. Compared to solar thermal adsorption and solar thermal desiccant cooling, solar thermal absorption cooling has the highest energy-saving potential [40]. It also shows great potential for refrigeration in places with high solar irradiation. Furthermore, it shows a high possibility of being commercially driven by low-grade solar thermal energy, making it more likely to work efficiently under low irradiation conditions [67].

2.1.3.1. Theoretical Background

Absorption cooling is a type of cooling technology that uses heat as its energy source. It operates based on the principle that when a liquid is vaporized, it absorbs heat from its

surroundings [68]. Absorption cooling systems use this principle to provide cooling by evaporating a refrigerant into a gas in a process known as absorption. The basic components of an absorption cooling system include an absorber, a generator, a condenser, an evaporator, and a pump. The refrigerant used in absorption cooling systems is typically water, ammonia, or lithium bromide. The cooling occurs through a repeated absorption cooling cycle shown in Figure 6.

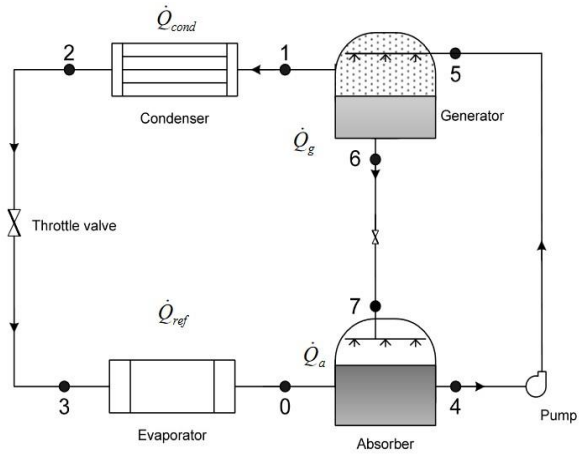

Figure 6. Schematic of absorption chilling cycle without heat exchanger [68].

The process starts in the absorber, where the refrigerant is mixed with an absorbent (usually water or lithium bromide) [51]. The mixture absorbs the vaporized refrigerant from the evaporator and creates a concentrated solution. The concentrated solution then flows to the generator where it is heated. The supplied heat (Q_g) is transferred to the generator and causes the refrigerant to vaporize and separate from the absorbent, creating a high-pressure gas. The high-pressure gas then flows to the condenser where it is cooled and condensed back into a liquid at high pressure. Heat (Q_{cond}) is rejected in the condenser and the temperature of the refrigerant drops. The liquid then flows to the evaporator through a throttling valve where it is expanded, and its kinetic energy is consequently decreased. This results in its temperature dropping further under low pressure. The refrigerant flows into the evaporator chamber where it absorbs any heat energy (Q_{ref}). The resulting evaporation provides a cooling effect. The process is completed when the vaporized refrigerant flows back to the absorber where it is absorbed by the absorbent and the cycle starts again. Before reabsorption, the absorbent is allowed to flow into the absorber chamber through a throttling valve, decreasing its pressure.

The solution is then pumped back into the generator chamber where the cycle repeats, resulting in refrigeration.

Overall, absorption cooling is an efficient and environmentally friendly alternative to traditional cooling technologies as it uses heat as its energy source rather than electricity. It is commonly used in large-scale industrial applications such as refrigeration, air conditioning, and district cooling systems.

2.1.3.2. Working Fluid

Thermodynamic properties of working fluids used in absorption chillers heavily influence the performance of an absorption cycle [69]. The most widely used working fluid pairs are ammonia/water and water/LiBr solutions.

Lithium bromide/water is a well-known absorption refrigeration pair that has been used for over 70 years [70]. In this system, water is the refrigerant and lithium bromide is the absorbent. The process works by absorbing the water vapor into the lithium bromide solution, thus causing a decrease in pressure and temperature. The cooled water is then circulated through the system to provide cooling.

Water/ammonia is another commonly used absorption refrigeration pair. In this system, ammonia is the refrigerant and water is the absorbent. The process works by absorbing the ammonia vapor into the water, resulting in a decrease in pressure and temperature. The cooled ammonia is then circulated through the system to provide cooling.

The main advantage of lithium bromide/water over water/ammonia is that lithium bromide is a non-toxic and non-flammable substance, making it a safer option for use in refrigeration systems [71]. Additionally, the use of water as the refrigerant in lithium bromide/water means that it is a more environmentally friendly option than water/ammonia which uses ammonia as the refrigerant. However, the obvious flaw with this working fluid pair is that water freezes at 0 °C, which implies that refrigeration temperatures at or below 0 °C cannot be achieved [70]. This, together with the crystallization of lithium bromide at moderate concentrations, puts this working fluid pair at a major disadvantage.

Nevertheless, the water/LiBr working fluid pair is still preferable to an ammonia/water solution due to its higher COP [55, 60]. Water/ammonia has a lower coefficient of performance (COP) than lithium bromide/water, which means it is less efficient at producing cooling. This makes it a less popular choice in industrial applications where high levels of cooling are required. In

addition, the efficiency of the ammonia/water solution is greatly reduced by the volatility of water which attaches to the ammonia vapor from the generator in the form of water vapor. This should not happen as ammonia is the refrigerant while water is absorbent in this working fluid pair. Rectifying this predicament requires a complex system design incorporating a distillation column and a rectifier to ensure that water vapor does not reach the condenser.

Overall, both lithium bromide/water and water/ammonia are effective absorption refrigeration pairs, but the choice between the two will depend on the specific requirements of the application and the preferences of the user.

2.1.3.3. Mathematical Representation

Absorption cooling can be mathematically represented using the following equations which can be used to model the behavior of an absorption cooling system and optimize its performance:

The thermodynamic cycle equation:

$$Q_c = Q_h - w \tag{9}$$

Where Q_c is the cooling effect or heat removed from the chilled space, Q_h is the heat input or heat absorbed from the heat source, and W is the work done by the system.

The thermodynamic cycle can be broken down into separate processes that occur during the absorption cycle. These processes are represented by the following equations:

Evaporation:

$$Q_{evap} = \dot{m} h_{vap} \tag{10}$$

Where Q_{evap} is the heat absorbed during evaporation, $\dot{m}$ is the mass flow rate of refrigerant, and h_{vap} is the enthalpy of vaporization.

Absorption:

$$Q_{abs} = \dot{m}h_{in} - \dot{m}h_{out} \quad (11)$$

Where Q_{abs} is the heat released during absorption, h_{in} is the enthalpy of the refrigerant entering the absorber, and h_{out} is the enthalpy of the refrigerant leaving the absorber.

Desorption:

$$Q_{des} = \dot{m}h_{out} - \dot{m}h_{in} \quad (12)$$

Where Q_{des} is the heat absorbed during desorption.

Condensation:

$$Q_{cond} = \dot{m}h_{vap} \quad (13)$$

Where Q_{cond} is the heat released during condensation.

The overall COP of the absorption cooling system is defined as:

$$COP = \frac{Q^{evap}}{Q_{abs}} \quad (14)$$

Where Q_{evap} is the heat absorbed during evaporation, and Q_{abs} is the heat released during absorption.

Where *COP* is a measure of the system's efficiency defined as the ratio of the cooling effect to the work done.

The equation for the performance ratio (PR):

Q_c

$$PR = \frac{}{Q_h} \tag{15}$$

Where *PR* is a measure of the system's effectiveness defined as the ratio of cooling effect to heat input.

The following chemical equation gives a representation of the water and lithium bromide fluid pair in the absorption process:

$$H_2O + LiBr + Q_a \rightarrow LiBr \cdot H_2O + Q_b \tag{16}$$

Where H_2O is water, *LiBr* is lithium bromide, Q_a is the heat input required to drive the absorption process, $LiBr \cdot H_2O$ is the resulting absorbent solution, and Q_b is the heat released during the absorption process.

Absorption systems can also be modeled with mathematical relationships based on mass and energy conservation as shown in (17) and (18).

$$\sum_i \dot{m}_i = 0 \tag{17}$$

$$\sum \dot{m}_{in} h_{in} + \sum \dot{P} = \sum \dot{m}_{out} h_{out} \tag{18}$$

Where $\dot{m}$ is the mass flow rate, h is the specific enthalpy, and $\dot{P}$ is the heat transfer rate measured in watts (W). The following trivial equations from (19) to (24) based on Figure 6 for the condenser, evaporator, throttling, pump, high concentration path, and low concentration path respectively, need to be solved first before solving for any other quantities.

$$\dot{P}_{cond} = \dot{m}_1 (h_2 - h_1) \tag{19}$$

$$\dot{m}_0 = \dot{m}_1 = \dot{m}_2 = \dot{m}_3 = \dot{P}_{ref}/(h_0 - h_3) \quad (20)$$

$$h_3 = h_2 \; and \; h_7 = h_6 \quad (21)$$

$$h_5 = h_4 \quad (22)$$

$$C_5 = C_4 \quad (23)$$

$$C_7 = C_6 \quad (24)$$

Where $\dot{P}_{cond}$ is the heat rejected in the condenser chamber, $\dot{P}_{ref}$ is the heat removed in the evaporation chamber, and C is the refrigerant/absorber solution concentration. The non-trivial equations for mass balance (generator solution, generator absorbent, pump, and throttling) are given from (25) to (30), followed by absorber and generator energy balance equations, respectively.

$$\dot{m}_5 - \dot{m}_6 = \dot{m}_1 \quad (25)$$

$$C_5\dot{m}_5 - C_6\dot{m}_6 = 0 \quad (26)$$

$$\dot{m}_4 - \dot{m}_5 = 0 \quad (27)$$

$$\dot{m}_6 - \dot{m}_7 = 0 \quad (28)$$

$$-\dot{m}_4 h_4 + \dot{m}_7 h_7 - \dot{P}_a = -\dot{m}_0 h_0 \quad (29)$$

$$\dot{m}_5 h_5 - \dot{m}_6 h_6 + \dot{P}_g = \dot{m}_1 h_1 \quad (30)$$

Where $\dot{P}_a$ is the absorber heat rejected and $\dot{P}_g$ is the generator heat from the source.

The preceding system of equations can be solved by assuming *C* and *h* are constant coefficients, and then defining a system matrix [S] and expressing it according to equation (31) as shown in equation (32).

$$[x] = [S]^{-1}[b] \quad (31)$$

$$\begin{matrix} 0 & 1 & -1 & 0 & 0 & 0 \\ 0 & C_5 & -C_6 & & & \\ & & & 0 & 0 & 0 \end{matrix} \begin{matrix} & & \\ & \dot{m}_4 & \dot{m}_1 \\ \dot{m}_5 & & 0 \end{matrix}$$

$$\begin{matrix} 10 & -01 & 01 & -01 & 0000 \\ -h_4 & 0 & 0 & h_7 & -1\ 0 \\ [\,0 & h_5 & -h_6 & 0 & 0 & 1] \end{matrix} \begin{matrix} \dot{m}\dot{m}_{67} \\ \dot{P}_a \\ [\dot{P}_g\,] \end{matrix} = \begin{matrix} -\dot{m}_{000} h_0 \\ \\ [\,\dot{m}_1 h_1\,] \end{matrix} \quad (32)$$

The fluid useful energy gain of the fluid used to transfer heat energy from solar thermal collectors to the generator chamber can be calculated using equation (33), where $\dot{m}$ is the mass flow rate of the fluid, C_p is the specific heat capacity of the fluid, and T_o is the outlet temperature.

$$Q_{solar} = \dot{m} C_P (T_o - T_i) \quad (33)$$

Temperature loss during precooling is not linear as it is rapid when the temperature difference between the produce and the refrigerator is high, and slower once the produce temperature approaches that of the precooling storage [24]. The produce is usually precooled to 7/8th of the

required temperature and the rest of the cooling will occur in cold transport or warehouse cold storage. This is shown by equation (34).

$$T_{final} = T_{initial\ product} - 7(T_{initial\ product} - T_{refrigerant})/8 \quad (34)$$

Where T_{final} is the final temperature required in precooling, $T_{initial}$ product is the initial temperature of the product before refrigeration, and $T_{refrigerant}$ is the temperature of the refrigerant.

2.1.3.4. Relevant Work

A configuration-based modeling and performance analysis of a single-effect solar absorption cooling system in TRNSYS was conducted by Khan et al. [73]. TRNSYS was used for simulation as it provides a reasonable approximation of the expected results without the need for expensive system testing rigs. In their study, the system was modeled to meet a peak cooling demand of 298 kW in subtropical Asia. The performance parameters targeted were solar fraction, collector efficiency, and primary energy savings which all varied with varying collector slope, system configuration, and collector area, respectively. Nevertheless, the system simulation was performed for air conditioning and there was no emphasis on cooling temperatures required and maintaining them at that level.

In addition, Assilzadeh et al. simulated a LiBr solar absorption cooling system in Malaysia for a 3.5 kW cooling requirement using evacuated tube collectors [74]. The collectors were tilted at 20 ° and covered an area of 35 m^2; there was also a hot storage volume of 0.8 m^3. The system parameters of interest in this study were the collector performance and the solar fraction. The maximum solar fraction that the system could achieve was 0.7. The authors of this study claim that system simulation was carried out in TRNSYS. However, there is no apparent methodology followed in the study that gives evidence of TRNSYS usage. Furthermore, the results are very vague and the system parameters used are too limited. The temperatures achieved by the absorption chiller are also not addressed.

A slightly larger cooling load of 4.5 kW was modeled by Agyenim et al. in Cardiff [75]. Vacuum tube collectors were used for thermal energy supply, but unlike in the previous system by Assilzadeh et al., the collector area was 12 m2 which is significantly lower.

Another study was conducted by Molero et al. comparing solar absorption configurations with and without cold storage in Madrid [76]. The simulations were performed for a cooling capacity of 10 kW. The set point temperature for the absorption chiller was 7 °C. The results showed that COP values were constant for set point temperatures higher than 8 °C but decreased significantly for COP values less than 8 °C. Although unlike Assilzadeh et al. the system configuration was given clearly and a less vague methodology was provided, the TRNSYS component configuration was not given. This makes it harder to objectively comment on TRNSYS results.

In contrast to many who have used TRNSYS to model absorption cooling, Somerse et al. model water/lithium bromide adsorption chillers in ASPEN Plus Software. The choice of ASPEN Plus was informed by the nature of their system which uses industrial waste heat as energy supply for the chiller. ASPEN Plus is more suitable for that as it performs steady-state modeling. Conversely, TRNSYS is more suited for solar thermal energy supply as it can model transient system performance [73].

Furthermore, solar energy was used in an absorption refrigeration cycle by Chen and Hihara who reported that there were significant variations in refrigeration capacity throughout the day due to the intermittency of solar radiation [77]. This results in the cooling system experiencing an increase in temperatures. This is a major problem for the refrigeration of food as it requires steady temperatures with minimum fluctuations. Again, it was not clear whether software simulation or mathematical modeling were used in this study. Not only that but neither the design cooling capacity nor target cooling conditions were mentioned in the study. Moreover, the premise of the study was to design a new absorption refrigeration cycle using solar energy, yet, neither the type nor area of solar collectors was specified. These factors impede a comprehensive and essential assessment of the system's performance parameters.

In pursuit of advancing solar thermal cooling technologies for higher COP, a Chinese team modeled a solar thermal absorption cooling system which resulted in an average collector efficiency of 37.6% and a solar fraction of 0.76 in the summer [11]. A system COP of 0.32 was found in summer, which is much lower compared to typical thermally driven COP values of 0.6-1.8 according to Shirazi et al. [78]. The system was designed for a cooling load of 99.8

W/m^2 for an area of 1,850 m^2 with a cooling set point of 25 °C. The total aperture area for collectors was 358 m^2 and the flow rate was 28.8 m^3/h. However, the cooling set point was too high, which is consistent with air conditioning. While the collector efficiency was relatively low, the high solar fraction showed the potential of solar thermal absorption cooling technology [24, 25].

2.2. Thermal Energy Supply

The preceding cooling technologies all require thermal energy for regenerative processes to sustain the continuous cooling cycle. These technologies generally have lower cooling capacities than their conventional cooling counterparts. However, their need for low-grade heat sources (80-100°C), such as industrial waste heat or solar thermal energy makes them worthy contenders for use in sustainable cooling [80].

Solar thermal collectors have been improved over the years to absorb solar radiation and convert it to heat energy at high temperatures. Collectors are pivotal to modeling any solar thermal cooling system; therefore, understanding their working principle is of key importance. For system reliability, an auxiliary heating unit is required in the system since solar radiation is an intermittent source of energy [81]. Additionally, tank storage is required to collect thermal energy when there is abundance and store it to be used when there is low or no availability of radiation.

2.2.1. Theoretical Background

Solar collectors are heat exchangers that are specialized to transform solar radiant energy into heat energy. However, incident radiation on the solar collectors is not all absorbed and converted to useful energy. Several mechanisms result in energy losses. The absorbed solar radiation is the difference between the incident radiation and the optical losses as given by equation (35). This equation emanates from the 1963 isotropic diffuse model, where each term is multiplied by the appropriate transmittance-absorptance product (τα) [82].

$$S = I_b R_b (\tau\alpha)_b + I_d (\tau\alpha)_d \left(\frac{1+\cos\beta}{2}\right) + \rho_g I (\tau\alpha)_g \left(\frac{1-\cos\beta}{2}\right) \quad (35)$$

Where *(1+cosβ)/2* is the view factor from the collector to the sky and *(1-cosβ)/2* is the view factor from the collector to the ground. The subscripts *b*, *d*, and *g* are the beam, direct, and ground radiation, respectively.

The first detailed experimentation on solar thermal collectors based on energy balance measurements on an array of collectors on a solar-heated building was performed in 1942 by Hottel and Woertz [82]. However, their calculations were based on mean plate temperature rather than inlet temperature. Their measured and calculated results were in agreement to within 13% before the effects of dust and shading were accounted for.

Thermal energy losses to the surrounding atmosphere occur through thermal processes such as conduction, convection, and radiation. This thermal energy lost can be represented as a product of the heat loss coefficient (U_L) and the difference between the mean plate temperature (T_{am}) and the ambient temperature (T_a) as shown in equation (36). The heat loss coefficient represents the sum of top, bottom, and edge loss coefficients through a collector.

$$Q_L = U_L(T_{pm} - T_a) \tag{36}$$

In steady-state conditions, the performance of solar collectors is defined by an energy balance equation where incident radiation is distributed into useful energy gain, thermal losses, and optical losses. The useful energy output (*Qu*) of a collector of area (*Ac*) can be described as the difference between the absorbed solar radiation and the thermal losses as shown in equation (37).

$$Q_u = A_c[S - U_L(T_{pm} - T_a)] \tag{37}$$

Since it is very tricky to measure or calculate the mean absorber plate temperature as it is a function of collector design, working fluid, and incident solar radiation, an equation that defines the useful energy gain can be expressed in terms of the inlet fluid temperature and heat removal factor (F_R) as shown in (38). The heat removal factor of a collector is a quantity that relates its

actual useful energy gain to the useful gain if the whole surface of the collector were at the fluid inlet temperature.

$$Q_u = A_c[G_T F_R(\tau\alpha)_{av} - F_R U_L(T_i - T_a)] \quad (38)$$

Where $(\tau\alpha)_{av}$ is the transmittance-absorptance product weighted across the proportions of beam, diffuse, and ground-reflected radiation on the collector surface. However, for simplicity, the subscript *av* is usually dropped, and the transmittance-absorptance product only represents beam radiation.

The efficiency of a solar thermal collector depends on the rate of heat transfer, which is influenced by factors such as the collector's design, the absorber material, and the properties of the fluid being heated [83]. The collector efficiency is used to measure the performance of solar thermal collectors. It may be important to determine the efficiency at a particular instant to measure the collector performance given particular inputs. Therefore, collector instantaneous efficiency for such a collector can be defined and expressed in terms of the heat removal factor, transmittance-absorptance product, heat loss coefficient, incident radiation, and inlet and ambient temperature as shown in (39).

$$\eta_i = F_R(\tau\alpha) - F_R U_L G(T_i - T_a) \quad (39)$$

When determining collector performance, it is assumed that the flow distribution is uniform in all of the risers in multiple collector units. Parts of the collector with low flow rates will have lower values of F_R than those with higher flow rates. This can be a problem in collector performance, especially for forced circulation collectors since natural circulation collectors self-correct. Weitbrecht et al. suggest that the efficiency of solar collectors is strongly related to the flow distribution between adjacent riser pipes in a collector [84]. Non-uniformity of flow rates in risers results in different temperatures at different parts of the pipes and this decreases the effectiveness of the solar collectors. The following equation represents the energy loss coefficient (ζ) at pipe junctions where the flow rate changes from downstream to upstream.

$$\zeta = \frac{\Delta h}{(v^2/(2g))} \quad (40)$$

Where Δh is the pressure difference between downstream and upstream, v is the fluid velocity, and g is the acceleration due to gravity.

In addition to thermal energy from the collector array, heat storage is also crucial for system performance beyond sunset. The total thermal power that is transferred from the heat source to the storage tank is defined by equation (41) [85].

$$\dot{P}_P = \dot{S}_P(T_P - T_I) \quad (41)$$

Where, $\dot{S}_P = \rho_P \dot{V}_P C_P$, given in kW/°C and ρ_P, $\dot{V}_P$, and C_P are the fluid density, production volume flow rate, and fluid-specific heat capacity, respectively.

The storage tank succumbs to some heat losses through the tank walls. This can be expressed in kW as shown in equation (42).

$$\dot{P}_S = A_S U_S (T_S - T_U) \quad (42)$$

Where A_S, U_S, T_S, and T_U are the tank area, the heat transfer coefficient of the tank, the average tank fluid temperature, and the ambient temperature, respectively.

An auxiliary boiler may be required for optimum system performance to provide thermal energy during days without adequate insolation, and to increase the heating fluid temperature to the required value.

2.2.2. Summary of Gaps in the Literature

Lesotho has a 59% electricity capacity deficit and a 50% poverty rate [86]. Considering the high solar potential of the country, these qualify Lesotho for implementing solar thermal cooling technologies to enhance agricultural yield. However, solar thermal cooling technologies have not been researched in Lesotho and the question of their viability in Lesotho's geographical setting remains. In 2018, Nkolisa et al. [17] developed an evaporative cooling system where they evaluated the quality of tomatoes after 20 days in cold storage. However, their focus was on the quality of tomatoes after storage, and no economic analysis was performed to determine if farmers can even afford such cold storage. This is a major concern, especially for smallholder farmers, since the cost of the system will inevitably outweigh its effectiveness.

Many other solar thermal cooling technologies have been modeled and reviewed by several authors such as Ullah et al., Imtiaz et al., and Valles et al. among others [7, 40, 63]. However, none of them performed an economic analysis of the cooling system. Some authors such as Desideri et al., Huang et al., and Narayanan, notably, performed an economic analysis on the designed cooling systems but the focus was placed on air conditioning, which requires significantly higher temperatures than refrigeration [63–65]. Furthermore, none of these systems address the need for cooling systems in the agricultural sector.

In addition, specific cooling power was addressed, notably by Ullah et al., Sapienza et al., and Chang et al. However, they only modelled or reviewed adsorption cooling [7], [92], [93]. It is apparent in the literature that researchers often overlook the specific cooling power of absorption cooling systems. This is because the specific cooling power is commonly considered and emphasized in the context of adsorption cooling systems due to their higher potential for achieving higher cooling capacities per unit mass of the working fluid.

2.3. System Performance Parameters

2.3.1. COP and Exergy Efficiency

The COP of an absorption chiller is defined as the ratio of the cooling effect produced to the heat input required. The cooling effect is the amount of heat removed from the chilled water and the heat input is the amount of heat required to drive the refrigeration cycle. COP is a measure of the efficiency of the chiller in producing cooling.

In an absorption chiller, the refrigeration cycle is driven by a heat source, usually steam or hot water, rather than a mechanical compressor. The refrigerant, typically water, is absorbed by a liquid absorbent such as lithium bromide or ammonia, which is then regenerated by heating. This process requires a significant amount of heat input, usually from a boiler or other heat sources such as industrial waste heat or solar thermal.

The COP of an absorption chiller is typically lower than that of a mechanical vapor compression chiller due to the additional energy required for the absorption and regeneration processes. However, absorption chillers can be more efficient when waste heat or low-grade heat sources are available for use as heat input.

COP can be estimated using equation (43), where t_f and t_0 represent the initial time and final time, T_{chill} and T_{hw} represent cold and hot water temperatures, respectively, and $\dot{m}Cp$ represents heat exchange.

$$COP_{cycle} = \frac{\int_{t0}^{tfcycle} cycle_t(\dot{m}Cp)_{chill}(T_{chill,in} - T_{chill,out})dt}{\int_{t0}^{tfcycle} cyclet(\dot{m}Cp)_{hw}(T_{hw,in} - T_{hw,out})dt} \quad (43)$$

The exergy efficiency of an absorption chiller can be defined as the ratio of the actual cooling output to the maximum possible cooling output that could be obtained if the chiller operated at the Carnot efficiency between the source and sink temperatures. Exergy efficiency is sometimes referred to as the second-law efficiency and it is used to evaluate the effectiveness of the system relative to an idealized or reversible system equivalent [94]. This is a more comprehensive comparison as it gives a more realistic representation of the system's efficiency.

The Carnot efficiency for cooling can be calculated using the following formula:

$$\eta_{Carnot} = \left(\frac{T_a}{T_c}\right) - 1 \quad (44)$$

Where T_c is the temperature of the cooling medium and T_a is the ambient temperature.

The exergy efficiency of an absorption chiller can be calculated using the following formula:

$$\eta_{exergy} = Q_c * \eta_{Carnot} \quad (45)$$

Where Q_c is the cooling output demand and η_{Carnot} is the Carnot efficiency.

The exergy efficiency of an absorption chiller is typically lower than the Carnot efficiency due to irreversibilities such as heat transfer and pressure drops in the system. The actual exergy efficiency depends on various factors such as the type of refrigerant and absorbent used, operating conditions, and design parameters of the chiller.

2.3.2. Primary Energy Savings (PES)

The PES model formulated by Sparber et al. and simplified by Siddique et al., is given in equation (46) [81], [95]. The reference system is an electrically operated absorption chiller. Variables Q_{boiler} and $Q_{cooling,ref}$ are the heat energy provided by the auxiliary boiler, and the cooling energy supplied by the conventional refrigerating system, respectively. The variables η_{boiler}, ε_{heat}, and ε_{el} are the efficiency of the boiler, the conversion efficiency of fossil fuel supplying the boiler, and the heat-providing electricity efficiency, respectively. COP_{ref} is the rated efficiency of the absorption chiller.

$$PES = 1 - \frac{\int Q_{boiler}}{\int Q_{cooling,ref}} \frac{\varepsilon_{heat}}{\left(\frac{COP_{ref}}{\varepsilon_{el}}\right)} \eta_{boiler} \quad (46)$$

The term inside the brackets in equation (46) is the ratio of the primary energy consumption of a solar thermal system contributed by an auxiliary boiler to the primary energy consumption of a reference absorption system using traditional energy sources to meet the same load. The values of ε_{heat} and ε_{el} are taken as 0.9 and 0.4, respectively.

2.3.3. Solar Fraction

The periodical solar fraction is modeled using equation (47). Where Q_{boiler} represents the thermal energy received from the auxiliary boiler and Q_{sun} represents the thermal energy received from the sun. The variables are integrated to account for a month or season, hence the integral sign. The solar fraction ranges from zero to one depending on the amount of insolation available.

$$SF = \frac{\int Q_{solar}}{\int Q_{solar} + \int Q_{boiler}} \quad (47)$$

Where, SF is the solar fraction, T_{final} is the final temperature required in precooling, $T_{initial}$ product is the initial temperature of the product before refrigeration, and $T_{refrigerant}$ is the temperature of the refrigerant.

2.4. Target Produce

One of the most-grown vegetables in Lesotho is cabbage which was found to cover 22.1% of all the land which grows fruits and vegetables in the 2009/2010 agricultural census [96]. According to Chinese research, cabbage can ideally be stored at a temperature of 4 °C and humidity of 90-95% [97]. Other common fruit and vegetable products in the country are tomatoes, green pepper, and green beans which are ideally stored in temperatures of 0-12 °C and humidity of 90-95% [98]. Therefore, this study focuses only on cabbage, tomato, green pepper, and green beans.

2.5. Economic Impact Metrics

2.5.1. Levelized Cost of Energy (LCOE)

The LCOE of a solar thermal cooling system is the levelized cost of energy associated with the generation of solar energy for cooling using solar thermal technology. The LCOE of a solar

thermal cooling system is typically calculated by considering the total lifetime costs of the system, including the costs of design, installation, operation, and maintenance, as well as the amount of energy cooling that it can produce over its lifespan [99].

The costs associated with a solar thermal cooling system include the cost of the collectors, the storage tanks, the pumps, and the control system. The system's efficiency, the solar resources available at the installation site, and the operating and maintenance costs of the system also affect the LCOE of the solar thermal cooling system.

Calculating the LCOE of a solar thermal cooling system requires a detailed analysis of the system design and operation, and it can vary depending on the specific installation site and the local energy market conditions. However, solar thermal cooling systems generally have higher upfront costs. Still, they can offer lower operating costs and zero fuel costs over their lifespan, leading to a potentially competitive LCOE when compared to conventional cooling systems.

LCOE can be determined using equation (48). This is a ratio of the total lifetime cost and total lifetime energy output [100]. Lower LCOE is desired because it implies that energy is produced for less, while higher LCOE implies high production costs over an assumed financial life and duty cycle.

$$LCOE = \frac{Lifetime\ \ Energy\ \ Production}{} = \frac{\sum_{t=1}^{n} I_t + (1M + r) + {}_tF_t}{\sum_{t=1}^{n} \frac{E_t}{(1+r)^t}} \quad Lifetime\ Cost \tag{48}$$

Where I_t is the investment expenditure, M_t is the operational and maintenance expenditures, F_t is the fuel expenditure, E_t is the cooling output, r is the discount rate, and n is the expected lifetime of the system. These variables, except for n, are accounted for over a year.

2.5.2. Net Present Value (NPV)

The NPV of a solar thermal cooling system is a financial metric that represents the present value of the system's future cash flows, discounted to account for the time value of money [101]. To calculate the NPV of a solar thermal cooling system, the costs, and benefits of the

system are estimated over its entire lifetime. The cash flows can be broken down into two categories: the initial investment (outflow) and the savings on energy costs (inflow) over the lifespan of the system.

The initial investment includes the costs associated with designing, installing, and commissioning the solar thermal cooling system. The savings on energy costs are generated by the reduced electricity consumption from the grid due to the use of solar thermal cooling instead of conventional cooling systems.

The NPV calculation involves discounting the estimated future cash flows to their present values using an appropriate discount rate, which represents the opportunity cost of investing in the solar thermal cooling system. If the NPV is positive, the investment is considered profitable, whereas if the NPV is negative, the investment is considered unprofitable.

The NPV of a solar thermal cooling system depends on several factors including capital costs, operating costs, energy savings, and the discount rate used. It is important to conduct a thorough financial analysis of the solar thermal cooling system to determine its NPV and assess the financial viability of the investment. Calculating the net present value of a solar thermal cooling system requires information such as the initial investment, operating costs, salvage value, and discount rate, among other factors.

The equation for calculating the NPV of a solar thermal cooling system is [102]:

$$NPV = -C + \sum \frac{(R-O)}{(1+d)_t} \tag{49}$$

Where C is the initial capital cost of the solar thermal cooling system, R is the annual energy cost savings generated by the system, O is the annual operating cost of the system, and d is the discount rate which represents the opportunity cost of investing in the system, and t is the year of the cash flow.

The first term, $-C$, represents the initial outflow of cash from the investment. The second term, $\Sigma((R - O) / (1 + d)^t)$, represents the discounted inflows of cash from the savings on energy costs generated by the system over its lifespan. The summation is performed over the entire lifespan of the system.

2.5.3. Savings to Investement Ratio (SIR)

The SIR of a solar thermal absorption cooling system depends on several factors including the initial cost of the system, the energy savings achieved, and the operating costs.

Generally, solar thermal absorption cooling systems have a higher upfront cost compared to traditional cooling systems, but they can provide significant energy savings over their lifetime. The SIR depends on the specific system design and location, as well as the cost of electricity in the area. To calculate the SIR of a solar thermal absorption cooling system, the initial investment cost and the expected energy savings over the lifetime of the system would need to be determined. Then, the total energy savings would be divided by the initial investment cost to determine the SIR.

Overall, solar thermal absorption cooling systems can be a cost-effective option for cooling buildings, particularly in areas with high electricity costs and abundant sunshine. However, it is important to carefully evaluate the costs and benefits of any investment in renewable energy technology to determine if it is the right choice for the specific situation.

The equation for calculating the SIR of a solar thermal cooling system is [103]:

$$SIR = \frac{NPV}{C} \tag{50}$$

Where C is the initial capital cost of the solar thermal cooling system.

2.5.4. Discounted Pay-Back Period (DPP)

The DPP is a financial metric used to estimate the length of time it takes for a project to recover its initial investment, taking into account the time value of money.

To calculate the DPP for a solar thermal absorption cooling system, the initial investment required to install the system, as well as the expected annual savings in operating costs compared to using conventional cooling systems would need to be determined. Once these values are available, a financial calculator or spreadsheet can be used to calculate the present value of the expected cash flows over the life of the project, discounted at an appropriate rate

to reflect the time value of money [104]. The DPP is the point at which the cumulative discounted cash flows equal the initial investment.

The equation for calculating the DPP of a solar thermal cooling system is:

$$DPP = t + \frac{-\sum \frac{F_t+1}{(1+t)}}{\sum \frac{F_t+1}{(1+t)^t}} C \quad (51)$$

Where *t* is the year when the cumulative discounted cash inflows from energy cost savings first exceed the initial investment cost of the system, *C* is the initial capital cost of the solar thermal cooling system, F_t is the net cash flow in year t (equal to the energy cost savings minus the operating cost of the system), and *d* is the discount rate which represents the opportunity cost of investing in the system

The denominator of the equation represents the discounted cash inflows from energy cost savings generated by the system after the payback period, while the numerator represents the remaining discounted cash outflows required to recover the initial investment cost.

3. Methodology

The presented methodology addresses the objectives brought forward in the introduction, which are to design and simulate a solar thermal cooling system to address the challenge of spoiling fresh agricultural produce in Lesotho. It also describes procedures involved in performing an economic analysis of the model, mathematical modeling, and software simulation.

The cooling system focuses on the pre-cooling of fresh vegetables as according to Yu and Jaenicke, fruit and fresh vegetables are a major source of food waste [105]. Pre-cooling temperatures of 0-12°C for perishable vegetables are targeted, as recommended by FAO [106].

Having reviewed the literature, it is evident that the cooling method with the highest potential is absorption cooling. This is mainly due to its relatively high COP, low-temperature performance, and relatively simple system design [44]. Additionally, it is also apparent from the reviewed literature that computer modeling helps simulate real-life cooling performance with high accuracy at lower costs as opposed to expensive system testing rigs. Therefore, TRNSYS was selected to perform the system simulation in this study. Furthermore, the literature shows TRNSYS' superiority and robustness in simulating solar thermal cooling systems, and model validation studies have shown that the mean error between TRNSYS software simulation results and measured results on a real system is under 10% owing to its extensive library of components [107, 108].

3.1. The Backdrop of the Simulation Area

Lesotho farmers are the main target market for the cooling system. Hence, Maseru was selected for simulation because it represents the largest portion of Lesotho, in terms of both population and land size. Furthermore, the focus is only on January, which is the peak month for vegetable harvest in Lesotho.

The design aims for a higher COP above 0.6, and this represents a relatively acceptable system performance that usually varies from 0.6 to 0.85 for absorption chillers. [32–37]. However, lower COP values are also likely to be found depending on factors such as system components and available energy resources.

The research is carried out using typical meteorological year (TMY) data for January, with Maseru as a case study. The solar irradiation data for Maseru can be seen in Figure 1 in the

literature review section. The simulation accounts for only the weather conditions in January as the peak vegetable harvest month and the warmest month in Lesotho [111]. This selection ensures that the system is tested under the most demanding operating conditions, providing insights into its performance during the period of highest cooling demand. By focusing on the month with the highest cooling load, the economic analysis can accurately assess the system's financial feasibility and profitability during the critical period.

Furthermore, an annual economic analysis enables comparisons with conventional cooling systems or alternative energy sources over the entire year. This evaluation provides a comprehensive understanding of the system's competitiveness and advantages compared to other available options. It also helps identify potential cost savings and revenue generation opportunities that may arise from integrating the solar thermal cooling system into the existing energy infrastructure.

TRNSYS assumes that one already knows their desired cooling capacity. Therefore, cooling load calculations are performed in the Danfoss Cool-Selector software which allows for the selection of other crucial inputs such as the dimensions of the cold room, the type of agricultural produce that will be stored in refrigeration, and the frequency of produce turnover.

When modeling a solar thermal absorption cooling system using TRNSYS, some common assumptions made in this study include:

a. Simplified heat transfer models: The model may use simplified heat transfer models for solar collectors, heat exchangers, and other components to simplify the calculations.
b. Maseru and Bloemfontein have similar climatic conditions.
c. Parasitic electrical components and other necessary power requirements are supported by solar PV.

3.2. System Design Area

The described solar thermal cooling system is modeled in TRNSYS. The load determination is carried out in the Danfoss Cool-Selector under Bloemfontein's climatic conditions shown in Figure 7. TRNSYS simulation is based on weather data from a typical meteorological year external data file provided by Meteonorm. Meteonorm is a program that provides a combination of reliable meteorological data sources and high-quality calculation models.

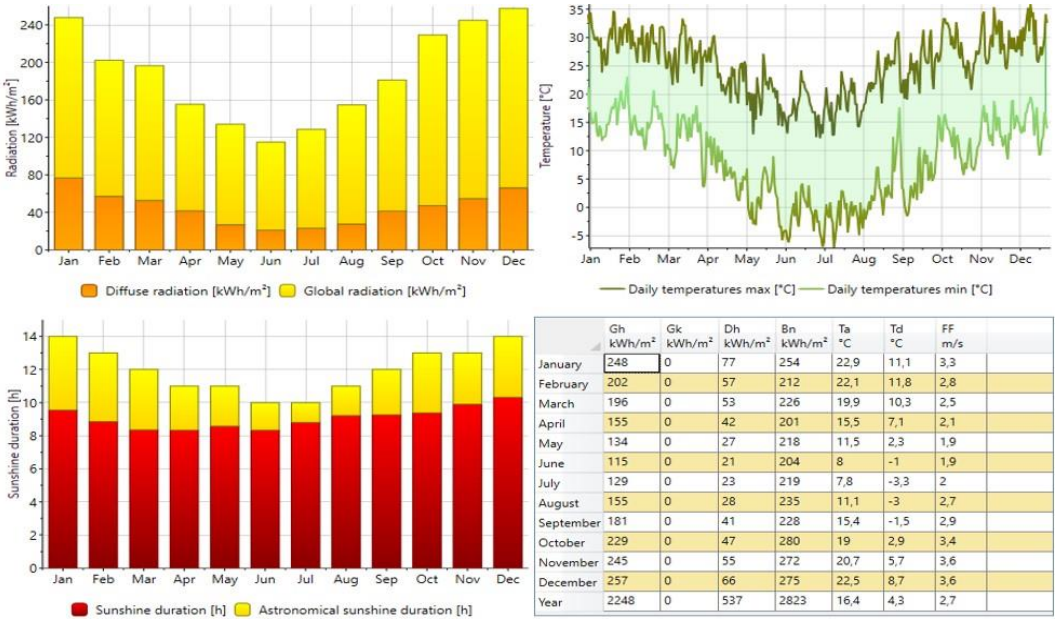

	Gh kWh/m²	Gk kWh/m²	Dh kWh/m²	Bn kWh/m²	Ta °C	Td °C	FF m/s
January	248	0	77	254	22,9	11,1	3,3
February	202	0	57	212	22,1	11,8	2,8
March	196	0	53	226	19,9	10,3	2,5
April	155	0	42	201	15,5	7,1	2,1
May	134	0	27	218	11,5	2,3	1,9
June	115	0	21	204	8	-1	1,9
July	129	0	23	219	7,8	-3,3	2
August	155	0	28	235	11,1	-3	2,7
September	181	0	41	228	15,4	-1,5	2,9
October	229	0	47	280	19	2,9	3,4
November	245	0	55	272	20,7	5,7	3,6
December	257	0	66	275	22,5	8,7	3,6
Year	2248	0	537	2823	16,4	4,3	2,7

Figure 7. Climate data for Bloemfontein produced by Meteonorm.

The closest available climate data used was for Bloemfontein (South Africa) and it can be assumed that it is closely similar to that of Maseru due to geographical proximity. This can be seen with similar radiation patterns between Bloemfontein and Lesotho in the summer and winter months as shown in Figure 8 [112].

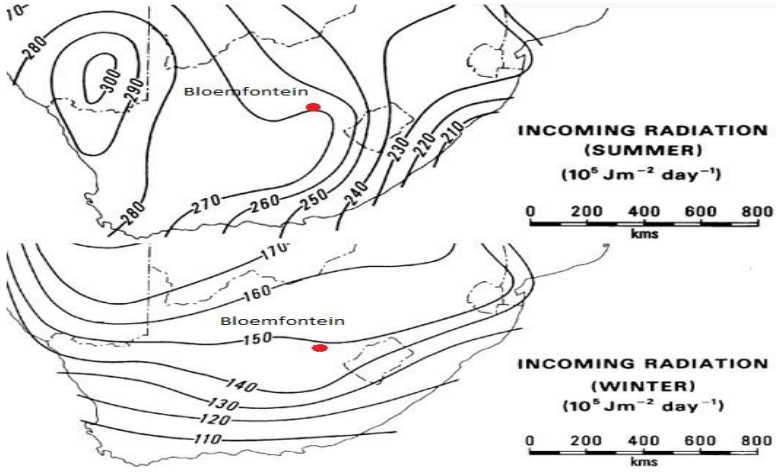

Figure 8. Irradiation patterns for Maseru relative to Bloemfontein in summer and winter *[112]*.

The similarities in climatic conditions between Lesotho and Bloemfontein are further corroborated in Figure 9, which shows daily maximum temperatures, nighttime temperatures, and sunshine hours per day

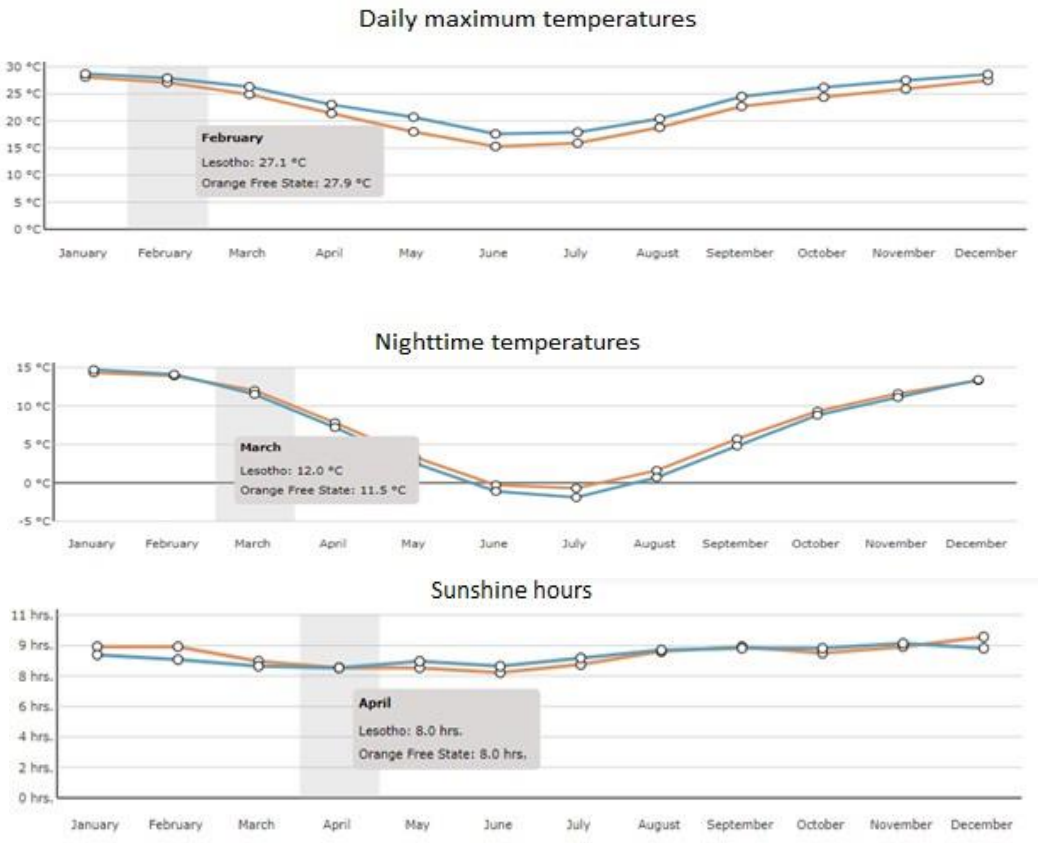

Figure 9. Lesotho and Bloemfontein daily maximum temperatures, night-time lows, and sunshine hour per day, respectively.

3.3. Description of the System Configuration

The system is composed of a solar thermal collector array, a hot water storage tank, a single effect absorption chiller, flow mechanisms (pumps and throttle valves), a refrigeration load, and an auxiliary boiler. The system configuration is shown in Figure 10.

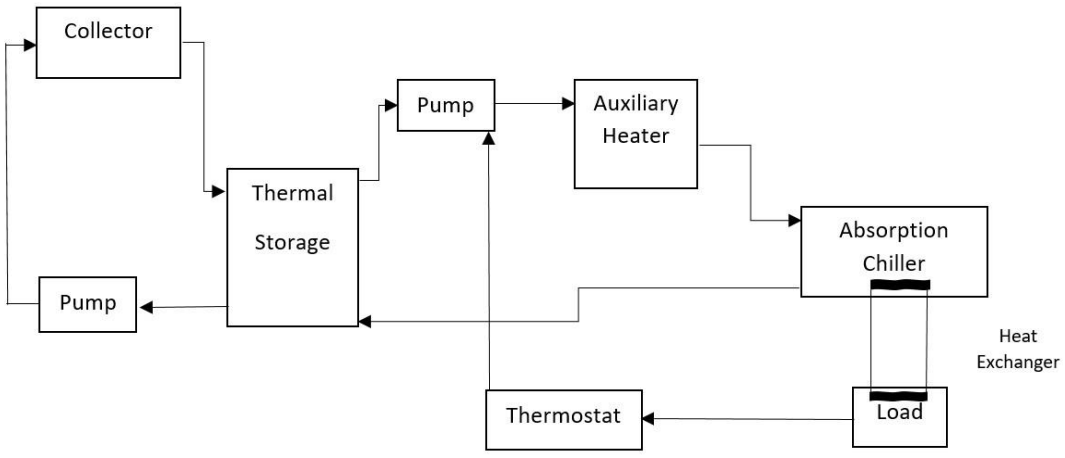

Figure 10. Solar thermal cooling system configuration.

Water is pumped from the bottom of the stratified thermal storage tank through the collector array when the temperature of the collector array is greater than that of the storage tank outlet. Otherwise, the circulation through the collector array stops until its temperature is greater than the storage outlet temperature. Another pump is used to pump the hot water from the storage tank outlet towards the top of the storage tank through the auxiliary heater. The auxiliary heater is only turned on when the inlet water temperature is less than the set point temperature. It raises the water temperature to the set point temperature of 98.89°C required as the heat supply for the absorption heater. The hot water coming into the absorption heater starts the absorption process and exits to return to the thermal storage tank. The absorption chiller's evaporator chamber is attached to the cooling load where heat is continuously absorbed from the load as cooling occurs. This keeps the temperature of the load at 6°C, which according to Sadi et al., is an adequate cooling temperature for cooling agricultural products [113].

3.4. Cooling Load Determination

The cooling load is modeled in Danfoss Cool-Selector as shown in Figure 11. The 75 mm thick polyurethane cold room with a volume of 64 m^3 and mass capacity of 17,280 kg was estimated to be adequate for the cold storage of agricultural produce from smallholder farmers. The daily turnover of the cold produce was estimated to be 20% which amounts to 3,556 kg per day. The inlet temperature of 20°C for fresh produce was based on the ambient temperature. The cold room was assumed to be built outside or in a room without any conditioning. As a result, belowfloor temperature and humidity were estimated to be 20°C and 56%, respectively [114]. The desired temperature and humidity for the cold room were set to 6.1°C and 95%, respectively.

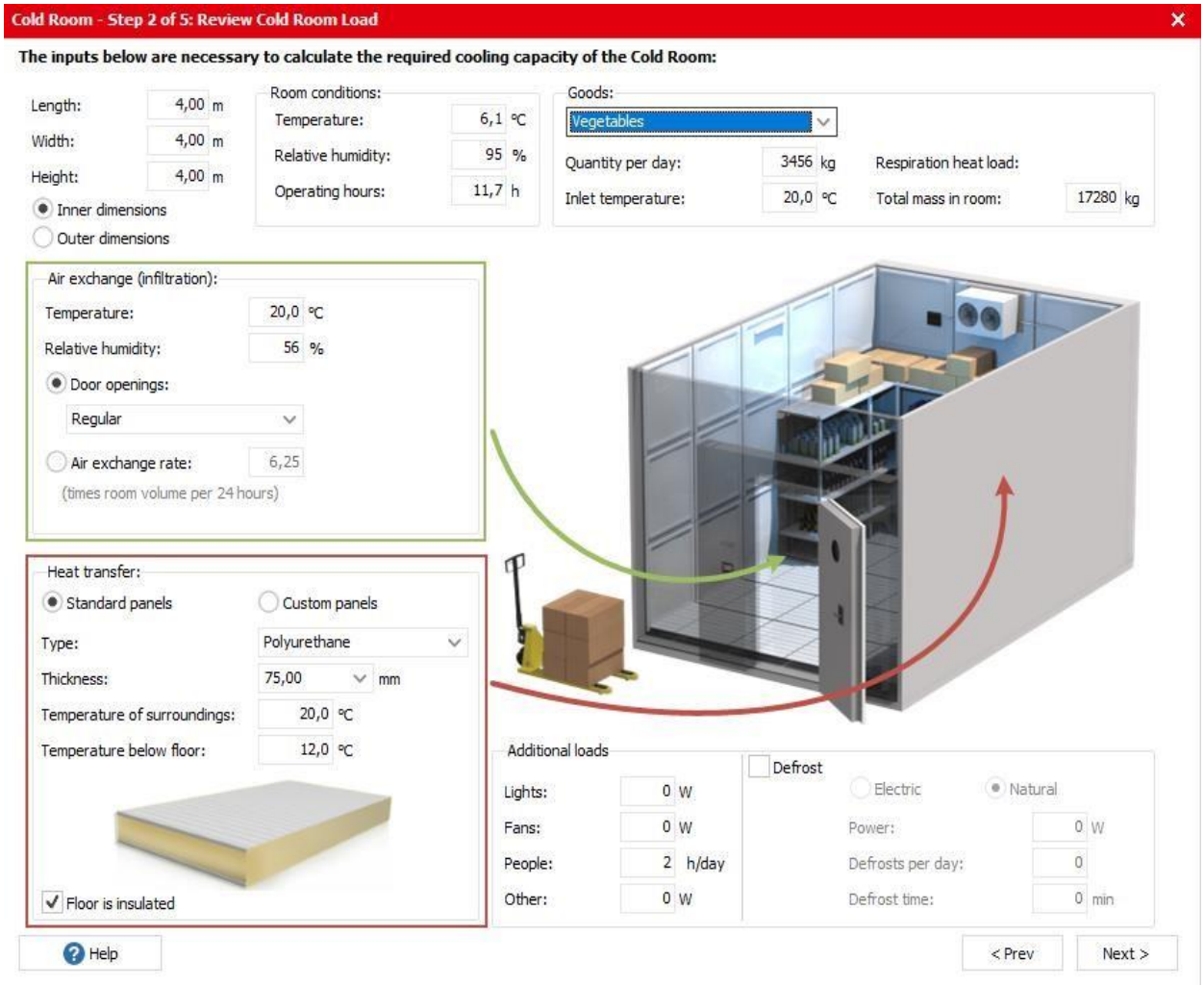

Figure 11. Cooling load inputs in Danfoss.

Some of the crucial parameters of the design of the cold room are summarized in Table 1.

Table 1. Load determination (Danfoss)

Calculated cold room load:	
Total cooling requirement	7.318 kW
Cold room details	
Temperature	6.1 °C
Relative humidity	95 %
Operating hours	11.7 h
Dimensions	
Length	4 m
Width	4 m
Height	4 m

Stored goods	
Type	Vegetables
Quantity per day	3,556 kg
Inlet temperature	20 °C

The cooling system load profile relative to ambient temperature for January is shown in Figure 12. The cooling load is expressed in TRNSYS as sensible load, which is the energy removed from the load through temperature reduction to facilitate chilling. It can be observed that during the day, when it gets warmer, the cooling load increases to a maximum of 26,270 kJ/h (7.3 kW), excluding the two extremes on the first and last day of January. This value is the system's peak cooling load. During the night, when it gets cooler and not much cooling is required, the cooling load decreases to 3,043 kJ/h (0.85kW), which is only 11.6% of the full load.

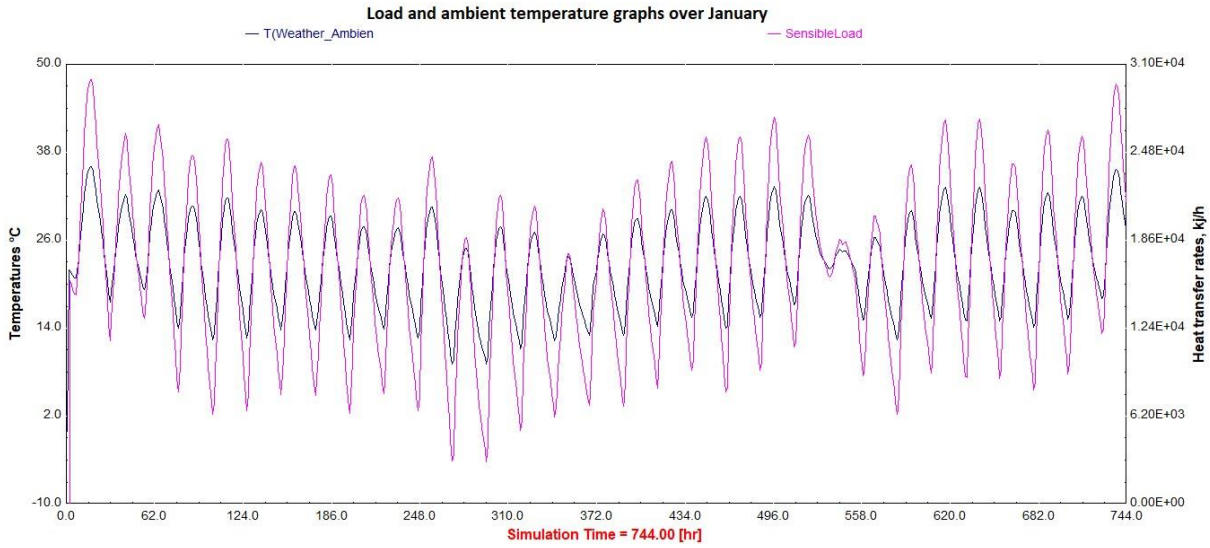

Figure 12. Cooling system load profile variation with ambient temperature for January.

3.5. TRNSYS Modeling

The described solar thermal absorption cooling system is simulated for Maseru in TRNSYS using Bloemfontein TMY weather data. The boiling-freezing effects of the fluid used in the system are not considered to allow simplicity. However, this is unlikely since the hot water temperature required for the system is 98.89°C, and the target refrigeration temperature is 6.1°C. A full TRNSYS pictorial schematic is shown in Figure 13.

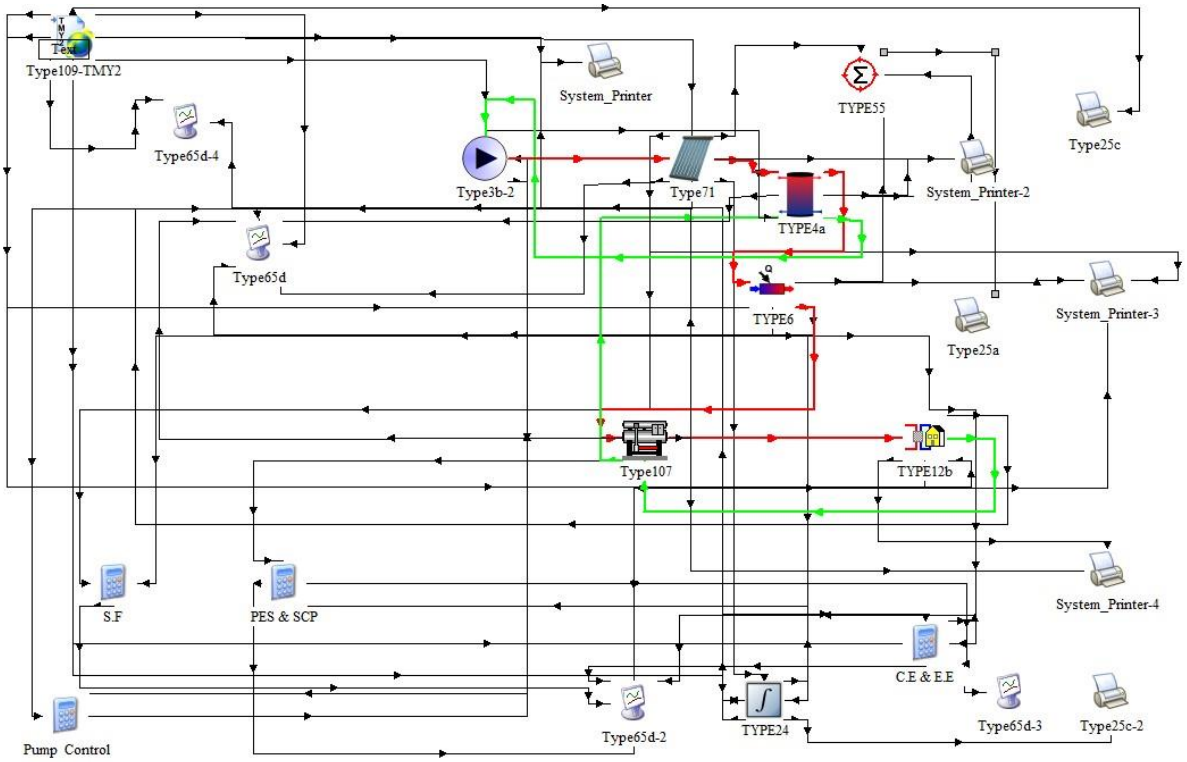

Figure 13. TRNSYS solar thermal cooling system schematic

3.5.1. Absorption Chiller

The absorption chiller used for the TRNSYS system simulation is a Type 107 hot water singleeffect absorption chiller. Type 107 has a catalog data external file which predicts the chiller performance based on the inlet temperature of hot water ($T_{hw,in}$), chilled water set point ($T_{chw,set}$), and entering cooling water temperature ($T_{cw,in}$). The absorption chiller is modeled in three scenarios, all with a rated capacity of 73.318 kW and a rated COP of 0.5, 0.65, and 0.8. In this study, the chiller is operated at 10% capacity for a cooling load of 7.318 kW. To determine the energy delivered to the chiller by the hot water (Q_{hw}), the following equation is used:

$$Q_{hw} = COP_{Rated} \frac{C_{Rated}}{} f\, DesignEnergyInput \quad (52)$$

Where $f_{designEnergyInput}$ is the actual current operating load, C_{Rated} is the chiller-rated capacity, and COP_{Rated} is the chiller-rated COP. The value of $f_{designEnergyInput}$ can be found in the absorption chiller external data file by first calculating the value of the fraction of the design load ($f_{designLoad}$) at which the chiller is required to operate. Then, the corresponding value of $f_{designEnergyInput}$ is determined concerning the inlet temperature of hot water, chilled water setpoint, and entering cooling water temperature as shown in Figure 14.

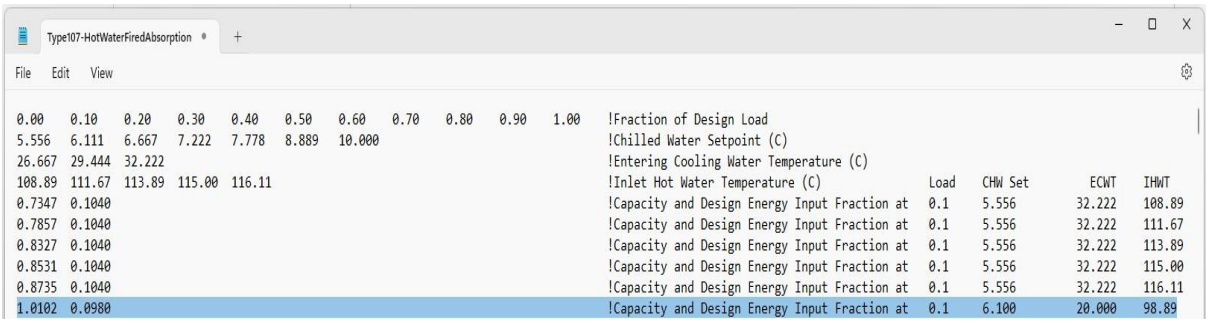

Figure 14. Type 107 absorption chiller external data file.

The following equation determines the value of $f_{designLoad}$.

$$f_{DesignLoad} = Capacity_{\frac{Q_{Remove}}{Rated}} \quad (53)$$

Where Q_{Remove} is the energy that must be removed from the chilled water stream to bring it from its entering temperature to the set point temperature which is equivalent to the cooling load.

The mass flow rate for chilled water entering the chiller can be determined using the following equation for the amount of energy to be removed from the chilled water stream.

$$Q_{Remove} = \dot{m}_{chw} Cp_{chw} (T_{chw,in} - T_{chw,set}) \quad (54)$$

Where $\dot{m}_{chw}$ is the mass flow rate of the chilled water, Cp_{chw} is the chilled water specific heat capacity, $T_{chw,in}$ is the inlet chilled water temperature, and $T_{chw,set}$ is the chilled water set point temperature.

Additionally, the following equation defines the chiller hot water stream outlet temperature. The equation is useful for finding the mass flow rates of the hot water stream and cold water stream when the hot water inlet temperature ($T_{hw,in}$), hot water outlet temperature ($T_{hw,out}$), hot water specific heating capacity (Cp_{hw}), and hot water energy (Q_{hw}) are already known.

$$T_{hw,out} = T_{hw,in} - \frac{\overline{Q^{hw}}}{\dot{m}_{hw} Cp_{hw}} \quad (55)$$

The energy balance equation for the chiller shown in the following equation is used to determine the energy rejection to the cooling water stream (Q_{cw}).

$$Q_{cw} = Q_{chw} + Q_{hw} + Q_{Aux} \quad (56)$$

Where Q_{Aux} is the energy attributed by various parasitic energy consumers in the system such as solution pumps, fluid stream pumps, and controls. In this study, the parasitic energy consumption is assumed to be zero for simplicity.

The mass flow rate of the cold water stream can then be determined using the following equation:

$$T_{cw,out} = T_{cw,in} + \frac{\overline{Q^{cw}}}{\dot{m}_{cw} Cp_{cw}} \quad (57)$$

Where $T_{cw,in}$ is the cold water inlet temperature, $T_{cw,out}$ is the cold water outlet temperature, Cp_{cw} is the cold water specific heating capacity, and Q_{cw} is the energy rejected to the cold water stream.

Type 107 absorption chiller is only applicable for catalog data sourced from different manufacturers' specifications. Therefore, input parameters for this absorption chiller have to be within operating limits. Table 2 shows the calculated input parameters for the Type 107 absorption chiller given different COP values.

Table 2. Input parameters for TYPE 107 absorption chiller.

Parameter	Description
Q_{remove}	7.318 kW
Q_{hw}	14.34 kW
Q_{cw}	21.66 kW
m_{chw}	628.75 kg/h
m_{hw}	1,232.08 kg/h
m_{cw}	1,846.68 kg/h
$f_{designLoad}$	0.1004
$f_{designEnergyInput}$	0.098

3.5.2. Solar Thermal Collectors

Type 71 evacuated tube solar thermal collectors are used in TRNSYS simulation to provide thermal energy for the cooling system. Since efficiency is essential in collector selection, the following thermal efficiency equation is used in TRNSYS to govern the performance of the collector.

$$\eta = a_0 - a_1 \frac{(T_i - T_a)}{G_T} - a_2 \frac{(T_i - T_a)^2}{G_T} \quad (58)$$

Where a_0, a_1, and a_2 are the thermal efficiency parameters representing the y-intercept, slope, and curvature of the collector efficiency versus temperature difference/radiation ratio curve, respectively. According to Quality Assurance in Solar Heating and Cooling Technology (QAiST), their values are given in Type 71 as 0.75, 0.832, and 0.0208, respectively [115]. The variables T_i and T_a are the collector inlet temperature and the ambient temperature, respectively.

3.5.3. Thermal Storage Tank

Type 4a stratified storage tank with uniform losses is used for this TRNSYS simulation. This is a hot water storage tank that stores the necessary thermal energy needed to reach the required 100 °C for regeneration in the chiller. Stratification of the storage tank improves system performance [116]. Figure 15 shows the energy balance diagram for the storage tank.

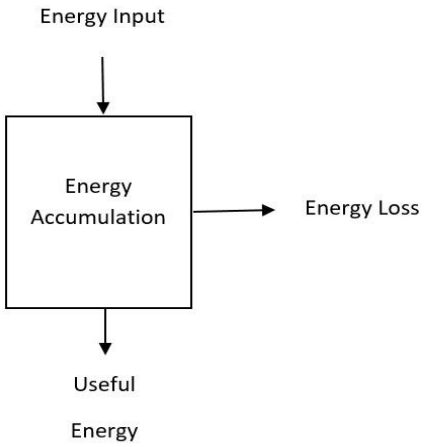

Figure 15. Energy balance diagram for the hot water tank.

3.5.4. Auxiliary Heater

Type 6 auxiliary heater is incorporated into the system in TRNSYS simulation to provide auxiliary thermal energy for low irradiation periods to keep the cooling temperatures within the required limits. The auxiliary heater only turns on when the inlet fluid temperature is less than the set point temperature of 98.89°C. Whenever the auxiliary heater is switched on, the following equation is used to model the heat energy (Q_{boiler}) required to increase the temperature of the heating fluid from the storage tank outlet temperature to the desired chiller inlet temperature.

Whenever the auxiliary heater is switched on, the following equation is used to model the heat energy (Q_{boiler}) required to increase the temperature of the heating fluid from the storage tank outlet temperature to the desired chiller inlet temperature.

$$Q_{boiler} = mC_P(T_o - T_i) \quad (59)$$

3.5.5. Other TRNSYS Components

The weather data is processed using the Type 109 Weather data reader and processor component of TRNSYS. The component is used to read and process weather data which includes solar radiation properties and ambient temperature for a given area as shown in Figure 16 and Figure 17, respectively. It does this by calculating the incident radiation on the surface of the solar collectors which are tilted at 30° towards the north, with a surface azimuth angle of 0° and consideration of 0.2 ground reflectance [117].

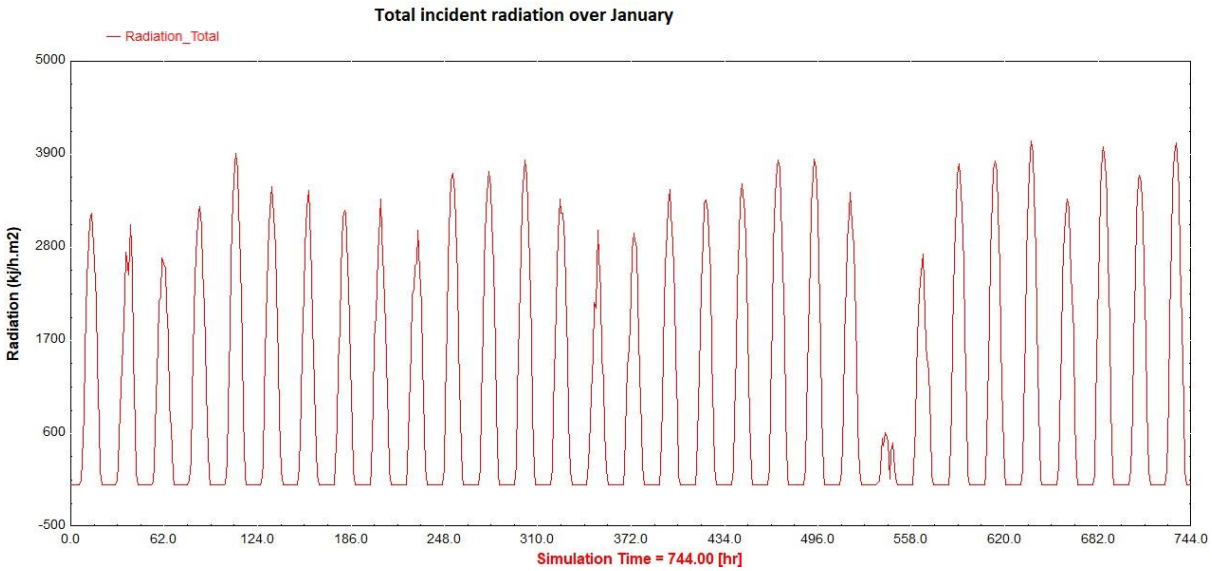

Figure 16. Maseru radiation profile for January.

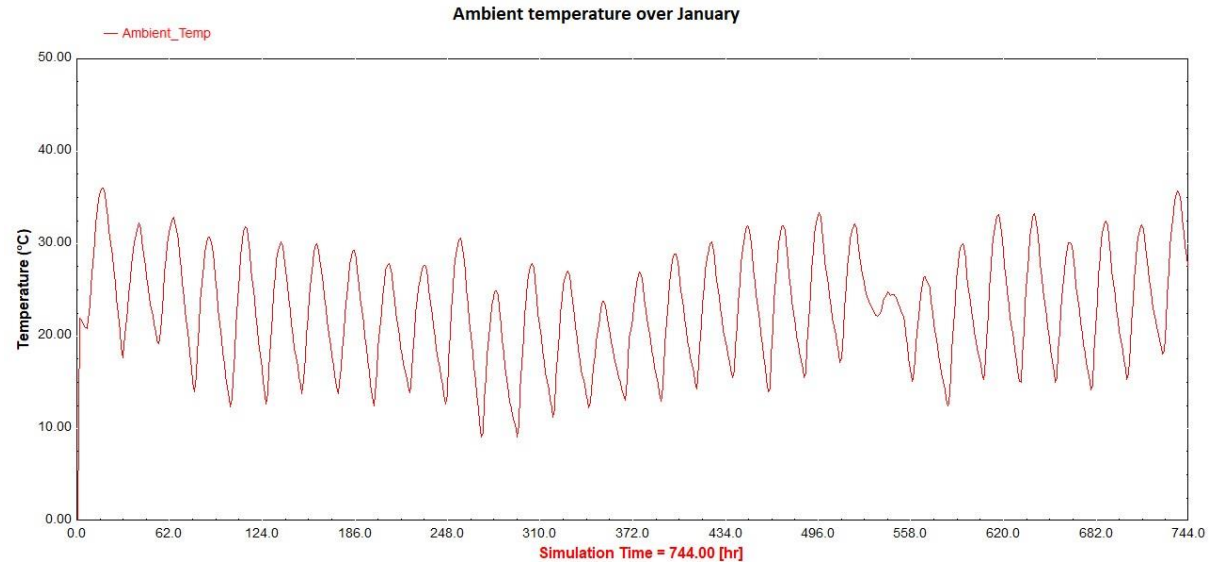

Figure 17. Maseru ambient temperature for January.

Supporting components used in the system include a Type 12b load, Type 3b-2 fluid pump, Type 65d online graphical plotter, Type 25 system printer, Type 24 quantity integrator, and Type 55 periodic integrator.

TRNSYS has several components that have different design parameters and the choice depends on factors such as the load for which it is designed and atmospheric conditions. Some of the most crucial TRNSYS system parameters are shown in Table 3.

Table 3. Typical operating parameters used in TRNSYS modeling.

Parameter	Description
Hot water single-effect absorption chiller	
Cooling load	7.318 kW
Chilled water set point	6.1°C
Chilled water flow rate	628.75 kg/h
Hot water inlet temperature	98.89 °C
Hot water flow rate	1232.08 kg/h
Cooling water inlet temperature	20°C
Cooling water flow rate	1846.68 kg/h
Solar collectors	
Fluid inlet flow rate	1232.08 kg/h
Slope	30°
Storage tank	
Tank type	Stratified
Hot side and cold side flow rate	1232.08 kg/h
Fluid density	1000 kg/m^3
Auxiliary heater	
Set point temperature	98.89°C

3.6. System Performance Metrics

3.6.1. Collector Efficiency

In this TRNSYS simulation, collector efficiency is measured monthly and seasonally. This collector efficiency (η) is expressed as the ratio of the useful gain (Q_{useful}) over a specific period to the incident radiation (G_T) and collector area (A_c) over the same defined period as shown in the following equation:

$$\eta = \frac{\int Q useful}{Ac \int GT} \tag{60}$$

3.6.2. Solar Fraction

The solar fraction was computed in TRNSYS to determine the contribution of solar energy to the system. The monthly or seasonal solar fraction is modeled in equation (47). The variables are integrated to account for a month or season. The solar fraction ranges from zero to one depending on the amount of insolation available.

3.6.3. Primary Energy Savings

Primary energy savings are computed in TRNSYS using equation (46). The values of ε_{heat}, ε_{elec}, and COP_{ref} are estimated as 0.7, 0.4, and 1.0 [71].

3.6.4. Exergy Efficiency

The exergy efficiency of an absorption chiller can be defined as the ratio of the actual cooling output to the maximum possible cooling output that could be obtained if the chiller operated at the Carnot efficiency between the source and sink temperatures. Exergy efficiency is sometimes referred to as the second-law efficiency and is used to evaluate the effectiveness of the system relative to an idealized or reversible system equivalent [94]. This is a more comprehensive comparison, giving a more realistic representation of the system's efficiency. Exergy efficiency considers not only the energy quantity, but also its quality from a thermodynamic perspective. Equations (44) and (45) give the exergy efficiency of an absorption chiller.

3.6.5. COP

The most important performance indicator for the absorption chiller is the coefficient of performance. COP is defined in TRNSYS as shown in the following equation.

$$COP = \frac{Q^{chw}}{Q_{aux}+Q_{hw}} \quad (61)$$

Where Q_{chw} is the energy removed from the chilled water stream, Q_{aux} is the energy drawn by parasitic energy consumers, and Q_{hw} is the energy removed from the hot water stream.

3.7. Economic Analysis

In this methodology section, the approach used to assess the economic viability of a solar thermal absorption cooling system is outlined. The economic analysis of the system was crucial in determining its feasibility and financial attractiveness for potential investment. MATLAB, a powerful computational tool widely used in engineering and financial analysis, was employed to evaluate the economic indicators, namely LCOE, NPV, SIR, and DPP.

The financial analysis encompasses several key steps, starting with data from the TRNSYS simulation to obtain the necessary input parameters. Data is gathered on solar radiation levels, system performance characteristics, capital costs, operational and maintenance expenses, and discount rates. With this data, mathematical models that estimate electricity generation, operating costs, and financial indicators are developed [118]. The implementation of the economic feasibility study involves leveraging MATLAB's capabilities to perform the required calculations.

Table 4 shows all the parameters used in determining the economic metrics. To determine the LCOE, NPV, SIR, and DPP for solar thermal absorption systems, the following method is proposed. According to Nikbakhti et al., the lifetime for these systems is assumed to be 20 years as is the case with other solar thermal absorption systems [119]. The discount rate applied was 7.75% according to the Central Bank of Lesotho [120]. The capital cost per kW was estimated at $6,000, and since the system capacity is 7.318 kW, the total initial investment

required was $42,828. Additionally, the annual operational and maintenance cost was estimated to be 4% of the capital cost each.

The annual returns for the solar thermal absorption systems are determined based on the energy savings achieved for each COP simulation. To calculate these annual returns, the energy savings resulting from each COP simulation were quantified. Once the energy savings were estimated, they were multiplied by the current Lesotho general-purpose electricity tariff rate of M1.9624 ($0.053) to determine the corresponding annual financial returns [121].

Table 4. Relevant parameters used in economic analysis.

Parameter	Value
System Lifetime	20 years
Discount rate	7.75%
Initial investment	$ 42,828
Annual operation cost	4%
Annual maintenance cost	4%

Firstly, the Total Capital Cost (TCC) is calculated by multiplying the system capacity with the capital cost per kW. This provides an estimate of the total investment required for the system. Subsequently, the annual operation and maintenance cost is determined by taking 4% of the TCC. These costs represent the ongoing expenses associated with the system. The Annual Energy Production (AEP) is calculated based on the annual average solar irradiance in Lesotho, which is 2000 kWh/m^2, multiplied by the system capacity [118]. This estimation indicates the annual energy output that the solar thermal absorption system is expected to generate.

To calculate the LCOE, the present value of the O&M costs and the present value of the energy production are needed. The present value of the O&M costs is obtained by discounting the annual O&M cost over the system lifetime using the chosen discount rate. Similarly, the present value of the energy production is obtained by discounting the AEP over the system's lifetime. The LCOE is then determined using equation (48). This metric provides an average cost of electricity generated by the solar thermal absorption system over its lifetime. Code snippet 1 (Appendix) shows the MATLAB code used to determine the LCOE for all COP values.

The NPV is calculated using equation (49). The present value of the annual returns is obtained by discounting the projected annual returns based on different COP simulations (0.5, 0.65, and 0.8) over the system lifetime. The MATLAB code used to evaluate the net present value of the investment for all COP values is shown in Code snippet 2 (Appendix).

The SIR is obtained by using equation (50). This ratio indicates the financial attractiveness of the project, with a higher SIR value indicating a more favourable investment. The MATLAB code snippet shown in Code snippet 3 (Appendix) incorporates the necessary calculations to determine the SIR for all the COP values.

Lastly, the DPP is determined by identifying the year in which the cumulative cash flow becomes positive using equation (51). The cumulative cash flow is calculated by summing the previous year's cumulative cash flow, and annual returns, and subtracting the TCC and O&M costs. The DPP represents the time it takes for the project to recover its initial investment. The MATLAB code snippet shown in Code snippet 4 (Appendix) determines the DPP for different COP values.

Validation and verification procedures are undertaken to confirm the accuracy of the MATLAB code and the results obtained. This is done through comparison with other established research studies.

4. Results and Discussion

The presented results and discussion addresses the aim of this research which is to design a solar thermal cooling system to mitigate the challenge of spoiling fresh agricultural produce and to perform an economic analysis of the model.

4.1. TRNSYS Analysis

The simulation was carried out for the entire month of January because it is the peak month for vegetable harvest in Lesotho and refrigeration is imperative. Three different scenarios were simulated with three different absorption chillers having COP rated at 0.5, 0.65, and 0.8. The cooling load was determined by Danfoss Cool-Selector software as 7.318 kW. This cooling load, which was used to design the absorption chiller, constitutes of 17,280 kg worth of fresh vegetables in a 64 m^3 storage room filled to 60% capacity and operating at 6.1°C.

4.1.1. Solar Fraction

The solar fraction which represents the fractional contribution of the solar thermal collectors to the system's energy demand serves as one of the primary metrics for evaluating the cooling system's effectiveness. In cases where the solar fraction is not equal to 1, the additional energy needed is provided by the auxiliary boiler. The results obtained from the TRNSYS simulation of a solar thermal absorption cooling system using different collector areas shown in Figure 18 provide valuable insights into the system's performance and its ability to meet cooling demand using solar energy for three different chiller-rated COP values (0.5, 0.65, and 0.8).

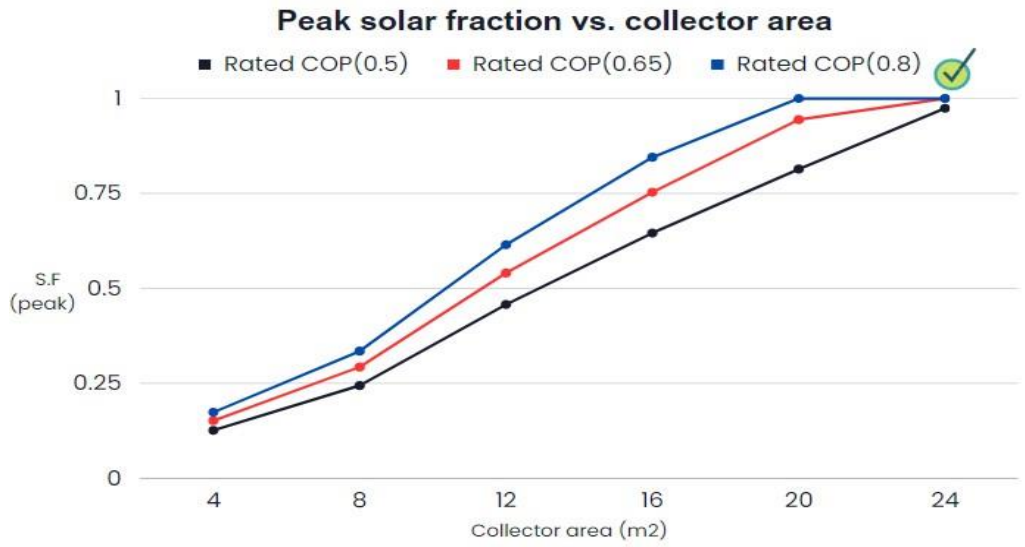

Figure 18. Variation of solar fraction with collector area for the system.

Starting with the simulation with a rated chiller COP of 0.5, when the collector area was 4 m^2, the solar fraction was found to be 0.1258, indicating that the solar thermal system can meet approximately 12.58% of the cooling load. As the collector area increased to 4 m^2, the solar fraction also increased to 0.2441, representing a significant improvement in system performance.

With further increases in the collector area to 8 m^2, 12 m^2, 16 m^2, and 20 m^2, the solar fraction increased to 0.4576, 0.6457, 0.8140, and 0.9743, respectively. The solar fraction values over January for the chiller rated COP of 0.5 and collector area of 12 m^2 are shown in Figure 19.

These results demonstrate a substantial enhancement in the system's efficiency and its ability to meet a larger portion of the cooling load through solar energy utilization. This aligns with the findings in a parametric study of a solar absorption cooling system by Sokhansefat et al.

[122]. Similarly, Sokhansefat et al. used evacuated tube collectors, a single-effect absorption chiller, an auxiliary heater, and a storage tank. Their simulation was carried out in TRNSYS with a collector area of 49.86 m^2 and a hot water storage tank capacity of 1 m^3.

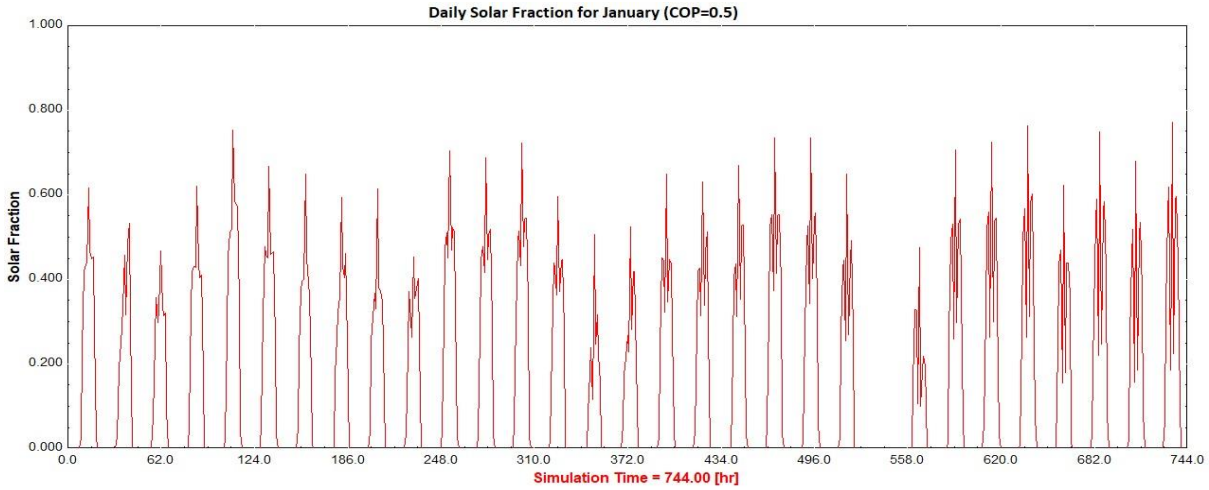

Figure 19. Hourly solar fraction for January when rated COP is 0.5.

When the rated chiller COP was 0.5, the solar fraction values were relatively low compared to the other two cases. This suggests that the chiller's efficiency was relatively low, requiring a larger portion of the cooling load to be met by non-solar sources. When the rated chiller COP was increased to 0.65 and 0.8, higher solar fraction values for all collector areas were observed. This indicates that the more efficient chiller allows the solar thermal system to supply a greater proportion of the cooling load. The solar fraction graphs over January for the rated COP of 0.65 and 0.8 are shown in Figure 20 and Figure 21.

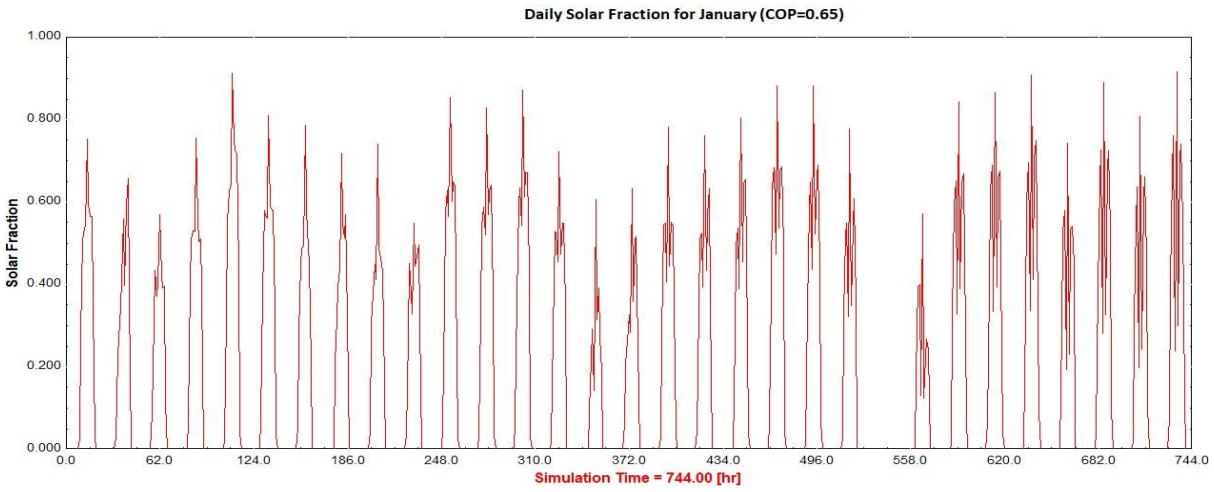

Figure 20. Hourly solar fraction for January when rated COP is 0.65.

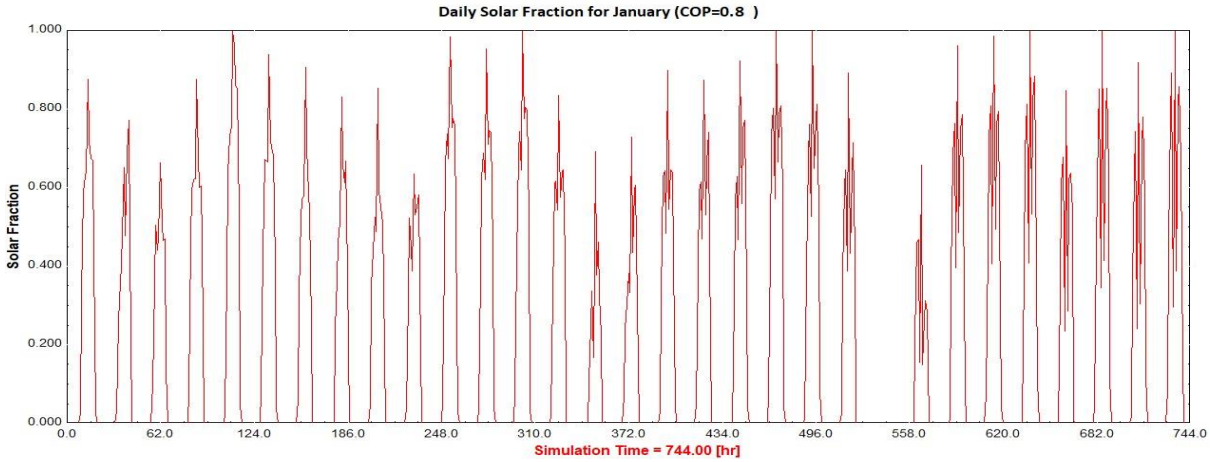

Figure 21. Hourly solar fraction for January when rated COP is 0.8.

Furthermore, with a collector area of 12 m^2, the solar fraction for the system with a chillerrated COP of 0.8 reached its maximum value of 1. This implies that the solar thermal system can fully meet the cooling load using solar energy alone with collector temperatures up to 111 °C as shown in Figure 22, achieving the optimal system sizing for the given conditions. Achieving a solar fraction of 1 is highly desirable as it signifies complete reliance on renewable energy sources for cooling needs. This is consistent with findings by Uçkan and Yousif confirming that the evacuated tube collectors can reach the solar fraction of 1 in the absorption cooling [123]. In their study, Uçkan and Yousif used TRNSYS to determine the effect of various solar collector types on a solar absorption cooling system. While the trends observed are similar, it is worth noting that the system sizes are not comparable as Uçkan and Yousif achieve a solar fraction of 1 with an evacuated tube collector area of 140 m^2 to support a cooling capacity of 35 kW.

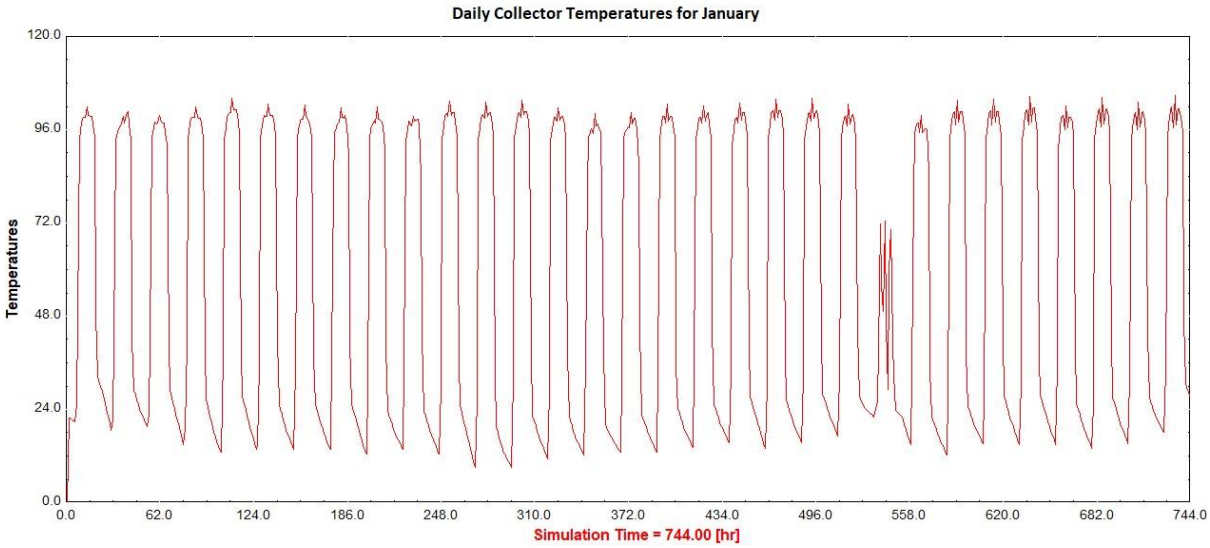

Figure 22. Hourly collector outlet temperatures for January.

The solar fraction values obtained for the different collector areas (4 m² to 24 m²) exhibit an increasing trend, which is generally expected, as can be seen in findings by Eicker and Pietruschka in their design of solar-powered absorption cooling systems [124]. However, the augmentation rate appears to diminish as the collector area gets larger. This trend is due to factors such as diminishing returns, system losses, and limitations in system efficiency. Nevertheless, across all three cases (rated COP of 0.5, 0.65, and 0.8), we observe a general trend where increasing the collector area leads to higher solar fractions.

The simulation results highlight the positive correlation between the collector area and solar fraction in a solar thermal absorption cooling system. A larger collector area allows for the capture of more solar energy, leading to a higher solar fraction and increased utilization of solar thermal energy for the cooling system. However, it is important to consider other factors such as cost, available space, and practical constraints when determining the optimal collector area for a specific solar thermal cooling system.

4.1.2. Collector Efficiency

The system's performance in terms of collector efficiency response to different collector slopes is shown in Figure 23.

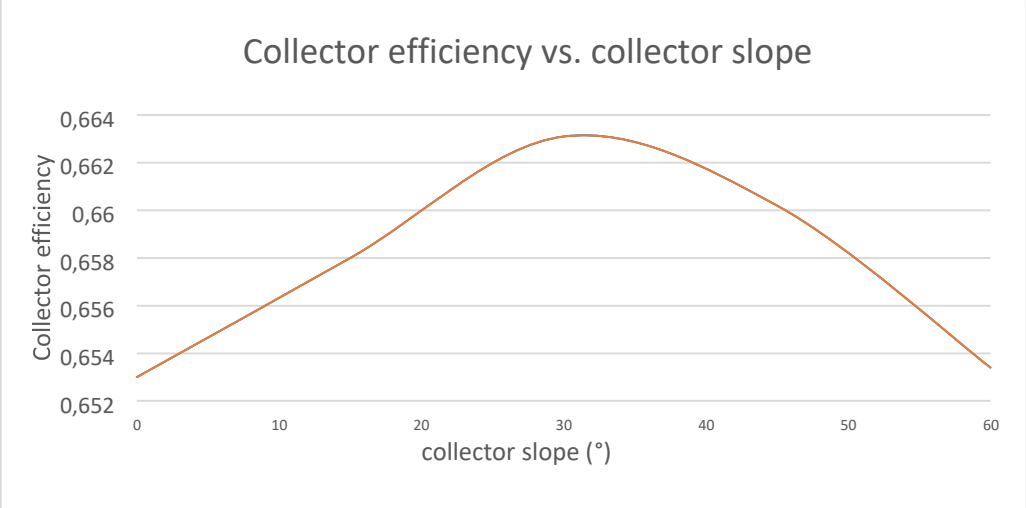

Figure 23. Collector efficiency graphs for collector slopes.

The results presented reveal the collector efficiency at various slope angles (0°, 15°, 30°, 45°, and 60°) for a solar thermal system in Maseru, Lesotho. The corresponding efficiency values for each slope angle are 0.653, 0.658, 0.6631, 0.6592, and 0.6534, respectively. These results demonstrate a slight variation in collector efficiency as the slope angle changes. The observed trend aligns with the expected behaviour of solar collectors and the influence of slope angle on efficiency. It is important to note that the collector efficiency peaked at a slope angle of 30°, which is closer to the optimal angle associated with the latitude of Maseru (29.3°).

At a slope angle of 0° (horizontal), the collector efficiency was 0.653. This relatively low efficiency can be attributed to reduced solar radiation absorption when the collector is parallel to the ground. In this position, the collector surface receives sunlight at a less optimal angle, resulting in lower energy capture and efficiency. The decrease in efficiency is due to the reduced exposure of the collector surface to the sun's rays, leading to decreased energy absorption. As the slope angle increased to 15° and 30°, the collector efficiency gradually improved, peaking at 30°. This trend can be explained by the increased alignment of the collector surface with the incident radiation as the slope angle approaches the optimal angle. At these angles, more solar radiation is incident on the collector surface, resulting in enhanced energy capture and higher efficiency. The improved alignment allows for better utilization of the available solar resource throughout the day, thus maximizing energy absorption.

However, at a slope angle of 45° and 60°, the collector efficiency decreased slightly to 0.6592 and 0.6534, respectively. This decline can be attributed to the steeper slope angle which

misaligns with the optimum incident radiation angle, hence limiting the energy absorption and decreasing the overall efficiency.

Additionally, it is noteworthy that the observed trends in collector efficiency remain consistent for different COP values (0.5, 0.65, and 0.8). This indicates that the COP does not directly influence collector efficiency as it primarily relates to the performance of the entire system, including components beyond the collector itself. Considering Maseru's latitude of 29.3°, it is expected that the collector efficiency would be higher at a slope angle closer to this latitude. The alignment of the collector surface with the sun's rays at a slope angle of 30° which is in proximity to the latitude, leads to higher energy capture and increased efficiency. This alignment ensures a more optimal angle of incidence for solar radiation throughout the year.

4.1.3. Primary Energy Savings (PES)

The fractional PES variation with the increasing collector area for the rated COP of 0.5, 0.65, and 0.8 are shown in Figure 24. The PES metric was simulated relative to a conventional electrical compression system.

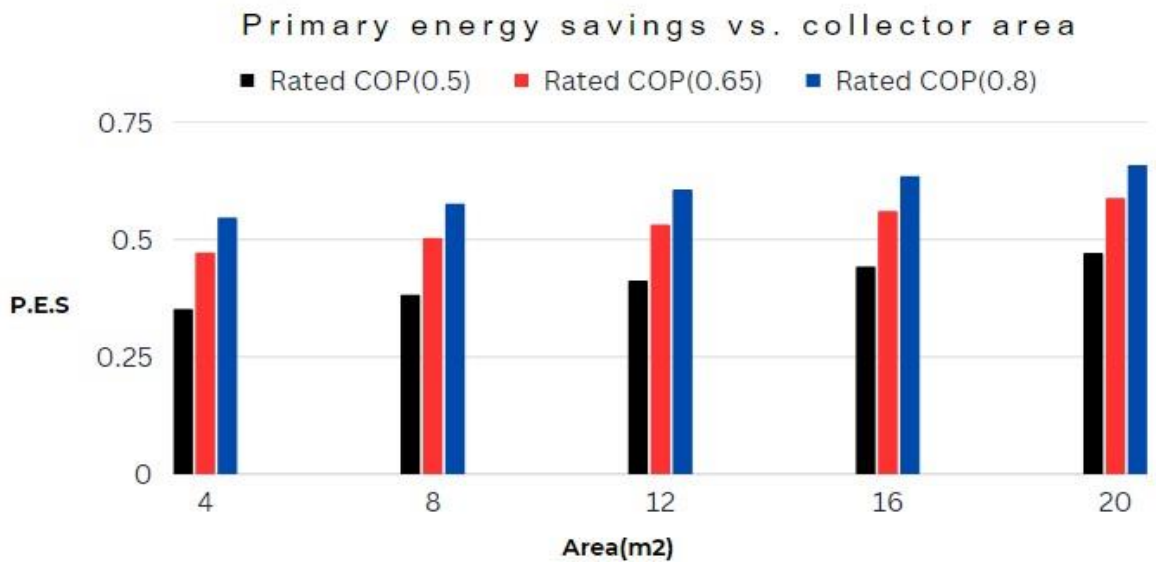

Figure 24. Monthly primary energy savings for different collector areas for January.

For a rated COP of 0.5, when powering the system with a collector area of 4 m^2, the simulation results yielded fractional primary energy savings of 0.3517. This indicates that the solar thermal

absorption cooling system could achieve approximately 35.17% monthly primary energy savings compared to a conventional electrical compression system. Having increased the collector area to 8 m^2, the fractional primary energy savings increased to 0.3826, indicating a higher level of monthly energy savings. This suggests that a larger collector area substantially reduces the primary energy consumption compared to the conventional electrical compression system.

With further increases in the collector area to 12 m^2, 16 m^2, and 20 m^2, the fractional primary energy savings continued to improve with values of 0.4123, 0.4418, and 0.4707, respectively. These results highlight the enhanced performance of the solar thermal absorption cooling system as the collector area increases, emphasizing the importance of larger collector areas for achieving significant primary energy savings.

For the COP of 0.65 and 0.8, the same trend was observed with the increasing collector area, and better yet, with much larger energy savings for higher COP. Energy savings observed for the rated chiller COP of 0.65 and 0.8 were 34% and 54% higher than those observed for the rated chiller COP of 0.5. This increase in energy savings due to an increase in COP can further be corroborated in Figure 25, Figure 26, and Figure 27. It can be observed that less auxiliary energy is required for a higher-rated COP. When the COP was 0.5, 0.65, and 0.8, the required auxiliary energy was 36,425 kJ/h, 29,092 kJ/h, and, 24,595 kJ/h respectively.

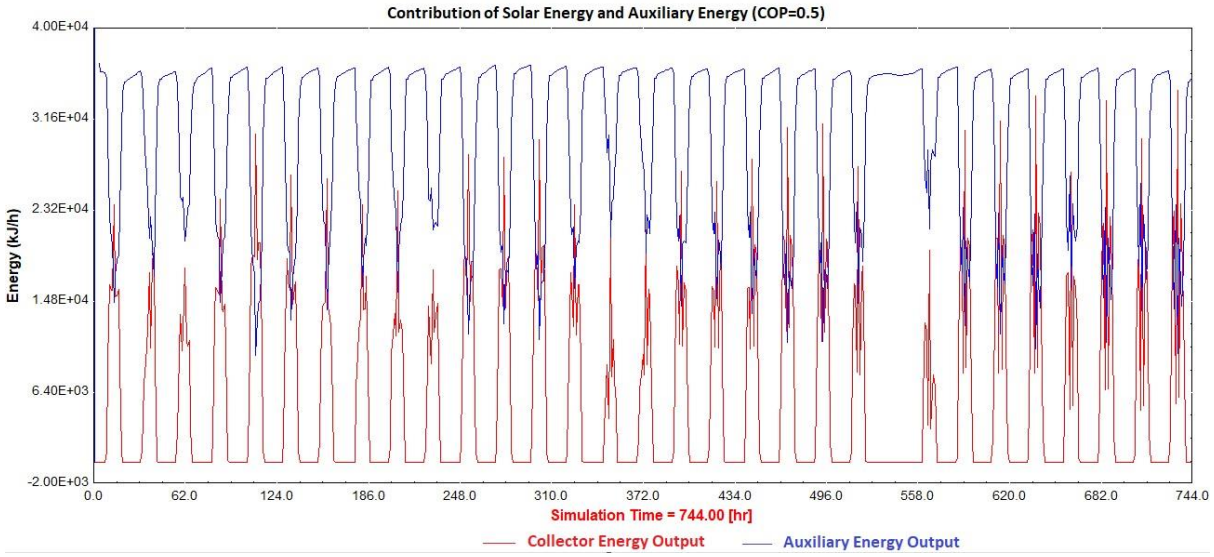

Figure 25. System contribution of collector and auxiliary energy for rated COP of 0.5.

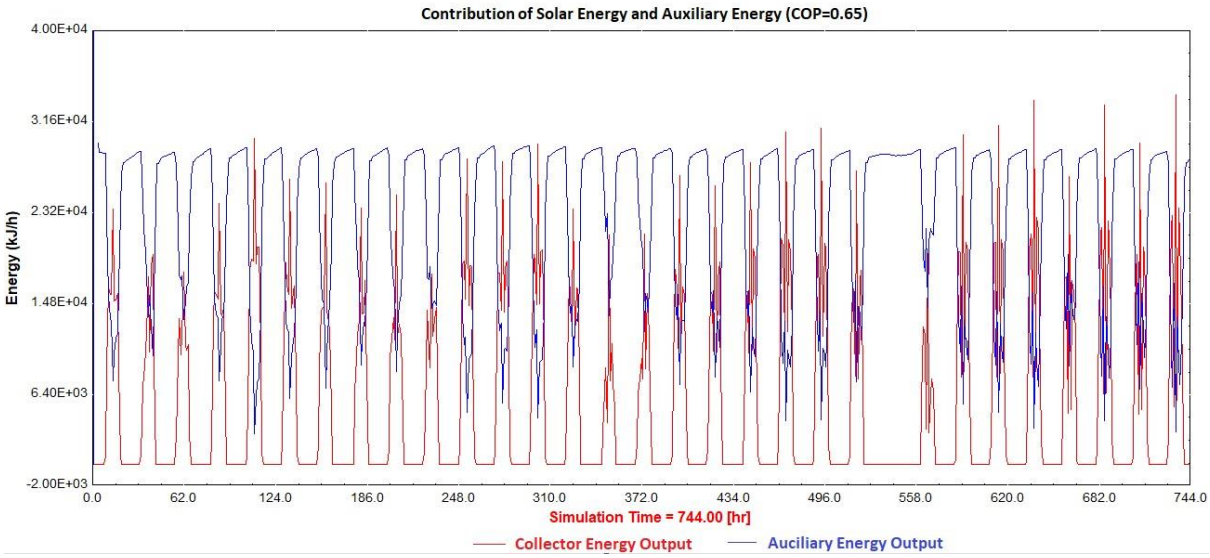

Figure 26. System contribution of collector and auxiliary energy for rated COP of 0.65.

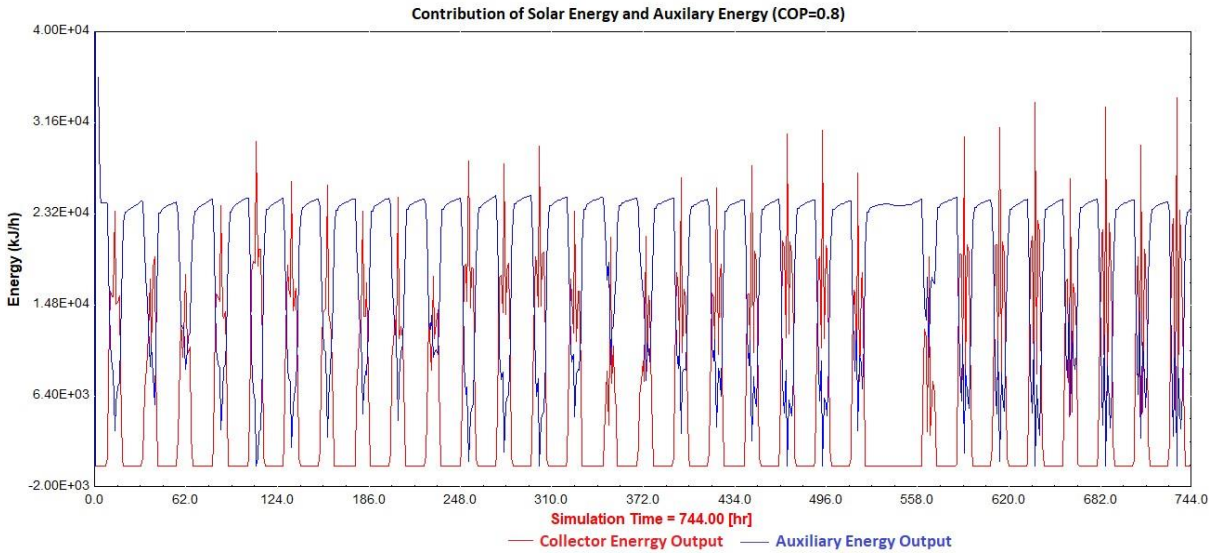

Figure 27. System contribution of collector and auxiliary energy for rated COP of 0.8.

The simulation results underscore the positive impact of increasing the collector area and COP on the fractional primary energy savings of a solar thermal absorption cooling system. Larger collector areas enable the system to capture more solar energy, resulting in higher energy savings and reduced reliance on conventional electrical compression systems. These results are congruent with the findings by Figaj et al. in the feasibility study of a small-scale hybrid dish/flat-plate solar collector system as a heat source for the absorption unit [125]. Their design supported a 17 kW cooling load. They used the optimum concentrator area of 1.6 m^2 per kW of the nominal cooling power of the absorption chiller which is similar to the designed solar

thermal absorption system for a 12 m^2 collector area and observed 50% primary energy savings. Additionally, a larger COP value implies that the absorption chiller can provide a greater amount of cooling while consuming less energy, signifying a more effective utilization of the heat source and efficient conversion of energy into cooling.

The results shown in Figure 28 are obtained from simulations of a solar thermal absorption cooling system considering the different chiller-rated COP values and varying hot storage volumes.

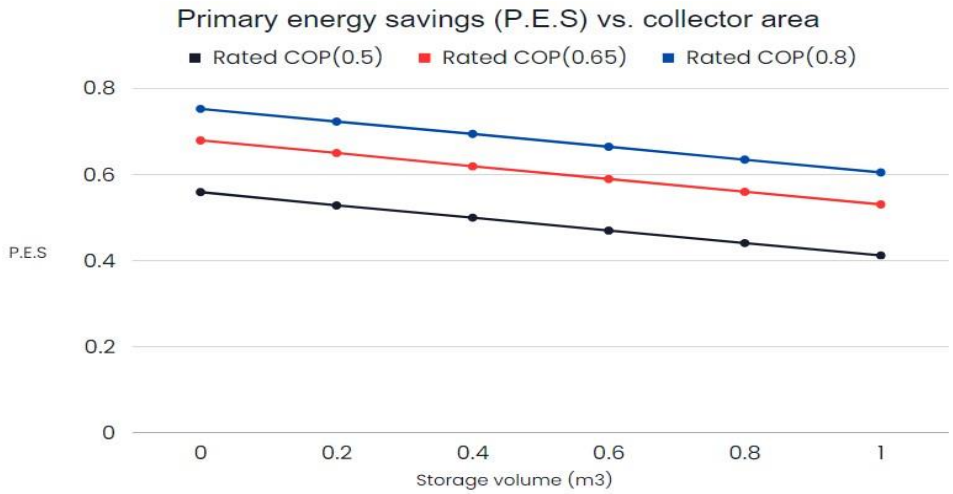

Figure 28. Primary energy savings variation with hot storage volume.

The system was first simulated for a rated chiller COP of 0.5. Without hot storage volume, the fractional primary energy savings of 0.5596 were observed. This result indicates that the system achieves approximately 55.96% monthly energy savings compared to the conventional electrical compression cooling system which was used as the reference. With a hot storage volume of 0.2 m^3, 0.4 m^3, 0.6 m^3, 0.8 m^3, and 1 m^3, the fractional primary energy savings decreased to 0.5286, 0.5002, 0.4702, 0.4411, and 0.4123, respectively. This suggests that the system achieves approximately 52.86%, 50.02%, 47.02%, 44.11%, and 41.23% energy savings compared to the reference. The simulation results demonstrate that as the hot storage volume increases, the primary energy savings of the solar thermal absorption cooling system decrease. This suggests that there is an optimal balance between the direct utilization of solar thermal energy and storage capacity for maximizing energy savings.

With a higher chiller-rated COP of 0.65, the primary energy savings are generally higher compared to the COP of 0.5, and for a chiller-rated COP of 0.8, the primary energy savings are significantly higher compared to the previous two cases. However, the trend remains the same, with the increasing hot storage volume leading to reduced energy savings. The highest savings are achieved without thermal storage, and as the storage volume increases, the energy savings decrease.

4.1.4. Exergy Efficiency

The exergy efficiency indicates the effectiveness of the system in converting available energy into useful cooling, taking into account the quality of the energy and the irreversibilities within the system. Figure 29 shows the relationship between the chiller-rated COP and the exergy efficiency.

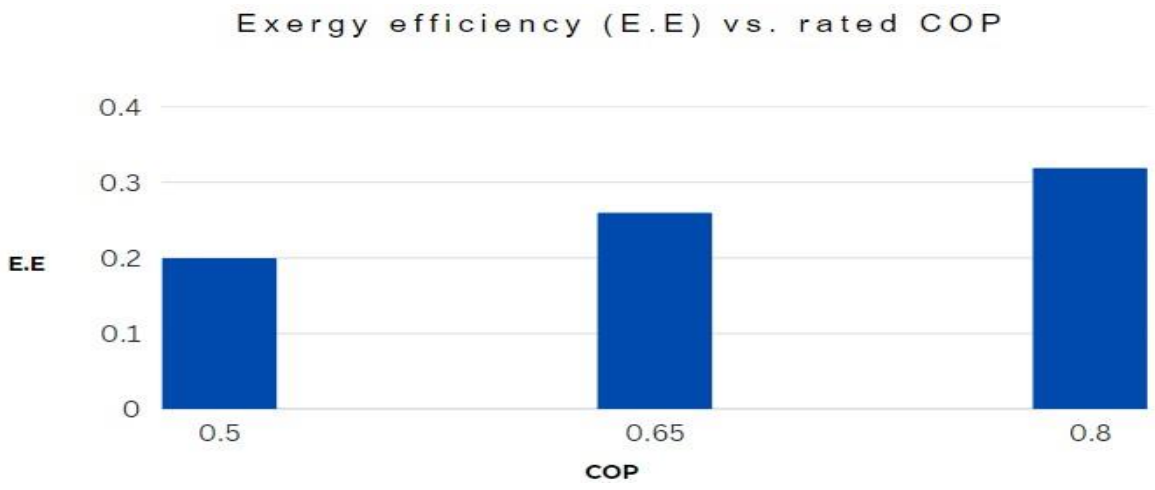

Figure 29. Exergy efficiency for different values of collector area.

Simulations were conducted with an elevated chiller-rated COP of 0.5, 0.65, and 0.8 yielding an increased exergy efficiency of 0.1992, 0.2591, and 0.3189, respectively. This discernible improvement suggests a more effective conversion of the available exergy input into useful work or cooling, demonstrating enhanced energy utilization capabilities within the system. Furthermore, Asadi et al. have provided supporting evidence for the validity of these results in their thermo-economic analysis and multi-objective optimization of absorption cooling systems driven by various solar collectors [113]. They found a closely similar exergy efficiency value

of 0.236 and COP of 0.66 for 10 kW while using evacuated tube collectors for a cooling load of 10 kW. Furthermore, these findings align with those by Aman et al. in the energy and exergy analysis of an absorption cooling system in Canada. Their cooling load was 10 kW and they used chiller generator temperatures from up to 90 °C, achieving the exergy efficiency of 0.32 [126]. Their slightly higher exergy efficiency is likely due to lower ambient temperatures in Canada. As the ambient temperature increases, the temperature difference decreases, resulting in a decrease in the Carnot efficiency. The Carnot efficiency represents the maximum possible efficiency of a heat engine operating between two temperature reservoirs. It is given by the temperature difference between the hot and cold reservoirs.

The outcomes of the simulation demonstrate a clear correlation between the chiller-rated COP and the exergy efficiency in the solar thermal absorption cooling system. The findings elucidate that an increase in the chiller-rated COP corresponds with a notable improvement in the exergy efficiency, indicating a heightened energy utilization and an enhanced conversion of available exergy input into useful cooling. These results underscore the critical importance of selecting chiller equipment with higher COP values to achieve superior energy efficiency and optimal performance within solar thermal absorption cooling systems.

4.2. Economic Impact Analysis

MATLAB was used for the economic impact analysis of the solar thermal cooling system to determine the cost implication and economic feasibility of the system. Four economic metrics (LCOE, NPV, SIR, and DPP) were evaluated for different system technical performance metrics to find a balance between high performance and economic viability.

The obtained results demonstrate that the LCOE for the solar thermal absorption cooling system is influenced by the rated COP as shown in Figure 30.

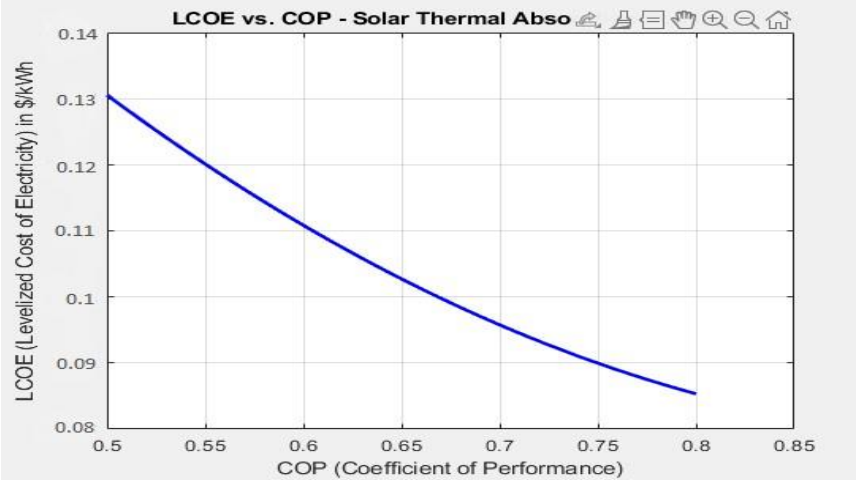

Figure 30. LCOE for variation for different COP values (0.5, 0.65, and 0.8).

Specifically, for a rated COP of 0.5, the LCOE was determined to be $0.13/kWh, indicating the cost associated with producing one kWh of electricity using the system under this particular COP. As the rated COP increases to 0.65, a reduction in LCOE was observed, resulting in a value of $0.103/kWh. This reduction signifies that electricity production costs decrease as the system's COP improves. Furthermore, at a rated COP of 0.8, the LCOE further declines to $0.085/kWh, underscoring the cost-effective nature of the system under higher COP values. A lower LCOE of $0.039/kWh was observed by Ayadi and Al-Dahidi with COP of 0.79 [99]. This could be due to a much higher cooling capacity of 160 kW which means their system is much larger, hence the larger energy production.

These findings highlight the significance of higher COP values in achieving lower LCOE for the solar thermal absorption cooling system. The increase in COP signifies enhanced energy efficiency, leading to substantial cost savings in system operation. A higher COP indicates that the system can deliver more cooling per unit of input energy, resulting in reduced operating costs, and consequently, a lower LCOE.

Drawing a comparison between these LCOE values and the average electricity cost of $0.10/kWh for refrigeration in Lesotho, several noteworthy observations arise: The first is, the solar thermal absorption cooling system demonstrates a less economical LCOE ($0. 0.13/kWh) at the lowest COP of 0.5 compared to the prevailing average electricity cost of $0.10/kWh. This suggests that the system presents a relatively costly alternative for refrigeration needs, lower than the conventional electricity costs at this specific COP value. However, as the COP rises, the LCOE proportionally decreases, indicating enhanced cost-effectiveness. At a COP of

0.65, the LCOE drops to $0.103/kWh. This establishes that the solar thermal absorption cooling system could be a viable and economical option when juxtaposed with the average electricity cost in the region. Lastly, at its peak efficiency with a COP of 0.8, the solar thermal absorption cooling system achieves a significantly reduced LCOE of $0.085/kWh, signifying substantial cost advantages in refrigeration operations compared to the prevalent regional electricity tariffs.

Collectively, these comparative insights imply that the solar thermal absorption cooling system, particularly at higher COP values, represents a more financially viable solution for refrigeration requirements than relying solely on the average electricity cost.

The NPV versus COP graph shown in Figure 31 represents the quantification of the present value of both cash inflows and outflows over the system's projected operational lifespan of 20 years while considering the time value of money discounted at an annual rate of 7.75%.

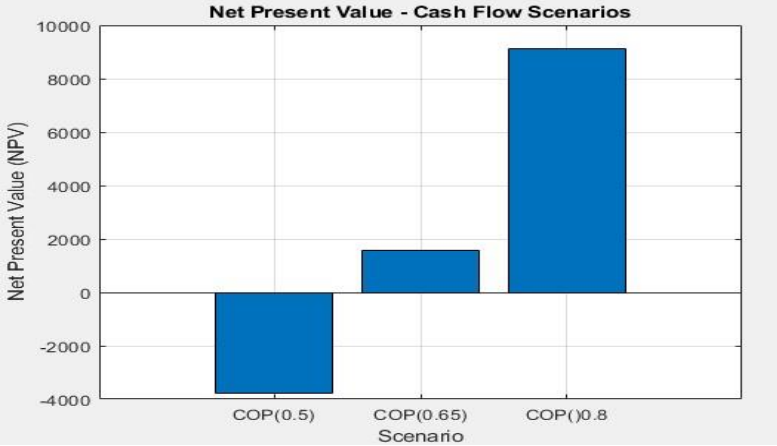

Figure 31. NPV for different COP values (0.5, 0.65, and 0.8).

When considering the solar thermal absorption cooling system with a COP of 0.5, the negative NPV of -$3,830 suggests a less favourable financial outlook. This indicates that the present value of cash outflows outweighs the present value of cash inflows over the projected operational lifespan. The negative NPV implies that the costs associated with the system including the initial investment and ongoing expenses exceed the expected benefits and cash inflows. Consequently, this indicates that the investment may not be financially attractive under these circumstances.

Conversely, a COP of 0.65 demonstrates a positive NPV of $1,790, therefore suggesting a more favorable financial scenario. The positive NPV indicates that the benefits and cash inflows

generated by the system outweigh the associated costs, resulting in a net positive value. This implies that the investment is expected to generate a profit and yield a satisfactory return on investment during the system's operational lifespan.

Furthermore, for a COP of 0.8, the solar thermal absorption cooling system exhibits a significantly higher NPV of $9,200. This notable positive NPV underscores the enhanced profitability potential of the investment. The substantial positive NPV suggests that the expected cash inflows including energy cost savings and potential revenue streams surpass the costs by a substantial margin, indicating a financially lucrative investment opportunity.

The NPV results underscore the critical role of the COP in assessing the financial feasibility of the solar thermal absorption cooling system. Higher COP values reflect increased energy efficiency, resulting in reduced operational costs and potentially higher financial returns. The positive NPV values observed for the COPs of 0.65 and 0.8 emphasize the positive impact of higher COP values on the investment's profitability.

The graph shown in Figure 32 indicates that for a COP of 0.5, the DPP is undefined as the cumulative discounted cash flows amount to -$3,768.5 in year 20. In contrast, for a COP of 0.65, the DPP was projected to be 18 years, while for a COP of 0.8, the DPP was expected to be 12 years considering the system's operational lifespan of 20 years.

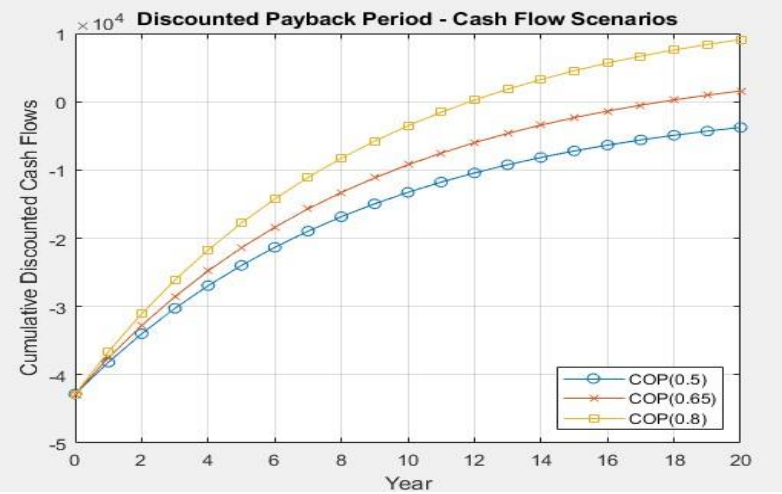

Figure 32. DPP for different COP values (0.5, 0.65, and 0.8).

The absence of a defined DPP for a COP of 0.5 signifies that the cumulative discounted cash flows fail to recover the initial investment within the 20-year time horizon. The negative cumulative discounted cash flows of -$3,768.5 indicate that the system's cash outflows continue to exceed the discounted cash inflows throughout the entire duration. This finding raises concerns about the system's financial sustainability, suggesting an inability to recoup costs and generate positive returns within the specified timeframe.

Conversely, a COP of 0.65 demonstrates a projected DPP of 18 years, indicating that the cumulative discounted cash flows from the solar thermal absorption cooling system are anticipated to surpass the initial investment within this timeframe. The positive DPP value suggests that the system achieves self-sufficiency and generates sufficient cash inflows to offset the discounted cash outflows by the end of the 18^{th} year. This implies an eventual return on investment, although, not within a reasonable timeframe.

Furthermore, for a COP of 0.8, the solar thermal absorption cooling system exhibits a relatively shorter DPP of 12 years. This implies that the system is expected to recover the initial investment and yield positive cumulative discounted cash flows within the initial 12 years of operation. This shorter DPP indicates a more accelerated return on investment for this specific COP scenario; it is closely similar to the pay-back period of 11 and 13.5 years found by Abed et al. for two scenarios in techno-economic analysis of solar-assisted combined absorption cooling cycle [127]. Their system design, with a cooling load of 5 kW and collector area and hot storage tank volume of 8.5 m^2 and 0.35 m^3 respectively, was also relatively comparable to the designed solar thermal absorption cooling system when the collector area was set to 12 m^2.

Within the context of a 20-year system lifespan shown in Figure 33, the SIR reaches 1 in year 17 for a COP of 0.5, year 15 for a COP of 0.65, and year 13 for a COP of 0.8.

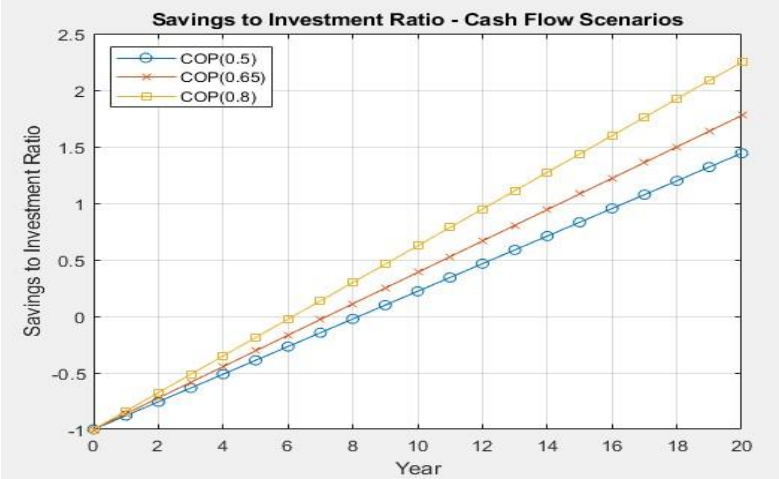

Figure 33. SIR for different COP values (0.5, 0.65, and 0.8).

For a COP of 0.5, the SIR reaching 1 in year 17 indicates that the cumulative savings gradually accumulate over the system's operational life, ultimately equalling the initial investment in the 17th year. The longer time required to achieve a SIR of 1 in this scenario can be attributed to the lower COP, which leads to slower savings accumulation and a comparatively delayed break-even point. While the investment eventually becomes financially sustainable, the extended recovery period raises concerns regarding the system's overall profitability and financial attractiveness.

Conversely, a COP of 0.65 demonstrates an earlier break-even point, with the SIR reaching 1 in year 15. The relatively higher COP contributes to more efficient energy utilization and cost savings, resulting in a faster recovery of the initial investment. This accelerated timeline indicates a favourable return on investment and enhances the system's financial prospects.

Furthermore, the highest financial performance was observed with a COP of 0.8, where the SIR reached 1 in year 13. The system's superior energy efficiency driven by the higher COP facilitates significant cost savings and a more rapid recoupment of the initial investment. The shorter time to achieve a SIR of 1 underscores the system's enhanced financial profitability and strengthens its value proposition. This outcome emphasizes the advantages of investing in a system with a higher COP as it leads to faster savings accumulation and an earlier break-even point.

The observed variations in the time required to reach a SIR of 1 for different COP values highlight the impact of energy efficiency on financial feasibility. The findings underscore the importance of higher COP values in achieving faster savings accumulation and earlier

breakeven points, ultimately contributing to improved financial profitability and the investment's attractiveness.

4.3. System Design Choice

The design of the optimal system starts with the choice of a chiller with a higher-rated COP value of favourably 0.8, as it results in higher solar fraction values and greater utilization of solar energy for meeting the cooling load. Moreover, a larger collector area is opted for, as it leads to higher solar fraction values and increased solar thermal energy utilization. The optimal collector area of 12 m^2 allows for higher solar fraction and higher primary energy savings without costly collector oversizing. The optimal storage volume of 0.2 m^3 was selected to allow adequate thermal storage without much trade-off with the primary energy savings. This is because an increase in thermal storage requires more auxiliary energy to get the tank to hot water set-point temperature.

In consideration of economic metrics, The LCOE showed that the system achieved its lowest value at a rated COP of 0.8 with an LCOE of $0.085/kWh. This indicates that the solar thermal cooling system becomes more cost-effective as the COP increases, resulting in lower electricity production costs. The NPV analysis demonstrated the most favourable outcome for a COP of 0.8. At this COP, the NPV reached $9,200, indicating a significant positive value. This positive NPV implies that the benefits and cash inflows generated by the system outweigh the associated costs, making the investment financially lucrative.

Regarding the DPP, the best performance was achieved with a COP of 0.8. The solar thermal cooling system exhibited a DPP of 12 years, indicating that the initial investment is expected to be recouped within this timeframe. This shorter DPP suggests a more rapid return on investment and enhances the financial feasibility of the system. Lastly, the SIR also highlighted the superior performance of the solar thermal cooling system at a COP of 0.8. The SIR reached 1 in year 13, indicating that the cumulative savings surpassed the initial investment within that timeframe. This accelerated break-even point further emphasizes the system's financial viability and attractiveness.

Considering both technical and economic factors, the optimal system choice from all the parametric analyses involves a chiller with a COP value of 0.8, a collector area of 12 m^2, and a 0.5 m^3 hot storage volume. This combination maximizes the system's ability to meet a cooling

load of 7.318 kW using solar energy. It also improves energy efficiency and offers costeffective operation compared to conventional electricity costs.

5. Conclusions and Recommendations

5.1. Conclusions

In CHAPTER ONE, a comprehensive exploration was made of the history and challenges of food preservation and refrigeration, tracing the shift from ancient methods to modern refrigeration. Innovations like Smock and Neubert's 1950 work on apple storage marked key advancements. However, fossil fuel-based electricity in conventional systems contributes to environmental issues, leading to interest in sustainable refrigeration such as solar thermal cooling.

CHAPTER TWO conducted a detailed literature review on solar thermal refrigeration, introducing its principles and components. Analysis was made on solar collectors, thermal storage, and the refrigeration cycle, covering components like compressors and evaporators. Adsorption, absorption, and desiccant cooling were explored, emphasizing their principles and performance metrics. Mathematical models and COP improvements were presented.

CHAPTER THREE, the methodology, outlined our systematic approach to designing, simulating, and economically analysing a solar thermal cooling system for fresh agricultural produce preservation in Lesotho. Absorption cooling's choice, its alignment with FAO storage recommendations, and system simplicity were justified. TRNSYS was selected for simulation due to its credibility. Also, the geographical and temporal focus was explained.

The economic analysis, a cornerstone, covered monthly and annual analyses, including costs, revenues from produce sales, and additional income from clean development mechanism projects. The simulation methodology, collector modelling, control strategies, and input specifics were described. Sensitivity analysis, essential for real-world uncertainties, outlined variations in collector efficiency, vegetable storage needs, and economic variables' impact on system performance and financial viability.

CHAPTER FOUR, the results, demonstrated the successful design and economic analysis of the cooling system. TRNSYS showed the system's efficiency in meeting cooling needs, emphasizing the significance of optimal sizing and hot storage volume on performance. The research demonstrates the effectiveness and economic viability of the designed solar thermal cooling system for preserving fresh agricultural produce. The economic impact analysis conducted using MATLAB provided essential insights into the cost implications and financial feasibility of the system. Metrics such as LCOE, NPV, SIR, and DPP were considered,

revealing that a chiller with a higher-rated COP value of 0.8, a collector area of 12 m^2, and a hot storage volume of 0.2 m^3 represents the optimal system design. This configuration maximizes solar energy utilization, resulting in higher solar fraction values and improved energy efficiency. It also offers cost-effective operation, with a lower LCOE of $0.085/kWh, a higher NPV of $9,200, a relatively short DPP of 12 years, and an early break-even point at year 13 according to the SIR analysis. These results underscore the financial feasibility and profitability of the solar thermal cooling system, making it an appealing investment option for refrigeration needs in the region. To enhance cost-effectiveness, it is recommended to consider larger-scale installations, invest in advanced materials and technologies, prioritize local manufacturing, explore government incentives, and implement proactive maintenance. Additionally, long-term financing options and hybrid system integration can further improve affordability.

5.2. Recommendations

While this research provides valuable insights, it is essential to acknowledge that it has a limited scope. This study primarily focuses on the technical and economic aspects of solar thermal cooling systems. Again, parasitic electrical energy consumers such as fluid-pumps, electronic sensors, and lights were not accounted for in this study. For future research, the following points could be considered:

- Exploring advanced optimization techniques, such as machine learning algorithms, for precise system parameter adjustments to boost overall performance.
- Developing dynamic models accommodating varying weather conditions and real-time demand fluctuations to enhance system reliability and accuracy.
- Conducting thorough analyses of market dynamics, policy frameworks, and regulatory incentives to assess readiness and potential obstacles for solar thermal cooling technology adoption.
- Conducting real-world implementation and monitoring for validation.

References

[1] R. C. Wiley, “Microbiological and Enzyme Considerations to Prevent Spoilage of MPR Fruits and Vegetables,” in *Preservation Methods for Minimally Processed Refrigerated Fruits and Vegetables*, 1994, p. 69. [Online]. Available: https://link.springer.com/chapter/10.1007/978-1-4615-2393-2_3

[2] L. Leistner, “Food preservation by combined methods,” *Food Research International*, vol. 25, no. 2, pp. 151–158, Jan. 1992, doi: 10.1016/0963-9969(92)90158-2.

[3] M. S. Tapia de Daza, S. M. Alzamora, J. W. Chanes, and G. Gould, “Combination of preservation factors applied to minimal processing of foods,” *Critical Reviews in Food Science and Nutrition*, vol. 36, no. 6, pp. 629–659, Jul. 1996, doi: 10.1080/10408399609527742.

[4] O. Adekomaya, T. Jamiru, R. Sadiku, and Z. Huan, “Sustaining the shelf life of fresh food in cold chain – A burden on the environment,” *Alexandria Engineering Journal*, vol. 55, no. 2, pp. 1359–1365, Jun. 2016, doi: 10.1016/j.aej.2016.03.024.

[5] S. Rodgers, “Preserving non-fermented refrigerated foods with microbial cultures—a review,” *Trends in Food Science & Technology*, vol. 12, no. 8, pp. 276–284, Aug. 2001, doi: 10.1016/S0924-2244(01)00093-0.

[6] World Bank, “Global Agricultural Trade and Developing Countries,” in *Fruits and vegetables: global trade and competition in fresh and processed product markets*, M. A. Aksoy and J. C. Beghin, Eds., The World Bank, 2004, p. 238. doi: 10.1596/0-82135863-4.

[7] K. R. Ullah, R. Saidur, H. W. Ping, R. K. Akikur, and N. H. Shuvo, “A review of solar thermal refrigeration and cooling methods,” *Renewable and Sustainable Energy Reviews*, vol. 24, pp. 499–513, Aug. 2013, doi: 10.1016/j.rser.2013.03.024.

[8] J. Sun, Y. Zuo, R. Sun, and L. Zhou, “Research on the conversion efficiency and preparation technology of monocrystalline silicon cells based on statistical distribution,” *Sustainable Energy Technologies and Assessments*, vol. 47, p. 101482, Oct. 2021, doi: 10.1016/j.seta.2021.101482.

[9] H.-M. Henning, T. Erpenbeck, C. Hindenburg, and I. S. Santamaria, “The potential of solar energy use in desiccant cooling cycles,” *International Journal of Refrigeration*, vol. 24, no. 3, pp. 220–229, May 2001, doi: 10.1016/S0140-7007(00)00024-4.

[10] A. R. Kalair, S. Dilshad, N. Abas, M. Seyedmahmoudian, A. Stojcevski, and K. Koh, “Application of Business Model Canvas for Solar Thermal Air Conditioners,” *Front. Energy Res.*, vol. 9, p. 671973, Jul. 2021, doi: 10.3389/fenrg.2021.671973.

[11] T. He *et al.*, “Application of Solar Thermal Cooling System Driven by Low Temperature Heat Source in China,” *Energy Procedia*, vol. 70, pp. 454–461, May 2015, doi: 10.1016/j.egypro.2015.02.147.

[12] K. Saikia, M. Vallès, A. Fabregat, R. Saez, and D. Boer, “A bibliometric analysis of trends in solar cooling technology,” *Solar Energy*, vol. 199, pp. 100–114, Mar. 2020, doi: 10.1016/j.solener.2020.02.013.

[13] R. Best and N. Ortega, “Solar refrigeration and cooling,” *Renewable Energy*, vol. 16, no. 1–4, pp. 685–690, Jan. 1999, doi: 10.1016/S0960-1481(98)00252-3.

[14] A. Al-Alili, Y. Hwang, and R. Radermacher, “Review of solar thermal air conditioning technologies,” *International Journal of Refrigeration*, vol. 39, pp. 4–22, Mar. 2014, doi: 10.1016/j.ijrefrig.2013.11.028.

[15] T. Brosnan and D.-W. Sun, “Precooling techniques and applications for horticultural products Ð a review,” *International Journal of Refrigeration*, p. 17, 2001.

[16] D. J. Wuebbles and A. K. Jain, “Concerns about climate change and the role of fossil fuel use,” *Fuel Processing Technology*, vol. 71, no. 1–3, pp. 99–119, Jun. 2001, doi: 10.1016/S0378-3820(01)00139-4.

[17] N. Nkolisa, L. S. Magwaza, T. S. Workneh, and A. Chimphango, “Evaluating evaporative cooling system as an energy- free and cost- effective method for postharvest storage of tomatoes (Solanum lycopersicum L.) for smallholder farmers,” *Scientia Horticulturae*, vol. 241, pp. 131–143, Nov. 2018, doi: 10.1016/j.scienta.2018.06.079.

[18] M. G. Gado, S. Ookawara, S. Nada, and I. I. El-Sharkawy, “Hybrid sorption-vapor compression cooling systems: A comprehensive overview,” *Renewable and Sustainable Energy Reviews*, vol. 143, p. 110912, Jun. 2021, doi: 10.1016/j.rser.2021.110912.

[19] World Bank, “Transforming Lesotho’s Farmers into Entrepreneurs,” Oct. 2022. Accessed: Jul. 05, 2023. [Online]. Available: https://www.worldbank.org/en/news/feature/2022/10/13/transforming-lesotho-sfarmers-into-entrepreneurs

[20] International Trade Administration, “Lesotho - Agricultural Sector,” Oct. 2021. https://www.trade.gov/country-commercial-guides/lesotho-agricultural-sector (accessed Jul. 05, 2023).

[21] International Fund for Agricultural Development, “Agriculture in Lesotho,” *IFAD*, 2020. https://www.ifad.org/en/web/operations/w/country/lesotho (accessed Jul. 05, 2023).

[22] M. Khesa, C. Nhemachena, G. Matchaya, and S. Nhlengethwa, “Africa agriculture transformation scorecard performance and lessons for Lesotho,” Jul. 2019, Accessed: Jul. 28, 2022. [Online]. Available: https://cgspace.cgiar.org/handle/10568/105913

[23] R. Mishra, S. K. Chaulya, G. M. Prasad, S. K. Mandal, and G. Banerjee, “Design of a low cost, smart and stand-alone PV cold storage system using a domestic split air conditioner,” *Journal of Stored Products Research*, vol. 89, p. 101720, Dec. 2020, doi: 10.1016/j.jspr.2020.101720.

[24] FAO, “Manual for the preparation and sale of fruits and vegetables,” 2004. https://www.fao.org/3/y4893e/y4893e06.htm#bm06.3.4 (accessed Dec. 13, 2022).

[25] C. Ziv and E. Fallik, “Postharvest Storage Techniques and Quality Evaluation of Fruits and Vegetables for Reducing Food Loss,” *Agronomy*, vol. 11, no. 6, p. 1133, Jun. 2021, doi: 10.3390/agronomy11061133.

[26] J. Ambuko, E. Karithi, M. Hutchinson, and W. Owino, "Modified Atmosphere Packaging Enhances the Effectiveness of Coolbot^{TM} Cold Storage to Preserve Postharvest Quality of Mango Fruits," *JFR*, vol. 7, no. 5, p. 7, Jun. 2018, doi: 10.5539/jfr.v7n5p7.

[27] M. Brian, S. Liako, L. Puselesto, and R. Montoeli, "Integration of post-harvest management in agricultural policy and strategies to minimise post harvest losses in Lesotho," *J. Dev. Agric. Econ.*, vol. 12, no. 2, pp. 84–94, May 2020, doi: 10.5897/JDAE2019.1082.

[28] G. R. Mugagga and H. B. N. Chamdimba, "Adoption of Solar Cooling in East Africa.," *Proceedings of the Sustainable Research and Innovation Conference*, p. 6, 2020.

[29] T. Peters, "The clean cold chain in agriculture in developing countries," Tropical Agriculture Association, United Kingdom, 36, Spring 2019. Accessed: Aug. 12, 2022. [Online]. Available: http://www.taa.org.uk

[30] T. A. Rantšo and M. Seboka, "Agriculture and food security in Lesotho: Government sponsored block farming programme in the Berea, Leribe and Maseru Districts," *Cogent Food & Agriculture*, vol. 5, no. 1, p. 1657300, Jan. 2019, doi: 10.1080/23311932.2019.1657300.

[31] Y. Duan *et al.*, "Postharvest precooling of fruit and vegetables: A review," *Trends in Food Science & Technology*, vol. 100, pp. 278–291, Jun. 2020, doi: 10.1016/j.tifs.2020.04.027.

[32] A. M. Elansari and Y. S. Mostafa, "Vertical forced air pre-cooling of orange fruits on bin: Effect of fruit size, air direction, and air velocity," *Journal of the Saudi Society of Agricultural Sciences*, vol. 19, no. 1, pp. 92–98, Jan. 2020, doi: 10.1016/j.jssas.2018.06.006.

[33] S. Bista, S. E. Hosseini, E. Owens, and G. Phillips, "Performance improvement and energy consumption reduction in refrigeration systems using phase change material (PCM)," *Applied Thermal Engineering*, vol. 142, pp. 723–735, Sep. 2018, doi: 10.1016/j.applthermaleng.2018.07.068.

[34] Government of Lesotho, "About Lesotho – Government Of Lesotho," 2023. https://www.gov.ls/about-lesotho/ (accessed Mar. 10, 2023).

[35] World Bank, "Solar resource maps of Lesotho," *SOLARGIS*, 2020. https://solargis.com/maps-and-gis-data/download/lesotho (accessed Oct. 30, 2022).

[36] R. Z. Wang and X. Q. Zhai, "Development of solar thermal technologies in China," *Energy*, vol. 35, no. 11, pp. 4407–4416, Nov. 2010, doi: 10.1016/j.energy.2009.04.005.

[37] Lesotho Electricity and Water Authority (LEWA), "The newsletter of the Lesotho Electricity and Water Authority," Maseru, Lesotho, 2, Sep. 2021. Accessed: Jul. 29, 2022. [Online]. Available: http://www.lewa.org.ls/library

[38] U. Eicker, D. Pietruschka, M. Haag, and A. Schmitt, "Systematic design and analysis of solar thermal cooling systems in different climates," *Renewable Energy*, vol. 80, pp. 827–836, Aug. 2015, doi: 10.1016/j.renene.2015.02.019.

[39] “Lesotho - Access To Electricity (% Of Population) - 2022 Data 2023 Forecast 1990-2020. Historical.” https://tradingeconomics.com/lesotho/access-to-electricity-percentof-population-wb-data.html (accessed Nov. 24, 2022).

[40] X. Q. Zhai, M. Qu, Yue. Li, and R. Z. Wang, “A review for research and new design options of solar absorption cooling systems,” *Renewable and Sustainable Energy Reviews*, vol. 15, no. 9, pp. 4416–4423, Dec. 2011, doi: 10.1016/j.rser.2011.06.016.

[41] B. R. Hughes, H. N. Chaudhry, and S. A. Ghani, “A review of sustainable cooling technologies in buildings,” *Renewable and Sustainable Energy Reviews*, vol. 15, no. 6, pp. 3112–3120, Aug. 2011, doi: 10.1016/j.rser.2011.03.032.

[42] O. Afshar, R. Saidur, M. Hasanuzzaman, and M. Jameel, “A review of thermodynamics and heat transfer in solar refrigeration system,” *Renewable and Sustainable Energy Reviews*, vol. 16, no. 8, pp. 5639–5648, Oct. 2012, doi: 10.1016/j.rser.2012.05.016.

[43] Y. Fan, L. Luo, and B. Souyri, “Review of solar sorption refrigeration technologies: Development and applications,” *Renewable and Sustainable Energy Reviews*, vol. 11, no. 8, pp. 1758–1775, Oct. 2007, doi: 10.1016/j.rser.2006.01.007.

[44] A. Ghafoor and A. Munir, “Worldwide overview of solar thermal cooling technologies,” *Renewable and Sustainable Energy Reviews*, vol. 43, pp. 763–774, Mar. 2015, doi: 10.1016/j.rser.2014.11.073.

[45] H. Z. Hassan, A. A. Mohamad, Y. Alyousef, and H. A. Al-Ansary, “A review on the equations of state for the working pairs used in adsorption cooling systems,” *Renewable and Sustainable Energy Reviews*, vol. 45, pp. 600–609, May 2015, doi: 10.1016/j.rser.2015.02.008.

[46] G. A. Florides, S. A. Tassou, S. A. Kalogirou, and L. C. Wrobel, “Review of solar and low energy cooling technologies for buildings,” *Renewable and Sustainable Energy Reviews*, 2002.

[47] F. Ziegler, “State of the art in sorption heat pumping and cooling technologies,” *International Journal of Refrigeration*, vol. 25, no. 4, pp. 450–459, Jun. 2002, doi: 10.1016/S0140-7007(01)00036-6.

[48] R. Wang and R. Oliveira, “Adsorption refrigeration—An efficient way to make good use of waste heat and solar energy☆,” *Progress in Energy and Combustion Science*, vol. 32, no. 4, pp. 424–458, 2006, doi: 10.1016/j.pecs.2006.01.002.

[49] D. S. Ayou, J. C. Bruno, R. Saravanan, and A. Coronas, “An overview of combined absorption power and cooling cycles,” *Renewable and Sustainable Energy Reviews*, vol. 21, pp. 728–748, May 2013, doi: 10.1016/j.rser.2012.12.068.

[50] Q. Cui, H. Chen, G. Tao, and H. Yao, “Performance study of new adsorbent for solid desiccant cooling,” *Energy*, vol. 30, no. 2–4, pp. 273–279, Feb. 2005, doi: 10.1016/j.energy.2004.05.006.

[51] C. Amaris, M. Vallès, and M. Bourouis, “Vapour absorption enhancement using passive techniques for absorption cooling/heating technologies: A review,” *Applied Energy*, vol. 231, pp. 826–853, Dec. 2018, doi: 10.1016/j.apenergy.2018.09.071.

[52] K. C. A. Alam, B. B. Saha, and A. Akisawa, “Adsorption cooling driven by solar collector: A case study for Tokyo solar data,” *Applied Thermal Engineering*, vol. 50, no. 2, pp. 1603–1609, Feb. 2013, doi: 10.1016/j.applthermaleng.2011.09.028.

[53] A. N. Shmroukh, A. H. H. Ali, and S. Ookawara, “Adsorption working pairs for adsorption cooling chillers: A review based on adsorption capacity and environmental impact,” *Renewable and Sustainable Energy Reviews*, vol. 50, pp. 445–456, Oct. 2015, doi: 10.1016/j.rser.2015.05.035.

[54] A. Allouhi, T. Kousksou, A. Jamil, T. El Rhafiki, Y. Mourad, and Y. Zeraouli, “Optimal working pairs for solar adsorption cooling applications,” *Energy*, vol. 79, pp. 235–247, Jan. 2015, doi: 10.1016/j.energy.2014.11.010.

[55] W. S. Teng, K. C. Leong, and A. Chakraborty, “Revisiting adsorption cooling cycle from mathematical modelling to system development,” *Renewable and Sustainable Energy Reviews*, vol. 63, pp. 315–332, Sep. 2016, doi: 10.1016/j.rser.2016.05.059.

[56] R. Z. Wang, “Adsorption refrigeration research in Shanghai Jiao Tong University,” *Renewable and Sustainable Energy Reviews*, vol. 5, no. 1, pp. 1–37, Mar. 2001, doi: 10.1016/S1364-0321(00)00009-5.

[57] J. Wang, E. Hu, A. Blazewicz, and A. W. Ezzat, “Simulation of accumulated performance of a solar thermal powered adsorption refrigeration system with daily climate conditions,” *Energy*, vol. 165, pp. 487–498, Dec. 2018, doi: 10.1016/j.energy.2018.09.080.

[58] M. Luberti, C. Di Santis, and G. Santori, “Ammonia/Ethanol Mixture for Adsorption Refrigeration,” *Energies*, vol. 13, no. 4, p. 983, Feb. 2020, doi: 10.3390/en13040983.

[59] P. Bourdoukan, E. Wurtz, and P. Joubert, “Comparison between the conventional and recirculation modes in desiccant cooling cycles and deriving critical efficiencies of components,” *Energy*, vol. 35, no. 2, pp. 1057–1067, Feb. 2010, doi: 10.1016/j.energy.2009.06.021.

[60] A. Gagliano, F. Patania, F. Nocera, and A. Galesi, “Performance assessment of a solar assisted desiccant cooling system,” *Therm sci*, vol. 18, no. 2, pp. 563–576, 2014, doi: 10.2298/TSCI120526067G.

[61] B. S. Davanagere, S. A. Sherif, and D. Y. Goswami, “A feasibility study of a solar desiccant air-conditioning system—Part I: psychrometrics and analysis of the conditioned zone,” *Int. J. Energy Res.*, vol. 23, no. 1, pp. 7–21, Jan. 1999, doi: 10.1002/(SICI)1099-114X(199901)23:1<7::AID-ER439>3.0.CO;2-U.

[62] B. Hyndman, “Heating, ventilation, and air conditioning,” in *Clinical Engineering Handbook*, Elsevier, 2020, pp. 662–666. doi: 10.1016/B978-0-12-813467-2.00092-4.

[63] N. Enteria *et al.*, "Development and construction of the novel solar thermal desiccant cooling system incorporating hot water production," *Applied Energy*, vol. 87, no. 2, pp. 478–486, Feb. 2010, doi: 10.1016/j.apenergy.2009.08.026.

[64] K. Mansuriya, B. D. Raja, and V. K. Patel, "Experimental assessment of a small scale hybrid liquid desiccant dehumidification incorporated vapor compression refrigeration system: An energy saving approach," *Applied Thermal Engineering*, vol. 174, p. 115288, Jun. 2020, doi: 10.1016/j.applthermaleng.2020.115288.

[65] H. Caliskan, H. Hong, and J. K. Jang, "Thermodynamic assessments of the novel cascade air cooling system including solar heating and desiccant cooling units," *Energy Conversion and Management*, vol. 199, p. 112013, Nov. 2019, doi: 10.1016/j.enconman.2019.112013.

[66] M. I. Karamangil, S. Coskun, O. Kaynakli, and N. Yamankaradeniz, "A simulation study of performance evaluation of single-stage absorption refrigeration system using conventional working fluids and alternatives," *Renewable and Sustainable Energy Reviews*, vol. 14, no. 7, pp. 1969–1978, Sep. 2010, doi: 10.1016/j.rser.2010.04.008.

[67] V. Boopathi Raja and V. Shanmugam, "A review and new approach to minimize the cost of solar assisted absorption cooling system," *Renewable and Sustainable Energy Reviews*, vol. 16, no. 9, pp. 6725–6731, Dec. 2012, doi: 10.1016/j.rser.2012.08.004.

[68] M. Sheykhi, M. Chahartaghi, M. M. Balakheli, B. A. Kharkeshi, and S. M. Miri, "Energy, exergy, environmental, and economic modeling of combined cooling, heating and power system with Stirling engine and absorption chiller," *Energy Conversion and Management*, vol. 180, pp. 183–195, Jan. 2019, doi: 10.1016/j.enconman.2018.10.102.

[69] J. Sun, L. Fu, and S. Zhang, "A review of working fluids of absorption cycles," *Renewable and Sustainable Energy Reviews*, vol. 16, no. 4, pp. 1899–1906, May 2012, doi: 10.1016/j.rser.2012.01.011.

[70] I. Horuz, "A comparison between ammonia-water and water-lithium bromide solutions in vapor absorption refrigeration systems," *International Communications in Heat and Mass Transfer*, vol. 25, no. 5, pp. 711–721, Jul. 1998, doi: 10.1016/S07351933(98)00058-X.

[71] C. Somers, A. Mortazavi, Y. Hwang, R. Radermacher, P. Rodgers, and S. Al-Hashimi, "Modeling water/lithium bromide absorption chillers in ASPEN Plus," *Applied Energy*, vol. 88, no. 11, pp. 4197–4205, Nov. 2011, doi: 10.1016/j.apenergy.2011.05.018.

[72] D. Micallef and C. Micaleff, "Mathematical model of a vapour absorption refrigeration unit," *Int. j. simul. model.*, vol. 9, no. 2, pp. 86–97, Jun. 2010, doi: 10.2507/IJSIMM09(2)3.153.

[73] M. S. A. Khan, A. W. Badar, T. Talha, M. W. Khan, and F. S. Butt, "Configuration based modeling and performance analysis of single effect solar absorption cooling system in TRNSYS," *Energy Conversion and Management*, vol. 157, pp. 351–363, Feb. 2018, doi: 10.1016/j.enconman.2017.12.024.

[74] F. Assilzadeh, S. A. Kalogirou, Y. Ali, and K. Sopian, "Simulation and optimization of a LiBr solar absorption cooling system with evacuated tube collectors," *Renewable Energy*, vol. 30, no. 8, pp. 1143–1159, Jul. 2005, doi: 10.1016/j.renene.2004.09.017.

[75] F. Agyenim, I. Knight, and M. Rhodes, "Design and experimental testing of the performance of an outdoor LiBr/H2O solar thermal absorption cooling system with a cold store," *Solar Energy*, vol. 84, no. 5, pp. 735–744, May 2010, doi: 10.1016/j.solener.2010.01.013.

[76] N. Molero-Villar, J. M. Cejudo-López, F. Domínguez-Muñoz, and A. Carrillo-Andrés, "A comparison of solar absorption system configurations," *Solar Energy*, vol. 86, no. 1, pp. 242–252, Jan. 2012, doi: 10.1016/j.solener.2011.09.027.

[77] G. Chen and E. Hihara, "A new absorption refrigeration cycle using solar energy," *Solar Energy*, vol. 66, no. 6, pp. 479–482, Sep. 1999, doi: 10.1016/S0038-092X(99)00042-0.

[78] A. Shirazi, R. A. Taylor, G. L. Morrison, and S. D. White, "Solar-powered absorption chillers: A comprehensive and critical review," *Energy Conversion and Management*, vol. 171, pp. 59–81, Sep. 2018, doi: 10.1016/j.enconman.2018.05.091.

[79] A. Hmida, N. Chekir, A. Laafer, M. E. A. Slimani, and A. Ben Brahim, "Modeling of cold room driven by an absorption refrigerator in the south of Tunisia: A detailed energy and thermodynamic analysis," *Journal of Cleaner Production*, vol. 211, pp. 1239–1249, Feb. 2019, doi: 10.1016/j.jclepro.2018.11.219.

[80] E. Bellos and C. Tzivanidis, "Parametric analysis and optimization of a cooling system with ejector-absorption chiller powered by solar parabolic trough collectors," *Energy Conversion and Management*, vol. 168, pp. 329–342, Jul. 2018, doi: 10.1016/j.enconman.2018.05.024.

[81] M. Z. Siddique *et al.*, "Performance analysis of double effect solar absorption cooling system with different schemes of hot/cold auxiliary integration and parallel-serial arrangement of solar field," *Energy*, vol. 245, p. 123299, Apr. 2022, doi: 10.1016/j.energy.2022.123299.

[82] J. A. Duffie and W. A. Beckman, "Solar Engineering of Thermal Processes," in *Solar Engineering of Thermal Processes*, 4th ed.2013, p. 928.

[83] L. Evangelisti, R. De Lieto Vollaro, and F. Asdrubali, "Latest advances on solar thermal collectors: A comprehensive review," *Renewable and Sustainable Energy Reviews*, vol. 114, p. 109318, Oct. 2019, doi: 10.1016/j.rser.2019.109318.

[84] V. Weitbrecht, D. Lehmann, and A. Richter, "flow distribution in solar collectors with laminar flow conditions," *Solar Energy*, vol. 73, no. 6, pp. 433–441, 2002, doi: doi:10.1016 / S0038–092X(03)00006–9.

[85] A. Araújo and V. Pereira, "Solar thermal modeling for rapid estimation of auxiliary energy requirements in domestic hot water production: On-off flow rate control," *Energy*, vol. 119, pp. 637–651, Jan. 2017, doi: 10.1016/j.energy.2016.11.025.

[86] T. N. Rateele and L. Z. Thamae, "An optimization approach for the economic dispatch incorporating renewable energy resources into Lesotho power sources portfolio," *Heliyon*, vol. 9, no. 4, p. e14748, Apr. 2023, doi: 10.1016/j.heliyon.2023.e14748.

[87] M. Vallès, M. Bourouis, and D. Boer, "Solar-driven absorption cycle for space heating and cooling," *Applied Thermal Engineering*, vol. 168, p. 114836, Mar. 2020, doi: 10.1016/j.applthermaleng.2019.114836.

[88] M. Imtiaz Hussain, C. Ménézo, and J.-T. Kim, "Advances in solar thermal harvesting technology based on surface solar absorption collectors: A review," *Solar Energy Materials and Solar Cells*, vol. 187, pp. 123–139, Dec. 2018, doi: 10.1016/j.solmat.2018.07.027.

[89] U. Desideri, S. Proietti, and P. Sdringola, "Solar-powered cooling systems: Technical and economic analysis on industrial refrigeration and air-conditioning applications," *Applied Energy*, vol. 86, no. 9, pp. 1376–1386, Sep. 2009, doi: 10.1016/j.apenergy.2009.01.011.

[90] B. J. Huang *et al.*, "System performance and economic analysis of solar-assisted cooling/heating system," *Solar Energy*, vol. 85, no. 11, pp. 2802–2810, Nov. 2011, doi: 10.1016/j.solener.2011.08.011.

[91] M. Narayanan, "Techno-Economic Analysis of Solar Absorption Cooling for Commercial buildings in India," *IJRED*, vol. 6, no. 3, p. 253, Nov. 2017, doi: 10.14710/ijred.6.3.253-262.

[92] A. Sapienza, S. Santamaria, A. Frazzica, and A. Freni, "Influence of the management strategy and operating conditions on the performance of an adsorption chiller," *Energy*, vol. 36, no. 9, pp. 5532–5538, Sep. 2011, doi: 10.1016/j.energy.2011.07.020.

[93] W.-S. Chang, C.-C. Wang, and C.-C. Shieh, "Design and performance of a solarpowered heating and cooling system using silica gel/water adsorption chiller," *Applied Thermal Engineering*, vol. 29, no. 10, pp. 2100–2105, Jul. 2009, doi: 10.1016/j.applthermaleng.2008.10.021.

[94] D. Milani, "Renewable Energy Integration in Combined Cooling, Heating, and Power (CCHP) Processes," in *Polygeneration with Polystorage for Chemical and Energy Hubs*, Elsevier, 2019, pp. 459–491. doi: 10.1016/B978-0-12-813306-4.00014-8.

[95] W. Sparber, A. Thuer, F. Besana, W. Streicher, and H. M. Henning, "Unified Monitoring Procedure and Performance Assessment for Solar Assisted Heating and Cooling Systems," p. 9, 2008.

[96] M. Sebitia, M. Sekoli, and P. Masupha, "Farmers' Perspective on Insect Pests that Affect Vegetables in Protected Structures with Emphasis to Tuta absoluta (Meyrick) in Lesotho," *Asian Journal of Advances in Agricultural Research*, vol. volume 15, pp. 33–40, Jun. 2021, doi: 10.9734/AJAAR/2021/v15i330156.

[97] Z. Zhu *et al.*, "Effects of modified atmosphere vacuum cooling (MAVC) on the quality of three different leafy cabbages," *LWT*, vol. 94, pp. 190–197, Aug. 2018, doi: 10.1016/j.lwt.2018.04.002.

[98] T. Bertelsmann-Scott, “the sadc epa: how can the agreement contribute to lesotho’s agriculture and agro-processing sector development?,” Southern African Institute of International Affairs, Jul. 2018.

[99] O. Ayadi and S. Al-Dahidi, “Comparison of solar thermal and solar electric space heating and cooling systems for buildings in different climatic regions,” *Solar Energy*, vol. 188, pp. 545–560, Aug. 2019, doi: 10.1016/j.solener.2019.06.033.

[100] S. Walker, “What is LCOE, Levelized Cost of Energy? The Concept Explained & Formula ...,” *Solar Edition*, Apr. 11, 2019. https://solaredition.com/what-is-lcoe/ (accessed Nov. 10, 2022).

[101] K. M. Bataineh and S. Alrifai, “Recent trends in solar thermal sorption cooling system technology,” *Advances in Mechanical Engineering*, vol. 7, no. 5, p. 168781401558612, May 2015, doi: 10.1177/1687814015586120.

[102] F. Esposito, A. Dolci, G. Ferrara, L. Ferrari, and E. A. Carnevale, “A Case Study Based Comparison between Solar Thermal and Solar Electric Cooling,” *Energy Procedia*, vol. 81, pp. 1160–1170, Dec. 2015, doi: 10.1016/j.egypro.2015.12.144.

[103] S. Paraschiv, N. Bărbuţă-Mişu, and L. S. Paraschiv, “Technical and economic analysis of a solar air heating system integration in a residential building wall to increase energy efficiency by solar heat gain and thermal insulation,” *Energy Reports*, vol. 6, pp. 459–474, Nov. 2020, doi: 10.1016/j.egyr.2020.09.024.

[104] S. El Marazgioui and A. El Fadar, “Impact of cooling tower technology on performance and cost-effectiveness of CSP plants,” *Energy Conversion and Management*, vol. 258, p. 115448, Apr. 2022, doi: 10.1016/j.enconman.2022.115448.

[105] Y. Yu and E. C. Jaenicke, “Estimating Food Waste as Household Production Inefficiency,” *American J Agri Economics*, vol. 102, no. 2, pp. 525–547, Mar. 2020, doi: 10.1002/ajae.12036.

[106] FAO, “Manual for the preparation and sale of fruits and vegetables,” *FAO.ORG*, Nov. 2022. https://www.fao.org/3/y4893e/y4893e06.htm (accessed Nov. 10, 2022).

[107] R. L. Shrivastava, V. Kumar, and S. P. Untawale, “Modeling and simulation of solar water heater: A TRNSYS perspective,” *Renewable and Sustainable Energy Reviews*, vol. 67, no. 3, pp. 126–143, 2017, doi: 10.1016/j.rser.2016.09.005.

[108] TRNSYS, “Welcome | TRNSYS : Transient System Simulation Tool,” *TRNSYS*, Oct. 31, 2022. https://www.trnsys.com/ (accessed Oct. 31, 2022).

[109] T. C. Roumpedakis *et al.*, “Performance Results of a Solar Adsorption Cooling and Heating Unit,” *Energies*, vol. 13, no. 7, p. 1630, Apr. 2020, doi: 10.3390/en13071630.

[110] A. A. Hassan, A. E. Elwardany, S. Ookawara, and I. I. El-Sharkawy, “Performance investigation of a solar-powered adsorption-based trigeneration system for cooling, electricity, and domestic hot water production,” *Applied Thermal Engineering*, vol. 199, p. 117553, Nov. 2021, doi: 10.1016/j.applthermaleng.2021.117553.

[111] Lesotho Meteorological Services, "Climate of Lesotho," 2023. https://www.lesmet.org.ls/home/open/Climate-of-Lesotho (accessed Jul. 18, 2023).

[112] R. E. Schulze and O. S. McGee, "Climatic indices and classifications in relation to the biogeography of southern Africa," in *Biogeography and Ecology of Southern Africa*, M. J. A. Werger, Ed., in Monographiae Biologicae, vol. 31. Dordrecht: Springer Netherlands, 1978, pp. 19–52. doi: 10.1007/978-94-009-9951-0_2.

[113] J. Asadi, P. Amani, M. Amani, A. Kasaeian, and M. Bahiraei, "Thermo-economic analysis and multi-objective optimization of absorption cooling system driven by various solar collectors," *Energy Conversion and Management*, vol. 173, pp. 715–727, Oct. 2018, doi: 10.1016/j.enconman.2018.08.013.

[114] worlddata.info, "Climate comparison: Lesotho / Orange Free State," *Worlddata.info*, 2023. https://www.worlddata.info/climate-comparison.php?r1=lesotho&r2=za-orangefree-state (accessed Apr. 11, 2023).

[115] QAiST (Quality Assurance in Solar Heating and Cooling Technology), "Topic report for WP2 Solar thermal collectors (Performance testing of evacuated tubular collectors)," no. 2.1, 2012.

[116] H. O. Njoku, O. V. Ekechukwu, and S. O. Onyegegbu, "Analysis of stratified thermal storage systems: An overview," *Heat Mass Transfer*, vol. 50, no. 7, pp. 1017–1030, Jul. 2014, doi: 10.1007/s00231-014-1302-8.

[117] K. K. Gopinathan, "Solar radiation on variously oriented sloping surfaces," *Solar Energy*, vol. 47, no. 3, pp. 173–179, 1991, doi: 10.1016/0038-092X(91)90076-9.

[118] B. M. Taele, L. Mokhutšoane, I. Hapazari, S. B. Tlali, and M. Senatla, "Grid electrification challenges, photovoltaic electrification progress and energy sustainability in Lesotho," *Renewable and Sustainable Energy Reviews*, vol. 16, no. 1, pp. 973–980, Jan. 2012, doi: 10.1016/j.rser.2011.09.019.

[119] R. Nikbakhti, X. Wang, A. K. Hussein, and A. Iranmanesh, "Absorption cooling systems – Review of various techniques for energy performance enhancement," *Alexandria Engineering Journal*, vol. 59, no. 2, pp. 707–738, Apr. 2020, doi: 10.1016/j.aej.2020.01.036.

[120] Trading Economics, "Lesotho Interest Rate - 2023 Data - 1980-2022 Historical - 2024 Forecast - Calendar," 2023. https://tradingeconomics.com/lesotho/interest-rate (accessed Jul. 18, 2023).

[121] Lesotho Electricity and Water Authority (LEWA), "Approved Electricity Tariffs & Charges," *Lesotho Electricity and Water Authority*, 2022. https://www.lewa.org.ls/approved-electricity-tariffs-charges/ (accessed Jul. 09, 2023).

[122] T. Sokhansefat, D. Mohammadi, A. Kasaeian, and A. R. Mahmoudi, "Simulation and parametric study of a 5-ton solar absorption cooling system in Tehran," *Energy Conversion and Management*, vol. 148, pp. 339–351, Sep. 2017, doi: 10.1016/j.enconman.2017.05.070.

[123] İ. Uçkan and A. A. Yousif, “Investigation of the effect of various solar collector types on a solar absorption cooling system,” *Energy Sources, Part A: Recovery, Utilization, and Environmental Effects*, vol. 43, no. 7, pp. 875–892, Apr. 2021, doi: 10.1080/15567036.2020.1766599.

[124] U. Eicker and D. Pietruschka, “Design and performance of solar powered absorption cooling systems in office buildings,” *Energy and Buildings*, vol. 41, no. 1, pp. 81–91, Jan. 2009, doi: 10.1016/j.enbuild.2008.07.015.

[125] R. Figaj, M. Szubel, E. Przenzak, and M. Filipowicz, “Feasibility of a small-scale hybrid dish/flat-plate solar collector system as a heat source for an absorption cooling unit,” *Applied Thermal Engineering*, vol. 163, p. 114399, Dec. 2019, doi: 10.1016/j.applthermaleng.2019.114399.

[126] J. Aman, D. S.-K. Ting, and P. Henshaw, “Residential solar air conditioning: Energy and exergy analyses of an ammonia–water absorption cooling system,” *Applied Thermal Engineering*, vol. 62, no. 2, pp. 424–432, Jan. 2014, doi: 10.1016/j.applthermaleng.2013.10.006.

[127] A. M. Abed *et al.*, “Techno-Economic Analysis of dual ejectors solar assisted combined absorption cooling cycle,” *Case Studies in Thermal Engineering*, vol. 39, p. 102423, Nov. 2022, doi: 10.1016/j.csite.2022.102423.

Appendix

```
% Input parameters
system_lifetime = 20; % Lifetime of the system in years
discount_rate =0.0775; % Discount rate 7.75 %
system_capacity = 7.318; % System capacity in kW
capital_cost = 6000; % Capital cost per installed kW
annual_operational_cost = 1713.12; % Annual operational cost per kW (4% of capital cost)
solar_irradiance = 2000 ; % Average annual solar irradiance in kWh/m^2
annual_maintenance_cost = 1713.12; % Annual maintenance cost per kW (4% of capital cost)
collector_area =12;
coll_efficiency = 0.6498;

% Define the COP values
COP_values = [0.5, 0.65, 0.8];

% Initialize arrays for LCOE and energy production
lcoe_values = zeros(length(COP_values), 1);
energy_production_values = zeros(length(COP_values), 1);

% Calculate LCOE for each COP value
for i = 1:length(COP_values)
    COP = COP_values(i);
    % Calculate total energy production over the system's lifetime
    energy_production = solar_irradiance * collector_area * coll_efficiency * COP * system_capacity * system_lifetime;
    energy_production_values(i) = energy_production;

    % Calculate the annualized capital cost
    capital_recovery_factor = (discount_rate * (1 + discount_rate)^system_lifetime) / ((1 + discount_rate)^system_lifetime - 1);
    annualized_capital_cost = capital_cost * system_capacity * capital_recovery_factor;

    % Calculate the annualized operational and maintenance cost
    annualized_operational_cost = annual_operational_cost * system_capacity;
    annualized_maintenance_cost = annual_maintenance_cost * system_capacity;

    % Calculate the total annualized cost
    total_annualized_cost = annualized_capital_cost + annualized_operational_cost + annualized_maintenance_cost;

    % Calculate the LCOE
    lcoe = total_annualized_cost / energy_production;
    lcoe_values(i) = lcoe;

    % Display the result
    fprintf('The LCOE for the solar thermal absorption cooling system with COP %.2f is $%.4f/kWh.\n', COP, lcoe);
end

% Smooth the LCOE curve with interpolation
COP_values_smooth = linspace(min(COP_values), max(COP_values), 100); % Generate a finer grid of COP values
lcoe_values_smooth = interp1(COP_values, lcoe_values, COP_values_smooth, 'spline'); % Use spline interpolation for smooth curve

% Plot the LCOE graphs
figure;
plot(COP_values_smooth, lcoe_values_smooth, 'b-', 'LineWidth', 2);

xlabel('COP (Coefficient of Performance)');
ylabel('LCOE (Levelized Cost of Electricity) in $/kWh');
title('LCOE vs. COP - Solar Thermal Absorption Cooling');
grid on;
```

Code snippet 1. MATLAB code giving LCOE for different COP values

```
% Cash flows (negative values for initial investments, positive values for returns)
cashFlows1 = [-42828 5229.238 5229.238 5229.238 5229.238 5229.238 5229.238 5229.238 5229.238 5229.238 5229.238 5229.238 5229.238 5229.238 5229.238
cashFlows2 = [-42828 5944.311 5944.311 5944.311 5944.311 5944.311 5944.311 5944.311 5944.311 5944.311 5944.311 5944.311 5944.311 5944.311 5944.311
cashFlows3 = [-42828 6952.838 6952.838 6952.838 6952.838 6952.838 6952.838 6952.838 6952.838 6952.838 6952.838 6952.838 6952.838 6952.838 6952.838
% Discount rate
discountRate = 0.075;

% Calculate discounted cash flows for each scenario
discountedCashFlows1 = cashFlows1 ./ (1 + discountRate).^(0:numel(cashFlows1)-1);
discountedCashFlows2 = cashFlows2 ./ (1 + discountRate).^(0:numel(cashFlows2)-1);
discountedCashFlows3 = cashFlows3 ./ (1 + discountRate).^(0:numel(cashFlows3)-1);

% Calculate Net Present Value (NPV) for each scenario
npv1 = sum(discountedCashFlows1);
npv2 = sum(discountedCashFlows2);
npv3 = sum(discountedCashFlows3);

% Plot NPV for each scenario
bar([1 2 3], [npv1 npv2 npv3]);
xlabel('Scenario');
ylabel('Net Present Value (NPV)');
title('Net Present Value - Cash Flow Scenarios');
xticks([1 2 3]);
xticklabels({'Scenario 1', 'Scenario 2', 'Scenario 3'});
grid on;
```

Code snippet 2. MATLAB code giving NPV for different COP values

```
% Cash flows (negative values for initial investments, positive values for returns)
cashFlows1 = [-42828 5229.238 5229.238 5229.238 5229.238 5229.238 5229.238 5229.238 5229.238 5229.238 5229.238 5229.238 5229.238 5229.238 5229.238
cashFlows2 = [-42828 5944.311 5944.311 5944.311 5944.311 5944.311 5944.311 5944.311 5944.311 5944.311 5944.311 5944.311 5944.311 5944.311 5944.311
cashFlows3 = [-42828 6952.838 6952.838 6952.838 6952.838 6952.838 6952.838 6952.838 6952.838 6952.838 6952.838 6952.838 6952.838 6952.838 6952.838

% Calculate savings to investment ratio for each scenario
savings1 = cumsum(cashFlows1);
savings2 = cumsum(cashFlows2);
savings3 = cumsum(cashFlows3);
investment = abs(cashFlows1(1)); % Initial investment

ratio1 = savings1 / investment;
ratio2 = savings2 / investment;
ratio3 = savings3 / investment;

% Plot savings to investment ratio for each scenario
plot(0:numel(cashFlows1)-1, ratio1, 'o-', 'DisplayName', 'Scenario 1');
hold on;
plot(0:numel(cashFlows2)-1, ratio2, 'x-', 'DisplayName', 'Scenario 2');
plot(0:numel(cashFlows3)-1, ratio3, 's-', 'DisplayName', 'Scenario 3');
xlabel('Year');
ylabel('Savings to Investment Ratio');
title('Savings to Investment Ratio - Cash Flow Scenarios');
legend('Location', 'northwest');
grid on;
hold off;
```

Code snippet 3. MATLAB code giving SIR for different COP values

```
% Cash flows (negative values for initial investments, positive values for returns)
cashFlows1 = [-42828 5229.238 5229.238 5229.238 5229.238 5229.238 5229.238 5229.238 5229.238 5229.238 5229.238 5229.238 5229.238 5229.238 5229.238
cashFlows2 = [-42828 5944.311 5944.311 5944.311 5944.311 5944.311 5944.311 5944.311 5944.311 5944.311 5944.311 5944.311 5944.311 5944.311 5944.311
cashFlows3 = [-42828 6952.838 6952.838 6952.838 6952.838 6952.838 6952.838 6952.838 6952.838 6952.838 6952.838 6952.838 6952.838 6952.838 6952.838
discountRate = 0.075;% Discount rate

% Calculate discounted cash flows for each scenario
discountedCashFlows1 = cashFlows1 ./ (1 + discountRate).^(0:numel(cashFlows1)-1);
discountedCashFlows2 = cashFlows2 ./ (1 + discountRate).^(0:numel(cashFlows2)-1);
discountedCashFlows3 = cashFlows3 ./ (1 + discountRate).^(0:numel(cashFlows3)-1);

% Calculate cumulative discounted cash flows for each scenario
cumulativeCashFlows1 = cumsum(discountedCashFlows1);
cumulativeCashFlows2 = cumsum(discountedCashFlows2);
cumulativeCashFlows3 = cumsum(discountedCashFlows3);

% Plot cumulative discounted cash flows for each scenario
plot(0:numel(cashFlows1)-1, cumulativeCashFlows1, 'o-', 'DisplayName', 'Scenario 1');
hold on;
plot(0:numel(cashFlows2)-1, cumulativeCashFlows2, 'x-', 'DisplayName', 'Scenario 2');
plot(0:numel(cashFlows3)-1, cumulativeCashFlows3, 's-', 'DisplayName', 'Scenario 3');
xlabel('Year');
ylabel('Cumulative Discounted Cash Flows');
title('Discounted Payback Period - Cash Flow Scenarios');
legend('Location', 'southeast');
grid on;
hold off;
```

Code snippet 4. MATLAB code giving DPP for different COP values.